Conformational Restriction of the NPF Motif to Target EHD1 and Endocytic Recycling

A dissertation submitted by

Alissa Jaclyn Kamens

In partial fulfillment of the requirements for the degree of

Doctor of Philosophy

in

Chemistry

Tufts University

May 2017

Advisor: Dr. Joshua A. Kritzer

Abstract

The development of specific inhibitors for the long-loop recycling pathway is critical for the study of vesicle trafficking and its involvement in the spread of metastasized cancer cells. Many of the proteins involved in this pathway are difficult to target due to the large and shallow protein-protein interactions they require to function. EHD1, a C-terminal EH domain-containing protein, is a promising target for this process due to its involvement in surface receptor recycling. In addition, many of its interacting proteins do so through an asparagine-proline-phenylalanine (NPF) motif, which forms a type 1 β-turn in the hydrophobic binding pocket of the EH domain of EHD1 (EHD1-EH). In the work described in this thesis, we have developed inhibitors of EHD1 by synthesizing a cyclic peptide with an NPF sequence. The incorporation of the NPF motif into a backbone macrocyclic peptide appeared to stabilize its naturally occurring β-turn, and the cyclic peptide inhibitors bound EHD1-EH more tightly than the corresponding linear controls. We then developed our best inhibitor of the first design series, cNPF1, into a fluorescent probe to further study EH domain binding and screen for stronger EH domain inhibitors. Our newest series of inhibitors utilize the NPF motif in conjunction with a new synthetic pathway to explore a variety of linkers with a series of binding epitopes. The bis-alkylation of thiol-containing peptides allowed for many linkers to be examined in the context of the same peptide sequence. We search for more beneficial binding conformations, while ideally improving passive cell penetration through the

incorporation of a hydrophobic linker. These higher affinity inhibitors will help us gather a better understanding of the effects of EHD1 in the context of cancer cell invasion.

Acknowledgements

First and foremost, I would like to thank Dr. Joshua Kritzer. Through Joshua's tutelage I have learned what it takes to truly be a scientist. He has taught me so much over the years, and I am forever indebted to his efforts. Being a member of the Kritzer laboratory has been a life-changing experience, and through it all I have come out stronger and ready to join the ranks of successful scientists. Joshua has been a guiding light through it all, and I will always appreciate his help and support of my work. Thank you so much for your aid and support, and for always listening to my concerns.

I would also like to thank Dr. James Baleja from the Tufts Sackler School. This project started as a collaborative effort with his team, particularly with Tiffany Corlin. Since then it has evolved into my thesis work and has provided me with countless opportunities. Collaborative work with Dr. Addy Alt-Holland, from the Tufts Dental School, was also very exciting for the development of this project, and I thank her for her efforts. Thank you also to Dr. Charles Mace and Jenna Walz for their help with mammalian culture-based experiments. Next I would like to thank my graduate committee, Dr. David Walt and Dr. Clay Bennett. Thank you for serving as my committee and providing me with the commentary and insight needed to improve my work. Thank you also to Dr. Robert Hammer, for serving as my external examiner.

A huge thank you goes to Dr. Robyn Eisert, a former postdoc of the Kritzer laboratory who contributed greatly to the progress of this project. I learned so much from working with her. What started as a mentorship soon progressed to a true friendship, and I am glad to have had this experience. I would also like to thank Kaley Mientkeiwicz for aiding in the expression of several proteins needed to complete this research, and for being an enthusiastic contributor and willing to learn the necessary experimental techniques.

I would next like to thank all members of the Kritzer laboratory for their help and contributions. I would particularly like to thank Dr. Justin Quartararo and Dr. Santosh Kumar Choudary. They trained me in many of the experimental techniques vital to the completion of this project, and their input and friendship was always valued. They were always there to answer the phone at crazy hours when I had a question about my work that I just couldn't wait to answer, and for that I am so thankful. Thank you also to Daniela Ortiz Bahamonde for being an understanding friend during my graduate school experience, and for essentially introducing me to the rest of the group.

At this point I must say thank you to my parents for their unyielding support all throughout my education. My mother, Barbara Kamens, and my father, Paul Kamens, always pushed me to work harder and value my scholarship. Without their help, I would never have made it to where I am today. I also want to thank

my brother, Ben Kamens, for additional support and occasional comic relief. And a big thank you goes to Sammie Kamens, the greatest dog ever.

Lastly, I would like to thank my fiancé, Will Marshall. He has been a light in the darkness, and a source of unending support. Will has been my rock and has always been there, no matter how rocky the road to a Ph.D. has gotten. Thank you for putting up with my late nights, crazy work schedule, and getting stuck in the lab (when I said I'd only be 20 minutes). Thank you to your family for being so understanding when I have to bow out of an event because I need to be in the lab. Thank you for making me a better person. I love you dearly, and I am privileged to have you in my life.

Table of Contents

1 Chapter 1. An introduction to the development of inhibitors for EHD1, a protein involved in the long-loop recycling pathway.

1.1 An introduction to long-loop recycling and cancer motility

Receptor recycling has long been established as an important contributor to cancer motility.[1] The recycling of integrins from the perinuclear recycling compartment (PNRC) back to the surface of the cell is particularly important for the migration of invasive cancers.[1-2] Integrins, heterodimeric proteins that bind components of the extracellular matrix (ECM), are key players in the formation of focal adhesion points.[2-3] Upon the disassembly of focal adhesions, integrins are endocytosed into the cell where they can later be recycled back to the cell surface to form new focal adhesion complexes.[1, 3-4] In metastasized cancers, there is an increase in the directional trafficking of integrins.[4-5] Recycling of integrins is directed towards the advancing lamellipodia, protrusions of the plasma membrane common in motile cancer cells.[6] This polarization in the trafficking of integrins enables the formation of additional adhesions at the leading edge of the cell.[6] These focal adhesions act as handholds by which the cell can pull forward and away from its previous location.[6-7] The trafficking of the components of focal adhesions, such as integrins, towards the advancing lamellipodia enables the cell to become motile and migrate.[6-7] Consequently, a better understanding of the

pathways involved in the transport of integrins will provide a better understanding of the ways in which metastasized cancers can spread.

When integrins are taken up into the cell, they follow one of three pathways (Figure 1.1).[8] First, the internalized integrins may be taken to the early endosome (EE).[8] The EE contains localized groups of proteins, known as Ras-related in brain (Rab) proteins, that determine the fate of internalized receptors.[8] Rabs are small GTPases that assist in the coordination of membrane trafficking.[9] Rab4-positive endosomes direct the recycled integrins back to the surface of the cell.[4, 10] This pathway, known as short-loop recycling, occurs on the order of 1-2 minutes.[1, 8] By contrast, Rab5- and Rab7-positive endosomes sort integrins to late endosomes, and eventually lysosomes, for subsequent degradation.[11]

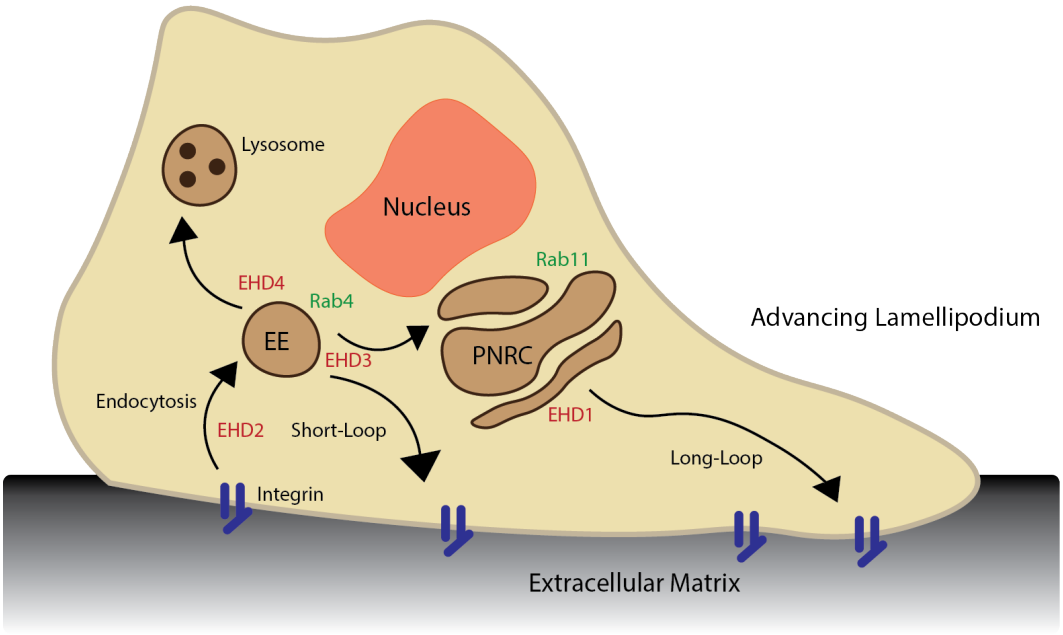

Figure 1.1. A schematic of the various vesicle trafficking pathways used to transport integrins. Selected proteins of the short-loop recycling pathway, the long-loop recycling pathway, and trafficking to the lysosome are shown in red and green. EE denotes the early endosome, while PNRC denotes the perinuclear recycling compartment. Adapted from Mosesson *et al.*[1]

In metastasized cancers, β1-integrins have been shown to be recycled using the long-loop recycling pathway.[1, 8] During long-loop recycling, β1-integrins are sent from the EE to the Rab11-positive PNRC, after which they are recycled back to the plasma membrane.[1, 3-4, 12] This process takes approximately 30 minutes.[4] Indeed there is an increase in the long-loop recycling of β1-integrins, and other adhesion components, in multiple metastasized cancers.[1, 6-7] As demonstrated by microscopy experiments and Monte Carlo simulations, this recycling of adhesion sites provides the cell with the additional traction needed to become motile and invasive.[6-7] While a few general recycling inhibitors exist, there are no inhibitors specific to the long-loop recycling pathway available. This pathway is challenging to target due to the involvement of many proteins that interact via broad, shallow protein-protein interfaces.[13] Ultimately, the discovery of an inhibitor specific to the long-loop recycling pathway would present an opportunity to explore the importance of this process in the context of cancer motility and metastasis.

1.2 Existing recycling pathway inhibitors

While there are no inhibitors specific to the long-loop recycling pathway, there are some molecules that are used as non-specific recycling inhibitors (Figure 1.2, Table 1.1). One of the most widely-used vesicle trafficking inhibitors is dynasore, which was discovered as an inhibitor of endocytosis.[14] Dynamin, the target protein, is a GTPase that facilitates the pinching off of vesicles during

clathrin-mediated endocytosis.[14-15] Dynasore is cell-penetrant and has an IC_{50} of 15 μM for *in vitro* experiments.[14] Although dynasore has been utilized to impede cancer cell motility, its target protein is not important to the long loop recycling process.[16] Other endocytic proteins have also been targeted with inhibitors to impede recycling and cancer invasion. NAV-2729 was developed to target ADP-ribosylation factor-6 (Arf6), a GTPase that serves as a molecular switch in vesicle trafficking of the plasma membrane and cell signaling.[17] However, Arf6 is also involved in trafficking at the plasma membrane.[18] Therefore, inhibitors for Arf6 may impact its cellular functions other than its involvement in long-loop recycling. As a result, other avenues must be explored to identify an inhibitor specific to the long-loop recycling pathway.

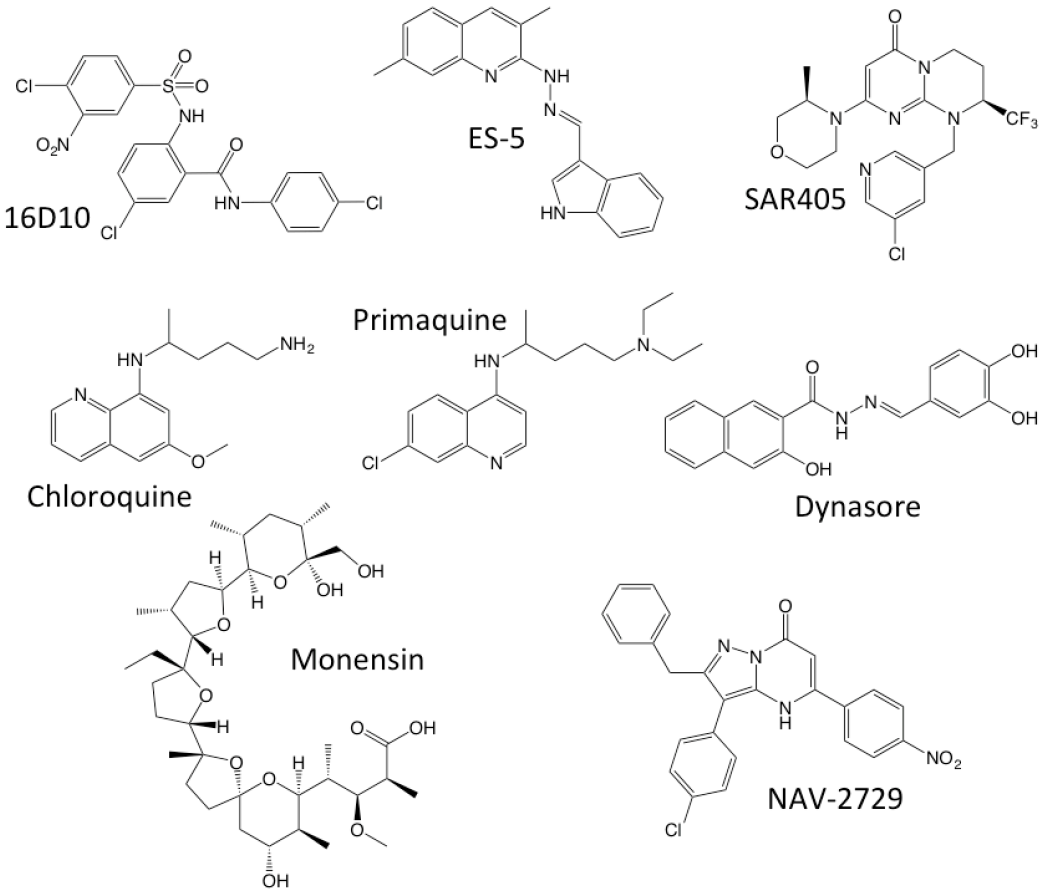

Figure 1.2. Compounds with known inhibitory effects on vesicle trafficking.[14, 17a, 19, 20 21]

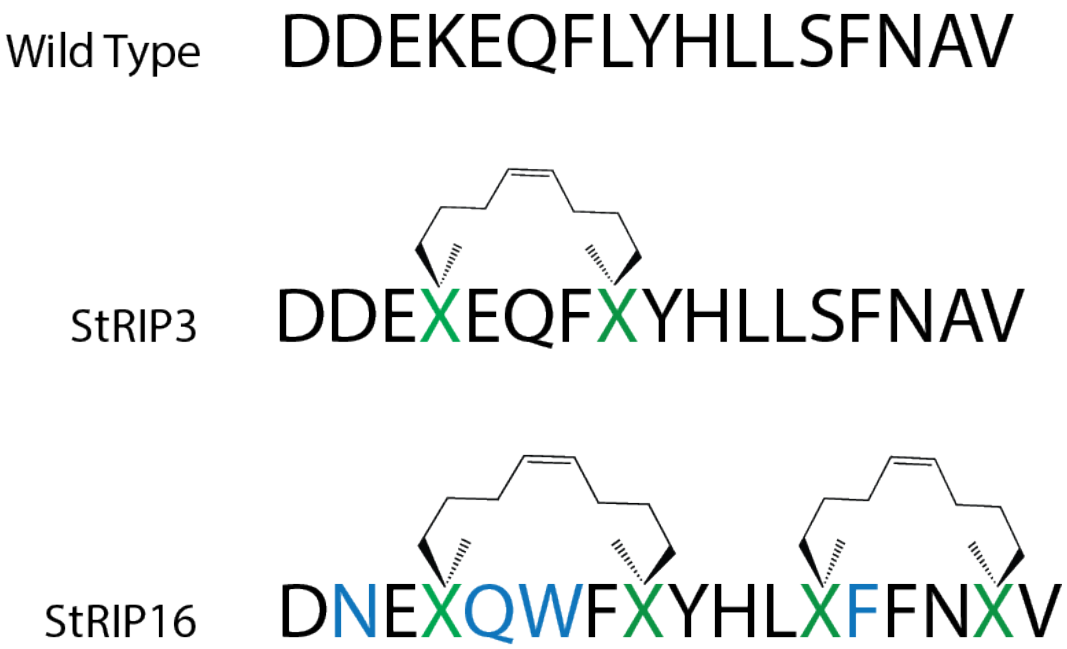

Figure 1.3. An overview of the Rab8a peptide-based inhibitors. The sequence for the wild type Rab6-interacting protein 1 is shown on top. The residues shown in green were replaced with α methyl, α alkenyl amino acids for hydrocarbon stapling. Residues altered between StRIP3 and StRIP16 were displayed in blue.[22]

Molecule	Effected Pathway	Target or Mechanism	References.
Dynasore	Endocytosis	Dynamin	[14-15]
NAV-2729	Long loop recycling and endocytosis	Arf6	[17]
Chloroquine	Transport between endosome and lysosome	Endosomal acidification	[19a, 19b]
Primaquine			
Monensin			
Endosidin-5	General membrane traffic	Unknown	[19c]
16D10	Golgi to plasma membrane	Endosomal acidification	[20]
SAR405	Endosome to lysosome	Vsp34	[21]
StRIP3	Long-loop and retrograde	Rab8a	[22]
StRIP16			

Table 1.1. A summary of the existing inhibitors related to or capable of the inhibition of the long-loop recycling pathway.

Other classes of molecules, such as lysosomotropic agents, have been designed to target intracellular trafficking beyond endocytosis. Lysosomotropic agents are comprised of weak bases and ionophores that raise the pH of intracellular compartments, such as endosomes and lysosomes.[19a, 19b] Exposure to lysosomotropic agents causes endosomal swelling and impairs protein secretion.[19b] Common lysosomotropic agents include chloroquine, primaquine, monensin, and ammonium chloride (Figure 1.2).[19b] Monensin has been used as a tool to block the trafficking between endosomes and lysosomes.[23] Both chloroquine and primaquine have also served as tools to probe endocytic transport.[23b, 24] They frequently serve as experimental controls while probing other components of recycling.[25] While these molecules make useful tools for examining vesicle trafficking, their effects on general endosomal pH underlines the need for a more precise inhibitor. [23 24]

In the search for inhibitors of long-loop recycling, multiple screening attempts have uncovered a few molecules that affect this pathway. In 2011, Drakakaki *et al.* identified endosidin-5 (ES-5) through a small molecule screen of inhibitors of membrane traffic (Figure 1.2).[19c] ES-5 caused the accumulation of endosomal transferrin in HeLa cells.[19c] In another study, medium-throughput small molecule screens in BSC1 cells identified some sulfonamide-containing compounds, including a compound designated 16D10, inhibited trafficking from the Golgi to the cell surface.[20] 16D10 was postulated to function similar to a lysosomotrophic agent (Figure 1.2).[20] A screen in HeLa cells discovered compound SAR405, a

small molecule which targets the protein vacuolar protein sorting 34 (Vps34).[21] This compound impedes vesicle trafficking between the endosome and the lysosome, as well as autophagy (Figure 1.2).[21] Although these molecules target proteins involved in related trafficking processes, further work is needed to find a specific long-loop recycling inhibitor.

Spiegel *et al.* used structure-based design to develop peptidic inhibitors of Rab8a, a Rab GTPase involved in long-loop recycling and transport from the Golgi network.[22, 26] Speigel *et al.* developed two hydrocarbon stapled α-helical peptides, StRIP3 and StRIP16 (Figure 1.3).[22] These peptides, which were designed based on Rab6-interacting protein 1, incorporated hydrocarbon staples to stabilize the α-helical secondary structure required for Rab binding.[22, 27] In addition, the incorporation of these hydrocarbon staples promoted the protease resistance and cell-penetrating capabilities of these peptides.[22, 27] StRIP3 had a dissociation constant (K_d) of 30 μM and StRIP16 had a K_d of 12.7 μM for GTP-bound Rab8a.[22b] However, these peptides bound more than one Rab protein *in vitro*.[22a] Further, cell-based assays suggested that StRIP16 had some off-target effects in mammalian cell culture, since it associated with membranes not associated with Rab8a.[22b] These results show that specificity remained a problem for these peptidic Rab8a inhibitors.

1.3 The EH domain and vesicle trafficking

The EH domain is found in many important components of vesicle trafficking.[28] This epidermal growth factor receptor tyrosine kinase substrate 15 (Eps15) homology (EH) domain was named for the protein in which it was initially discovered, Eps15.[29] First identified in 1993, this domain has since been discovered in other established pieces of endocytic machinery, such as EHD1 and intersectin.[28-29] EH domain-containing proteins are present within many different endocytic pathways.[28, 30] They function as adaptor proteins, in which EH domains cooperate with other interaction domains to coordinate multiple protein-protein interactions.[28, 31] Ultimately, an analysis of the importance of EH-domain containing proteins in the context of the long-loop recycling pathway, may provide a window into targeting this process for a better understanding of the pathway's involvement in the motility of cancer cells.

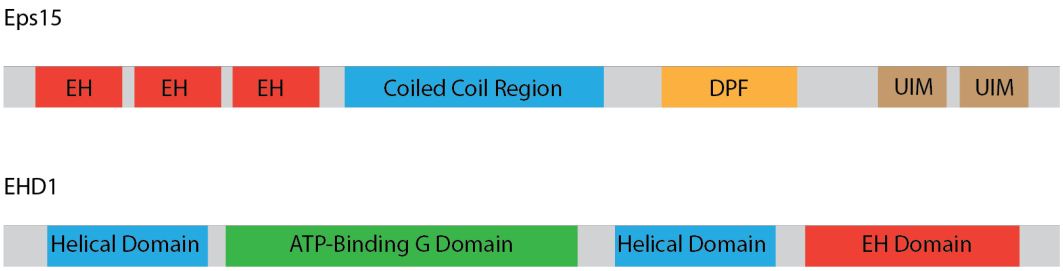

Figure 1.4. The domain organization of representative N-terminal and C-terminal EH domain-containing proteins. Human Eps15 (top) is an N-terminal EH domain-containing protein involved in clathrin-mediated endocytosis. It contains three EH domains (red) at its N-terminus, followed by a coiled coil region (blue) and a DPF-rich region (yellow). Its contains two ubiquitin interaction motifs (UIMs) at its c-terminus. Human EHD1 (bottom) has its EH domain near its C-terminus (red). Its N-terminal region consists of an ATP-binding G domain (green) flanked by helical domains (blue). This image was adapted from Rumpf *et al.* and Naslavsky *et al.*[32]

1.4 Differences between the N and C-terminal families of EH domain-containing proteins

EH domain-containing proteins can be divided into two groups: those with N-terminal EH domains and those with C-terminal EH domains (Figure 1.4).[33] Both groups function as scaffolding and adaptor proteins for vesicle trafficking.[33] Proteins with N-terminal EH domains, such as Eps15, function primarily in cellular internalization processes such as endocytosis.[28b, 34] N-terminal EH domain-containing proteins were first discovered by Fazioli *et. al*.[29] Eps15 contains three EH domains located in its N-terminal region. These EH domains are followed by a coiled-coiled region, and then a region containing multiple Asp-Pro-Phe (DPF) motifs and two ubiquitin interaction motifs (Figure 1.4).[28b, 34] Eps15 functions as an adaptor protein during clathrin-mediated endocytosis.[28b, 34] It is believed to aid in vesicle formation through its interactions with other adaptor proteins known to be involved in the endocytic machinery.[28b, 34]

Meanwhile, C-terminal EH domain-containing proteins are involved in intracellular transport.[32b, 33] There are four known paralogs with different, but occasionally overlapping, roles in intracellular trafficking.[32b] EHD1 has been linked with transport from the PNRC back to the surface of the cell.[35] EHD2 has been connected to direct cellular internalization; it localizes to calveolae-containing structures and membranes rich in phosphatidylinositol 4,5-bisphosphate.[36] Both EHD3 and EHD4 have been established as proteins involved

in transport from the sorting endosome to either the recycling endosome or the lysosome for subsequent degradation through their interactions with Rab11-FIP2 and Rab5-positive endosomes respectively.[32b, 37] EHD1-4 have a very similar domain structure (the structure of EHD1-EH is shown in Figure 1.4). They consist of an N-terminal helical domain, an ATP-binding G Domain, a second helical domain, and a C-terminal EH domain.[32b, 36a] There is a high degree of sequence identity, roughly 70%, among EHD1-4,[32b, 36a]

1.5 Validation of EHD1 as a target for developing vesicle trafficking inhibitors

EHD1 is a C-terminal EH-domain-containing protein involved in long-loop endocytic recycling and retrograde transport. EHD1 is directly involved in the recycling of β1 integrins to the plasma membrane.[33, 36a, 38] As a result, we judged that EHD1 could be an excellent target to block receptor recycling in a manner that would reduce cancer motility.

EHD1 was first discovered in 1999 by Mintz *et al*., and it was soon revealed to colocalize with known components of the recycling machinery.[35a, 39] It was then shown to be involved in the trafficking of major histocompatibility factor I (MHCI) and the transferrin receptor from the PNRC back to the plasma membrane.[35] It was also demonstrated to associate with other adaptor proteins relevant to the long-loop recycling pathway, such as rabenosyn-5 and MICAL-

L1.[40] EHD1 knockdown via siRNA resulted in the delayed recycling of transferrin and other proteins through the long-loop recycling pathway in HeLa cells.[40a, 41] Meanwhile, knockout of EHD1 in mouse embryonic fibroblasts (MEFs) slowed the recycling of internalized transferrin.[42] This early work suggested that EHD1 was an important component of intracellular trafficking.

In addition to the established connections to the pathway of interest, aberrations in EHD1 expression have been linked with several conditions and disease states.[32b] An increase in EHD1 expression in monocytes was connected with *Asperigillus Fumigatus* infections.[32b, 43] EHD1 was detected in secretions from prostate cancer cells.[32b, 44] Expression of EHD1 above basal levels in cutaneous T cell lymphoma has also been observed.[32b, 45] More recently, a link has been established between EHD1 intracellular protein levels and the prognosis for non-small cell lung cancer (NSCLC).[46] Increased expression of EHD1 in biopsied tumor tissue correlated with a poorer survival rate of NSCLC patients.[46] A study of 100 patients revealed that those with NSCLC that tested positive for EHD1 expression had an average overall survival (OS) of 23.9 months, while those negative for EHD1 expression had an average OS of 70.0 months.[46] Furthermore, the overexpression of EHD1 in NSCLC cells correlated to an increased resistance to cisplatin cancer therapies.[47] These studies demonstrated that targeting EHD1 may have long term benefits in the understanding of cancer progression.

The implied importance of EHD1 in cancer spurred additional studies of its relevance to integrin recycling via the long-loop pathway. The Caplan group probed this by knocking down expression of EHD1 in HeLa cells via siRNA.[38] The trafficking of transferrin and β1-integrins were monitored with fluorescence by confocal microscopy.[38] After a series of pulse-chase experiments, both transferrin and the β1-integrins remained accumulated in the PNRC.[38] These results indicated that EHD1 was key for the transport of these proteins from the PNRC back to the surface of the cell.[38] Additional studies were conducted to observe the impact of EHD1 knockdown on cell motility. Scratch test experiments revealed that knockout of EHD1 reduced the ability of MEFs to migrate and form filopedia.[38] In a separate study, EHD1 was shown to be necessary for the trafficking of the tyrosine kinase Src, an oncoprotein responsible for cell invasion and migration.[48] EHD1 has been shown to colocalize and interact with several other important pieces of endocytic machinery (Table 1.2). Ultimately, EHD1 has been demonstrated to be a potential player in the trafficking of integrins and cell motility.

Protein	Interaction Type	Reference
SNAP29	EH domain – NPF motif	[49]
AP-2 α-adaptin	Not characterized	[49]
Rabenosyn-5	EH domain – NPF motif	[40a]
Syndapin I	EH domain – NPF motif	[50]
Syndapin II	EH domain – NPF motif	[50]
Rab11-FIP2	EH domain – NPF motif	[37a]
MICAL-L1	EH domain – NPF motif	[51]
Snapin	EH domain	[52]

Table 1.2. A collection of proteins known to interact with EHD1. These proteins are known to be adaptors and other pieces of endocytic machinery important to the long-loop recycling pathway. This table was adapted from Naslavsky *et al.*[32b]

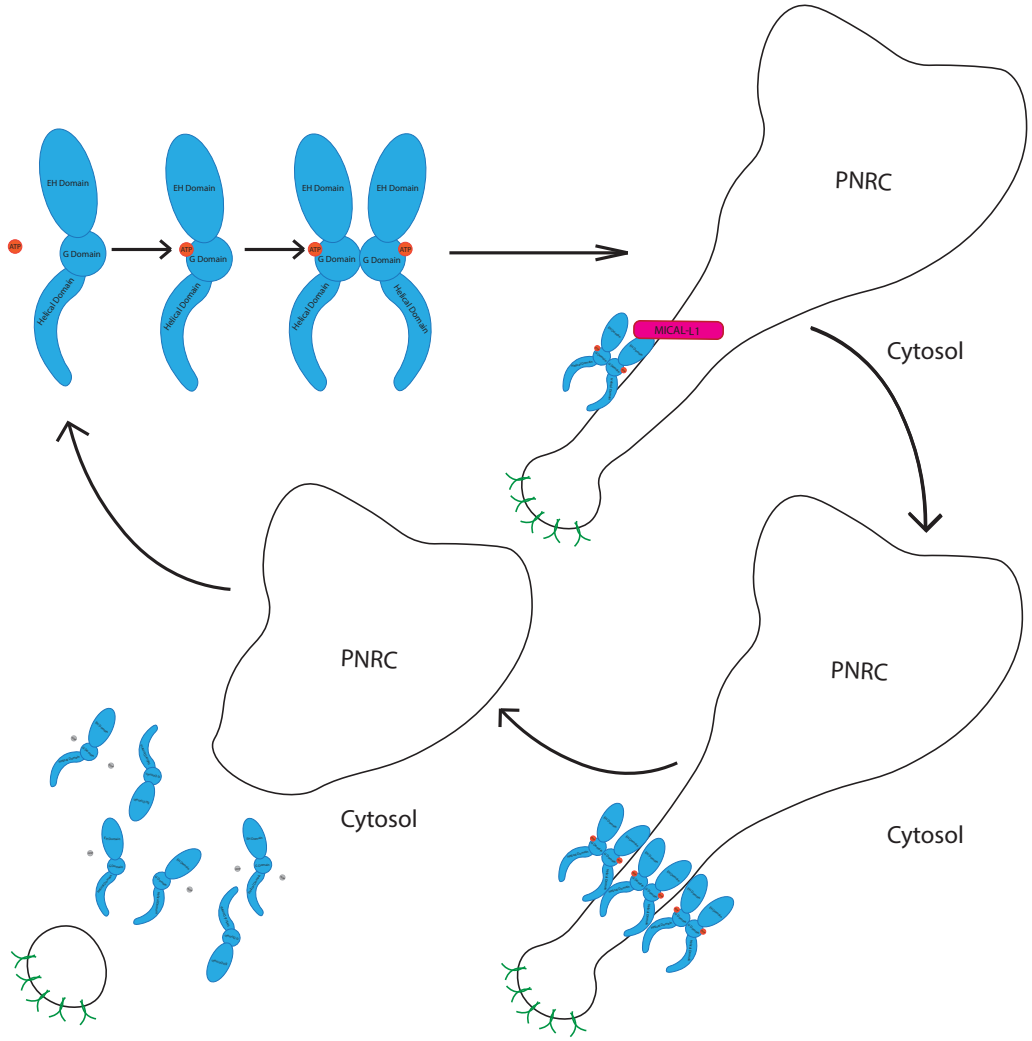

Figure 1.5. A schematic of the mechanism of EHD1 in vesicle scission. EHD1, depicted in blue, binds ATP (red) and dimerizes. The EHD1 dimers are then recruited to budding tubular vesicles via interactions between adaptor proteins (pink) and their EH domains. Receptors to be recycled are shown in green. After EHD1 forms oligomers on this budding tubular vesicle, ATP hydrolysis (ADP shown in gray) generates a conformational change and subsequent vesicle separation. This figure was adapted from Zhang *et al.* and Giridharan *et al.*[53]

EHD1 is believed to act as a pinchase, and aids in vesicle fission from the PNRC.[54] It is recruited to tubule-shaped vesicles as they bud from the PNRC.[40b] EHD1 binds ATP and then dimerizes (Figure 1.5).[55] The ATP-bound EHD1 dimers are then recruited to the budding tubular vesicle by adaptor proteins including MICAL-L1.[53b] The EHD1 dimers then form oligomers surrounding the budding vesicle.[55-56] Hydrolysis of the bound ATP generates a change in the EHD1 conformation, which destabilizes the vesicle membrane and ultimately promotes membrane fission.[53a, 56] According to this model, the application of an inhibitor of EHD1 would therefore prevent the scission of vesicles from the PNRC for subsequent return to the plasma membrane.

1.6 The structure and homology of the EH domain

EH domains are named for the protein in which they were initially discovered: Eps15, a scaffolding protein involved in the cellular uptake of epidermal growth factor receptors (EGFRs).[28b, 34] The tyrosine in Eps15 that is phosphorylated by the kinase domain of EGFR is not present in the EH domain.[34] The sequence homology is extremely high between various EH domains, especially among those of the same family.[28b] The second EH domain of Eps15 shares 49.5 % sequence identity with the EH domain of EHD1.[57] Meanwhile, the EH domain of EHD1 shares 58.7 %, 81.5 %, and 68.5 % sequence identity with the EH domains of EHD2, EHD3, and EHD4 respectively.[32b]

Each EH domain is approximately 100 amino acids in length.[36a] They consist of two helix-turn-helix motifs for calcium binding, connected by an anti-parallel β-sheet (Figure 1.6).[36a, 58] The helix-turn-helix motifs are similar to EF hands; however, in most EH domains only the second motif actually binds calcium ions.[28b, 58-59] The calcium ion has no impact on target binding, and appears to have a solely structural purpose.[28b, 58-59] Most of the EH domain's known binding partners interact with an Asn-Pro-Phe (NPF) motif that binds in a hydrophobic pocket between helices 2 and 3.[58-60] Binding of an NPF motif has little effect on the EH domain's overall structure.[59] The EH domain has also been shown to be capable of directly interacting with phosphotidylinositols.[57] The residues responsible for this interaction also lie between helices 2 and 3.[57] However, the side chains involved are positioned on the opposite face of the protein, which enables simultaneous binding of phosphotidylinositols and NPF-containing adaptor proteins.[57, 61]

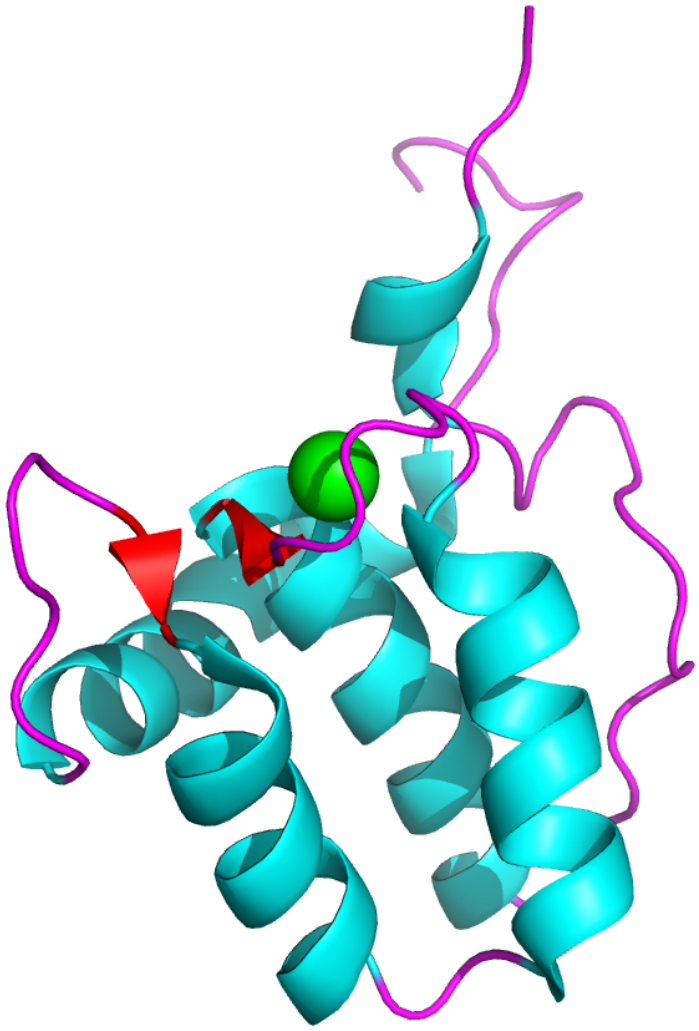

Figure 1.6. The EH domain of EHD1 EH. Helical structures are depicted in cyan, β-sheets are shown in red, and coil regions are shown in magenta. The calcium ion is represented by the green sphere. The EH domain is presented with the NPF binding site in front. This binding site is located between helices 2 and 3. PDB ID: 2KFF.[59]

1.7 EH domains and NPF motifs

As previously mentioned, the majority of known interactions with EH domains occur with proteins that contain an asparagine-proline-phenylalanine (NPF) motif.[62] NPF-containing proteins were initially identified while screening for interaction partners of EH domain-containing proteins.[62] Most of the known proteins with NPF motifs are involved in endocytic pathways.[28b, 32b, 36a] Many have additional functions in recycling, such as rabenosyn-5 and MICAL-L1 (Molecules Interacting with CasL-Like1).[28b, 32b, 36a] Most NPF proteins also contain other protein-protein interaction domains and motifs, facilitating multiprotein complexes important for vesicle trafficking (Figure 1.7).[28b, 32b, 36a]

NPF binding occurs in a hydrophobic binding pocket between helices 2 and 3 of the EH domain (Figure 1.8).[63] When bound to an EH domain, the NPF motif forms a type 1 β-turn, with its structure stabilized by an intramolecular hydrogen bond between the Asn and the residue immediately C-terminal to the NPF motif.[59, 63] The Phe residue is bound deeply in the hydrophobic binding pocket, which is formed by Lys^{468}, Met^{471}, Val^{472}, Asn^{478}, Leu^{481}, and Trp^{485} of EHD1.[59] Trp^{485} is particularly important for NPF binding, since mutating this position to alanine prevents the binding interaction entirely.[32b] A hydrogen bond between the γ-NH_2 of the Asn of the NPF peptide and the carbonyl oxygen of Gly^{482} of EHD1 provides additional selectivity for the NPF motif over similar sequences, such as DPF and GPF.[59, 63a]

While there is a high degree of both structural and sequence homology among the EH domains of both N-terminal and C-terminal EH domain-containing proteins, there is an important difference that enables selective binding for one class over the other. In C-terminal EHDs, the binding pocket is surrounded by large regions of positive surface potential (Figure 1.9).[58, 60, 64] This structural feature promotes the binding of NPF motifs with negatively charged residues C-terminal to the binding epitope.[58, 60, 64] In fact, several known binding partners of EHD1 have negatively charged residues in this position.[33] MICAL-LI, for instance, has two glutamic acids C-terminal to the NPF motif that are able to form salt bridges with nearby lysine residues on the EH domain surface.[60] This interaction provides additional electrostatic contributions, while allowing for the selective binding of C-terminal EH domains.[59-60, 64] By contrast, EH domains from N-terminal EH domain-containing proteins have regions of either negative or neutral surface potential surrounding the NPF binding pocket.[33, 63b] As a result, the NPF motifs of their interacting proteins may be flanked with positively charged residues to confer selectivity.[33, 63b]

Figure 1.7. The domain organization of several proteins identified as binding partners of EHD1 via an NPF-EH domain interaction.[53b, 64] The NPF motifs are displayed as red bars. Each protein contains at least two NPF motifs, each capable of binding one EH domain.[63b, 64] Rabenosyn-5 is a Rab5 effector important for endosomal fusion.[65] Rab11-Fip2 is a Rab11-binding protein involved in receptor recycling.[66] MICAL-L1 is an adaptor protein that recruits endocytic machinery to tubular recycling endosomes.[53b] Syndapin2 is an additional adaptor protein in vesicular recycling.[50] C2H2: Zn-finger domain, FYVE: phosphatidylinositol binding domain, Rab4: Rab4 binding helix, Rab5: Rab5 binding helix, C2: phospholipid binding domain, Rab11: Rab11 binding domain, CH: calponin homology domain, Lin11, Isl-1, Mec-3 domain, CC: coiled coil domain, F-BAR: FCH-Bin-amphiphysin-Rvs domain, SH3: Src homology 3 domain.[53b, 64]

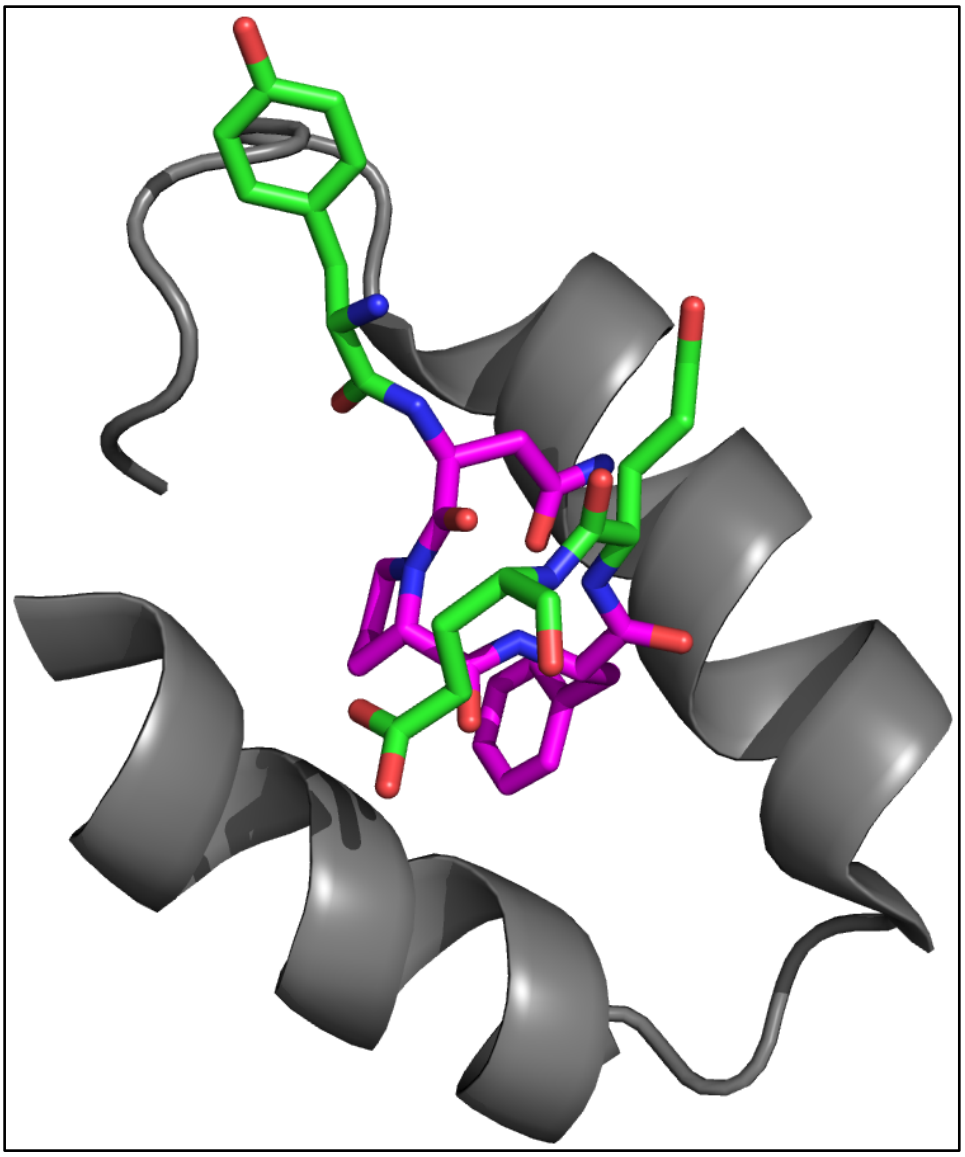

Figure 1.8. An NPF peptide (YNPFEE) in the hydrophobic binding pocket of EHD1 (PBD ID: 2KSP).[60] The NPF motif is shown in magenta, and the flanking residues are shown in green. The peptide binds between helices 2 and 3, shown in grey. The NPF motif forms a type I β-turn when in the binding pocket. The two negatively charged residues C-terminal to the NPF motif form salt bridges with nearby lysines on the EH domain.

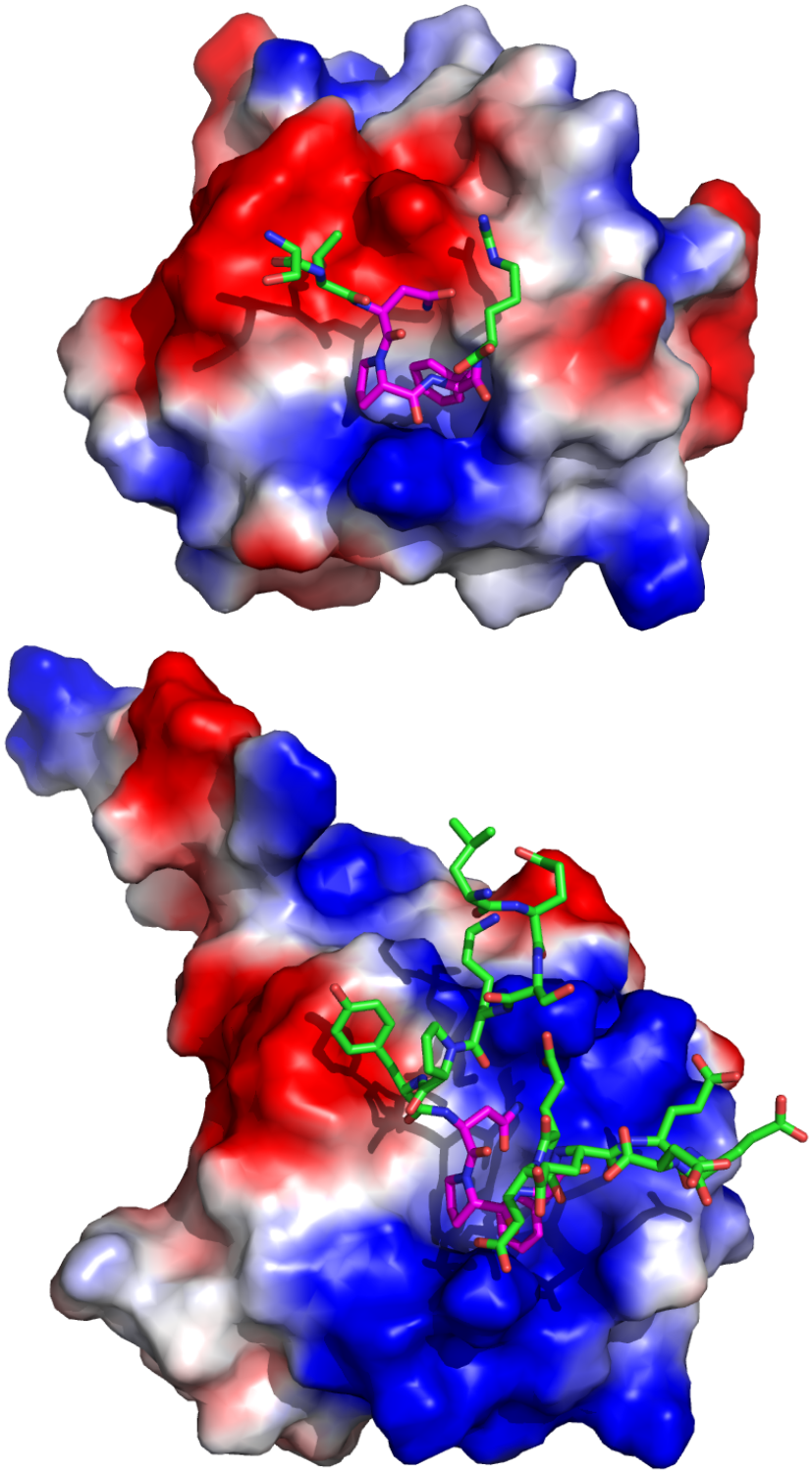

Figure 1.9. The EH domains of Eps15 (top, PBD ID: 1F8H) and EHD1 (bottom, PBD ID: 2KSP), bound to NPF-containing binding partners.[60, 63b] The NPF motif is shown in magenta, and the flanking residues are shown in green. Regions of positive surface potential are displayed in blue, while regions of negative surface potential are displayed in red.

1.8 Existing peptidic ligands of EHD1-EH

Prior to our work in this area, several peptides had already been explored and tested for affinity to EHD1-EH (Table 1.3). Peptides based on known binding partners of EHD1-EH were utilized as tools to better understand the NPF-EH-domain interaction. Sequences from both rabenosyn-5 and Rab11-Fip2 were used as peptides for study of the residues surrounding the binding epitope.[64] With EHD1-EH, the rabenosyn-5-based peptide had a K_d of 18.9 μM, while the Rab11-Fip2-based peptide had a K_d of 145 μM.[64] The sequence of MICAL-L1 was also used to generate a peptide for further study of the NPF interaction with EHD1. The MICAL-L1 peptide had a K_d of 57 μM.[60] Though each of these peptides has a relatively low binding affinity for EHD1-EH, they were useful starting points for the development of EHD1-EH inhibitors.

Some additional peptides that bind EH domains were discovered in studies that searched for higher-affinity ligands. In separate studies, three disulfide-linked NPF peptides were identified as higher affinity ligands (relative to their linear counterparts) for specific EH domains. The first interacted with the first EH domain of intersectin, an N-terminal EH protein involved in endocytosis, with an IC_{50} of 3 μM.[67] Later, a similar strategy was used to develop a ligand for the second EH domain of Eps15, Eps15-EH2.[63b] This ligand was an NPF-containing peptide cyclized via the formation of a disulfide bond. It had 47-fold improved affinity for Eps15-EH2 over its linear counterpart, with a K_d of 12 μM.[63b] The

third example involved a Reps1-EH binding peptide that was initially discovered through yeast two-hybrid screening. Its sequence was further optimized to incorporate cysteine residues and a disulfide crosslink.[68] The resulting cyclic peptide had a similar affinity for the EH domain compared to its linear counterpart (K_d = 45 μM), but a much slower off-rate.[68] Altogether, these three studies suggested that the cyclization of NPF-containing peptides could improve their affinities for their target EH domains, possibly through the stabilization of the β-within the NPF motif.[63b, 67-68]

Peptide Sequence	Targeted EH Domain	K_d (μM)	Experimental Conditions	Refs.
Ac-GPSLNPFDEED-NH_2	EHD1-EH	1.23	25 mM MOPS 1 mM $CaCl_2$ pH = 7.0	[64]
		18.9	25 mM MOPS 1 mM $CaCl_2$ 150 mM KCl pH = 7.0	[64]
Ac-YESTNPFTAK-NH_2	EHD1-EH	151	25 mM MOPS 1 mM $CaCl_2$ pH = 7.0	[64]
		145	25 mM MOPS 1 mM $CaCl_2$ 150 mM KCl pH = 7.0	[64]
NPFEEEEED	EHD1-EH	57	100 mM KCl 20 mM deuterated Tris 2 mM $CaCl_2$ pH = 7.0	[60]
		185	400 mM KCl 20 mM deuterated Tris 2 mM $CaCl_2$ pH = 7.0	[60]
DC*TNPFRSC*WR	Int-EHa	IC_{50} = 3 μM	25 mM Tris•HCl 145 mM NaCl 3 mM KCl pH = 7.5	[67, 69]
SSDC*TNPFRSC*WRS	Eps15-EH2	12	100 mM KCl 20 mM Tris 2 mM $CaCl_2$ pH = 7.0	[63b]
EYEC*TNPFTAKC*	Reps1-EH	65	10 mM NaCl 10 mM Imidazole 2 mM $CaCl_2$ pH = 6.7	[68]

Table 1.3. A collection of known peptidic ligands of EHD1 and known cyclic peptide ligands of EH domain-containing proteins. An asterisk (*) denotes a place where cysteine has been crosslinked to form a disulfide bond.

1.9 Conclusion

This chapter has highlighted the need for inhibitors specific to the long-loop recycling pathway.[1-2] The EH domain of EHD1 presents an attractive opportunity to specifically inhibit long-loop recycling.[38-39] The existing peptidic EH domain ligands demonstrate the feasibility of developing an inhibitor for EHD1-EH.[60, 64] Studies on cyclic peptide EH domain ligands demonstrate a useful strategy for stabilizing the type 1 β-turn.[63b, 67-69] In this thesis, we describe efforts to exploit this strategy to produce improved cyclic peptide inhibitors of EHD1-EH. Ultimately, the development of EHD1 inhibitors would be useful for biological studies that assess the importance of long-loop recycling to cancer metastasis and invasion.

2 Chapter 2. Structured cyclic peptides that target the EH domain of EHD1-EH

2.1 Introduction

Endocytosis and vesicle trafficking are intricate and highly regulated processes.[2] The deregulation of endocytosis and vesicle trafficking is critical for the development of malignant and invasive cancers.[1, 70] An increase in the long-loop recycling pathway is observed in motile cancer cells, where it moves β1-integrins towards the advancing lamellipodium.[1, 70] This change in integrin trafficking enables cancer cell migration; therefore, the proteins involved in the long-loop recycling pathway are potential targets for the prevention of invasion.[7d, 38, 71]

While some chemical tools for altering vesicle trafficking are available, no inhibitor specific to the long-loop recycling pathway has been found to date.[19c, 20, 71-72] The protein-protein interaction domain known as the EH domain (epidermal growth factor receptor tyrosine kinase substrate 15, or Eps15, homology domain) has been found in several proteins associated with endocytosis and vesicle trafficking, including long-loop recycling.[28b] Selective inhibitors of EH domains would thus be a novel way to target long-loop recycling in an effort to block cancer cell invasion.[28b, 32b]

The EH domain is named for Eps15, the protein in which it was initially discovered.[29, 39a] EH domains are about 100 amino acids in length, have a high degree of sequence homology, and consist of two calcium-binding helix-loop-helix motifs connected by an anti-parallel β-sheet.[28b, 58, 63a, 73] EH domain-containing proteins can be divided into two groups: those with N-terminal EH domains and those with C-terminal EH domains.[28b, 33] Proteins from both categories function as scaffolding and adaptor proteins for vesicle trafficking.[33-34] Proteins with N-terminal EH domains, such as Eps15, are primarily involved with endocytosis while proteins with C-terminal EH domains are more involved in intracellular vesicular transport.[28b, 33-34] One such protein, EH-domain-containing protein 1 (EHD1), is involved in long-loop endocytic recycling and retrograde transport.[36a] Genetic knockdown of EHD1 prevents recycling of β1 integrin to the plasma membrane, which demonstrates the protein's importance to the recycling pathway.[33, 36a, 38, 42] The deregulation of EHD1 has been implicated in cancer metastasis.[32b] Furthermore, inhibition of vesicle-trafficking proteins may inhibit tumor cell invasion; therefore, this protein is an ideal target to probe the effects of vesicle trafficking on cancer cell proliferation.[16, 32b]

The structures and sequences of known EHD1 binding partners have been studied.[33] The majority of these EHD1 effectors, which are also involved in regulating endocytosis, interact with EH domains through a common asparagine-proline-phenylalanine (NPF) motif.[36a, 40b, 51, 53b, 62, 74] This motif binds in a hydrophobic pocket between helices 2 and 3, and complex formation does little to

change the structure of the EH domain .[60, 63a] When in the binding pocket, the NPF motif forms a type 1 β-turn stabilized by an internal hydrogen bond between the carbonyl oxygen of the asparagine side-chain and the amide proton of residue C-terminal to the phenylalanine.[59-60, 63]

The sequences of some NPF-containing proteins have been further examined to investigate their selectivity for C-terminal EH-domains over N-terminal EH domains.[33] Proteins known to interact with EHD1 typically contain negatively charged residues C-terminal to the NPF sequence, and these sequences bind to C-terminal EH domains more tightly than those flanked by other residues.[33, 60, 64] The naturally-occurring EHD1 binding partners with negatively charged side-chains, such as MICAL-L1 and Rabenosyn-5, are thought to be better able to displace the water molecules adhering to the area surrounding the solvent-accessible binding pocket, which has positive surface potential.[33, 40b, 58, 64] The first two negatively charged residues following the NPF motif form salt bridges with two lysine residues adjacent to the binding pocket.[60] For this reason, C-terminal EH domains have higher affinity for peptides with negatively charged residues following the NPF motif.[64] This specificity is not observed for N-terminal EH domains because these domains have negative surface potential. Thus, the incorporation of negatively charged residues is a potential method to control selectivity for peptide ligands binding to C-terminal EH domains.[59, 63b]

Previous attempts to identify peptide and protein binding partners of EH domains have utilized yeast two-hybrid screens, phage-display selections, and pull-down assays.[40, 62] However, all identified EHD1-EH binding partners are relatively low-affinity, with K_d values no lower than 18 μM under physiological salt conditions (Table 1.2).[64] In this chapter, we describe the development of a new cyclic peptide inhibitor of the EHD1 EH domain (EHD1-EH) with a lower K_d. An NMR solution structure and docked model of the cyclic peptide bound to EHD1-EH provide a promising starting point for further ligand design. These novel inhibitors were also used as the basis of a fluorescence polarization assay suitable for screening for EH domain inhibitors.

2.2 Cyclic peptides as a tool to target protein-protein interactions

Conformationally constrained peptides have long been used as a method to target protein-protein interactions.[75] They make particularly attractive candidates for inhibitor design as they can be designed to incorporate the exact binding epitope for the target protein. Cyclizing a peptide is advantageous because it can result in molecules with improved cell penetration, proteolytic stability, target affinity and selectivity.[75]

Our group chose to make cyclic peptides to target EHD1-EH, with the long-term goal of generating cell-penetrant inhibitors capable of blocking EHD1 function in live cells. Cyclic peptides often have advantages in cell permeability over their

linear analogs.[76] The linkage of the N and C termini generates a peptide with fewer degrees of freedom, which can stabilize the peptide's structure. For instance, the incorporation and stabilization of a β-turn, such as the NPF motif, within a cyclic peptide was shown to improve a peptide's cell-penetrating abilities.[76-77] The underlying cause of this improvement appears to be the desolvation of backbone hydrogen bond donors and acceptors by the cyclic peptide structure.[76, 78] By producing cyclic analogs of EHD1-EH ligands, we sought to use these principlates to design peptidic inhibitors with greater likelihood of penetrating cell membranes.

We were also looking to design peptides with increased proteolytic stability.[79] Cyclic peptides are more proteolytically stable than their linear counterparts due to their locked conformations. The free N- and C-termini of linear peptides are targeted by exoproteases, and head-to-tail cyclization removes this liability.[80] Thus, we designed our first round of inhibitors as backbone macrocyclic peptides to improve their proteolytic stability.

Lastly, conformational restriction can be another advantage in targeting protein-protein interactions because it can lead to better affinity and target selectivity. The incorporation of a binding epitope, particularly one that takes on the structure of a loop when in the binding pocket of its target, into a cyclic peptide forces the sequence into its natural binding conformation.[78a, 81] The binding epitope of a cyclic peptide is pre-organized into a complimentary shape to fit in the binding

cavity.[81-82] The number of conformations available to a cyclized peptide is reduced relative to its linear counterpart, which may promote the formation of the desired structure in solution.[83] This pre-organization of the desired binding epitope may alter the entropic cost of binding, either through the peptide structure or the organization of water molecules surrounding the binding pocket, and thus lead to improved target affinity.[84] In the case of the NPF-EH domain interaction, the conformational constraints of a backbone macrocyclic peptide have been designed to hold the binding motif, NPF, in the shape in which it exists in the hydrophobic binding pocket.[59]

2.3 Cyclization improves the affinity of NPF-containing peptides for EHD1-EH

We chose to develop cyclic peptides as EH domain ligands, hypothesizing that cyclization would stabilize the β-turn and pre-organize the binding epitope.[78a] Cyclic NPF peptides were briefly explored in the context of N-terminal EH domain-containing proteins.[63b, 67-68] Despite their negative charge, cyclic peptides presented an opportunity to develop ligands with greater cell-penetrating capabilities and proteolytic resistance than their linear counterparts.[78a, 85] The consensus sequence among these ligands shows two or more negatively charged residues following the NPF motif.[33, 60, 64] We also incorporated a tyrosine immediately preceding the NPF motif for the spectrophotometric determination of the concentration of peptide, since tyrosine can be found in that position in some

EHD1 binding partners.[33] Our initial cyclic inhibitor, cNPF1, consisted of a head-to-tail cyclic peptide with the sequence YNPFEEGG (Figure 2.2). Two glycine residues were added to serve as a flexible cyclization linker. A linear peptide with the same sequence was synthesized as a control to directly assess the effects of cyclization (Figure 2.2).

Previously, ITC or NMR were used to determine peptide-EH domain dissociation constants, and these experiments were typically performed using low-NaCl or no-NaCl conditions to promote higher affinity.[60, 64] In line with these prior reports, we first analyzed ligand binding to EHD1-EH by ITC (Figure 2.3) with no NaCl, and then repeated the experiments under low-salt (15 mM NaCl) and physiological salt (150 mM NaCl) conditions. At 150 mM NaCl, the linear control had a dissociation constant (K_d) of 35.7 ± 3.7 μM, while cNPF1 had a K_d of 9.9 ± 0.8 μM (Table 1). The fourfold improvement in K_d value was consistent across the different salt conditions, which suggested that the effects of cyclization were charge-independent. This is consistent with cyclization promoting a conformation of the NPF that is favorable for EHD1-EH binding.

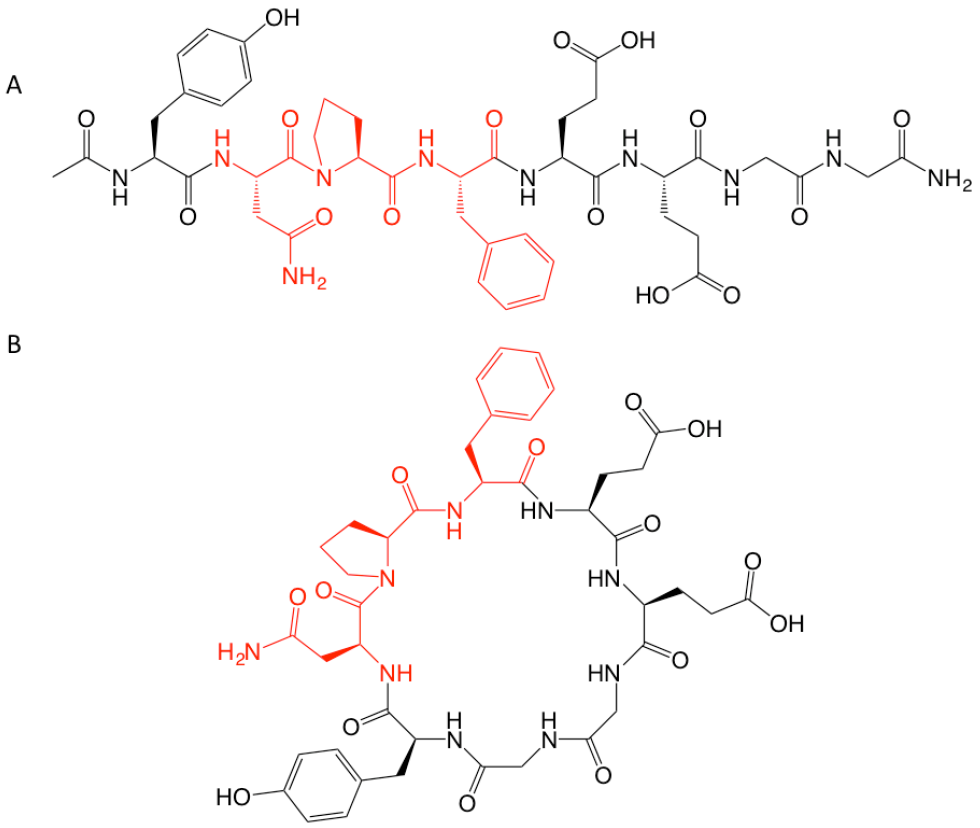

Figure 2.1. (A) The linear NPF peptide. The N-terminus was acetylated and the C-terminus was amidated to keep the same number of charges as cNPF1. (B) The head-to-tail cyclic peptide cNPF1. The NPF sequence is highlighted in red.

The improvement in binding affinity was largely due to more favorable enthalpy for the cyclic peptide (Table 2.1). Interestingly, the change in entropy (ΔS) of the linear peptide, observed by ITC, was more thermodynamically favorable than that of cNPF1 at lower salt concentrations. The relative entropic penalty observed for cNPF1 has been seen in other cyclic molecules designed to target other proteins; evidently, the preorganization of a binding epitope does not always result in entropically favored protein-ligand interactions.[82b, 82c, 86] Overall, results from ITC binding experiments indicated that the NPF motif and flanking residues are able to make enthalpically favorable contacts with EHD1-EH within the context of a cyclic scaffold.

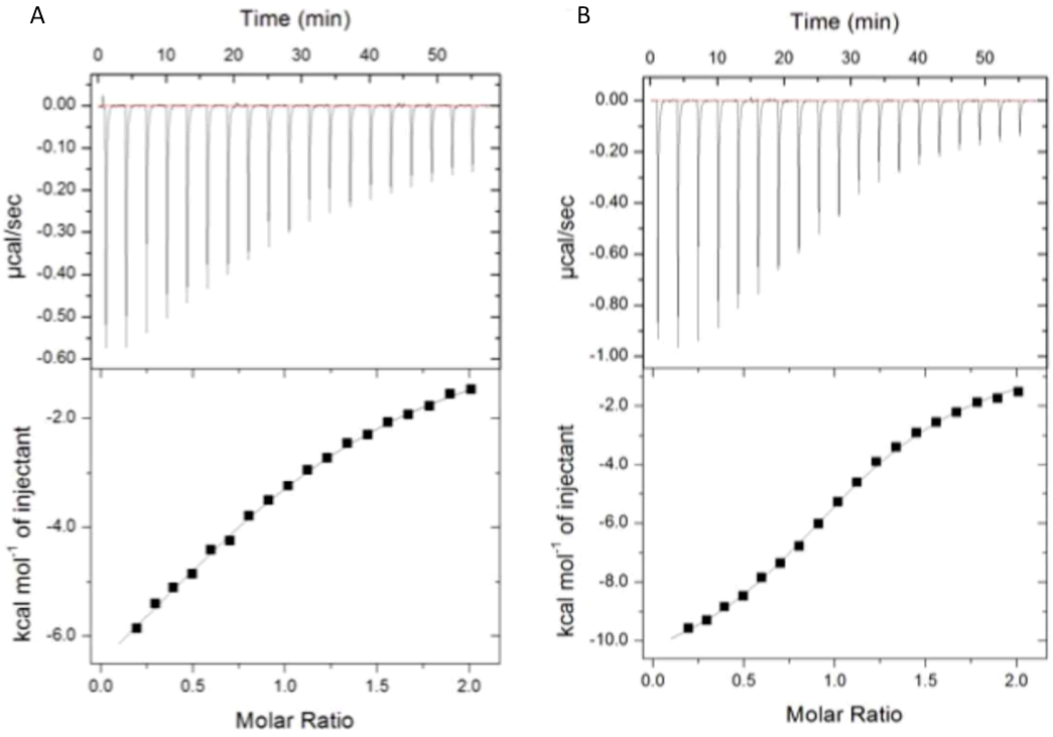

Figure 2.2. Raw ITC data from a representative experiment for the linear NPF (A) and cNPF1 (B) respectively. Both representative experiments were run in 25 mM MOPS (pH 6.8), 1 mM $CaCl_2$, and 150 mM NaCl at a temperature of 20°C. The experiments under each salt condition were performed in triplicate, with each experiment done on a different day.

Table 2.1. Binding data obtained for Linear and Cyclic Inhibitors of EHD1-EH		
	Linear NPF	cNPF1
Sequence	Ac-YNPFEEGG-$CONH_2$	-YNPFEEGG-
K_d (μM) 0 mM NaCl	5.6 ± 0.6	1.6 ± 0.3
ΔH (cal/mol) 0 mM NaCl	-9900 ± 190	-11800 ± 130
TΔS (cal/mol) 0 mM NaCl	-2,600 ± 160	-3,700 ± 220
K_d (μM) 15 mM NaCl	9.4 ± 1.2	2.5 ± 0.5
ΔH (cal/mol) 15 mM NaCl	-9340 ± 490	-11700 ± 880
TΔS (cal/mol) 15 mM NaCl	-2,500 ± 550	-3,900 ± 900
K_d (μM) 150 mM NaCl	35.7 ± 3.7	9.9 ± 0.8
ΔH (cal/mol) 150 mM NaCl	-11100 ± 1220	-11900 ± 100
TΔS (cal/mol) 150 mM NaCl	-4,800 ± 1400	-4,800 ± 100

These values were averages and standard deviations of three independent experiments.

2.4 Fluorescence polarization assay to identify EHD1-EH inhibitors

While ITC provides a great deal of data, it requires high concentrations of materials and time-consuming dialysis steps. To develop a more rapid and convenient assay for the discovery of EHD1-EH inhibitors, we modified cNPF1 with fluorescein to monitor direct EHD1-EH binding using fluorescence polarization (FP). Specifically, one glycine in the linker was replaced with lysine, and the lysine amine was conjugated to fluorescein on resin to generate cNPF1^{Flu} (Table 2.2, Scheme 2.2). We also synthesized a linear control, Lin^{Flu}, which consisted of the YNPFEE sequence conjugated to fluorescein with a linker of two β-alanine residues.

FP direct binding assays were performed with each probe, and the experiments were initially conducted with 15 mM NaCl to determine the binding affinity of each probe under low-salt conditions (Figure 2.3-4). We repeated the assays at 150 mM NaCl to determine affinities under physiological salt conditions.[87] We anticipated a lower target affinity under these higher salt concentrations due to the screening of the charges relevant for EH domain binding.[60, 64] In 15 mM NaCl, cNPF1^{Flu} had a K_d of 3.4 ± 0.4 μM, and the linear probe had a K_d of 7.2 ± 0.7 μM. In 150 mM NaCl, cNPF1^{Flu} had a K_d of 20.8 ± 2.9 μM, and the linear probe had a K_d of 48.0 ± 6.1 μM. At 150 mM NaCl, the FP values did not saturate at the highest protein concentration tested. Normally, this would make curve fitting challenging, since it would be difficult to determine the upper bound (the value

which corresponds to probe 100% bound to protein). To more accurately fit binding curves to the data at physiological salt, we used the upper bounds from curve fits to data obtained at 15 mM NaCl. All probes bound with a poorer affinity at higher salt concentrations, confirming the importance of electrostatic interactions surrounding the binding pocket. Under both conditions cNPF1^{Flu} bound more tightly than the linear probe. These data confirmed the findings from the ITC data that cyclization improved affinity for EHD1-EH.

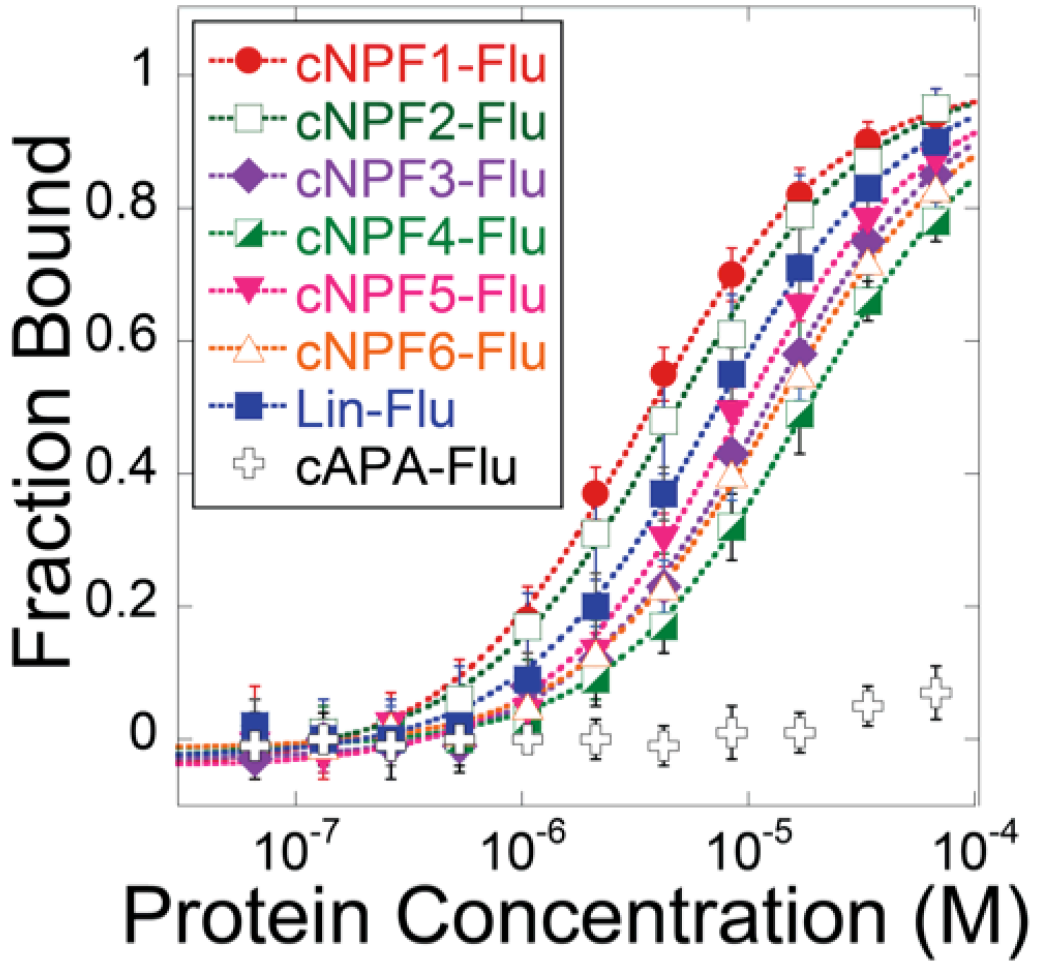

Figure 2.3. Representative FP direct binding assays of peptide ligands of EHD1-EH under low-salt conditions (15 mM NaCl). Probes were tested at 100 nM. The lines are curve fits of Equation 2.1. Error bars represent standard deviation from three independent experiments, each of which was an average of three technical replicates. cAPA served as a negative control to verify that the NPF motif was necessary for the observed binding.

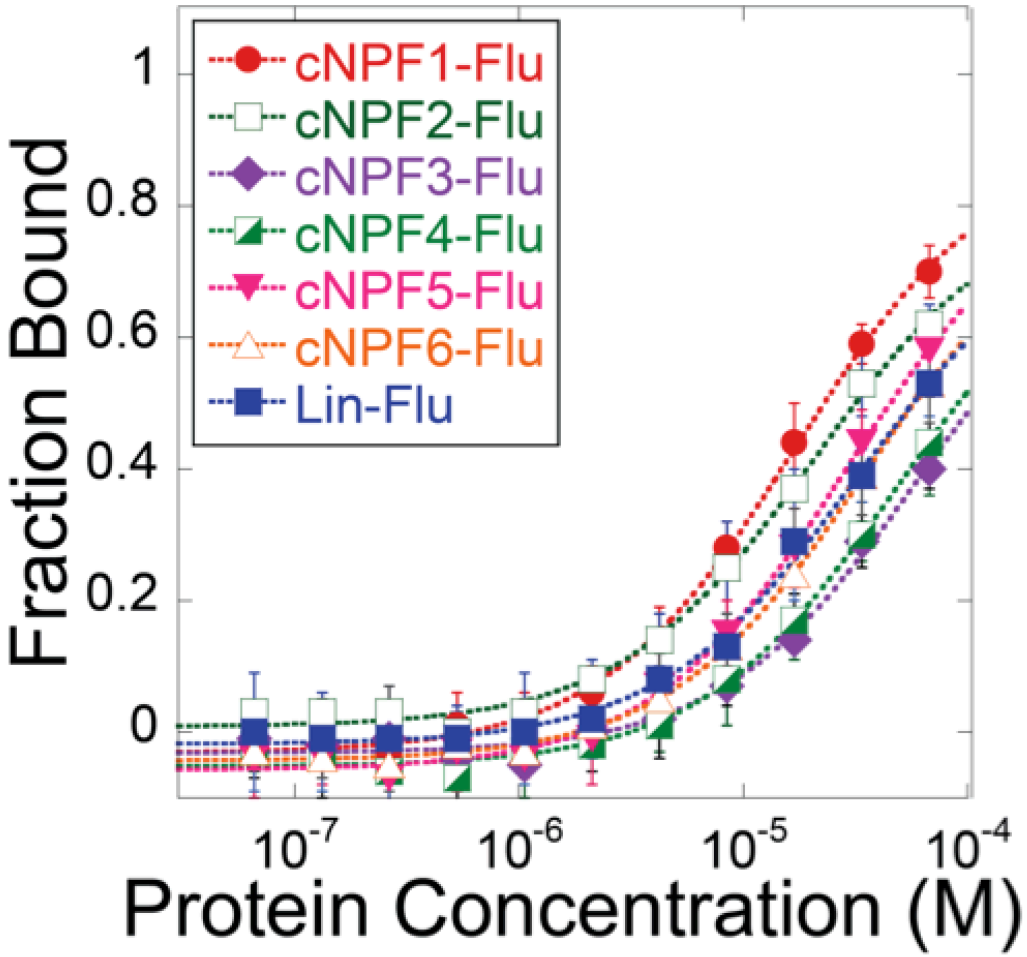

Figure 2.4. Representative FP direct binding assays of peptide ligands of EHD1-EH under physiological salt conditions (150 mM NaCl). Probes were tested at 100 nM. The lines are curve fits of Equation 2.1. Error bars represent standard deviation from three independent experiments, each of which was an average of three technical replicates.

2.5 Optimizing a Cyclic Peptide Scaffold for the NPF motif

For macrocyclic protein ligands, macrocycle size and conformation can have large effects on binding affinity.[81, 88] Therefore, we varied the glycine residue to observe effects of varying linker length (Table 2.2, Figure 2.4), and performed direct binding assays at both 15 and 150 mM NaCl. cNPF3^{Flu} omitted the glycine, decreasing the linker length. This resulted in a K_d of 83.8 ± 4.2 μM, which is fourfold greater than cNPF1^{Flu}. It is possible that the smaller macrocycle size destabilized the β-turn of the NPF motif. By contrast, an increase in the macrocycle length had little effect on binding affinity. cNPF2^{Flu} incorporated a longer linker, γ-aminobutyric acid in place of glycine, which brought the macrocycle length up to 26 atoms. cNPF2^{Flu} bound EHD1-EH with a Kd of 4.8 ± 1.1 μM, which is similar to the affinity of cNPF1^{Flu}. Of the cyclic peptides tested here, those with a macrocycle of 24 atoms or more had a greater affinity for EHD1-EH; however, further testing is needed to fully support this conclusion.

Table 2.2. Binding data obtained for each probe of EHD1-EH

Peptide	Sequence	Macrocycle Length[a]	K_d (μM) 15 mM NaCl	K_d (μM) 150 mM NaCl
Lin NPF (FAM)	(FAM)-βAla-βAla-YNPFEE-$CONH_2$	N/A	7.2 ± 0.7	48.0 ± 6.1
$cNPF1^{Flu}$	-YNPFEEGK(FAM)-	24	3.4 ± 0.4	20.8 ± 2.9
$cNPF2^{Flu}$	-YNPFEE-GABA-K(FAM)-	26	4.8 ± 1.1	28.5 ± 9.7
$cNPF3^{Flu}$	-YNPFEEK(FAM)-	22	11.7 ± 0.9	83.8 ± 4.2
$cNPF4^{Flu}$	-YNPFAEGK(FAM)-	24	18.5 ± 2.8	67.7 ± 11.0
$cNPF5^{Flu}$	-YNPFEAGK(FAM)-	24	9.0 ± 0.6	35.1 ± 2.3
$cNPF6^{Flu}$	-YNPFEQGK(FAM)-	24	12.5 ± 2.6	47.8 ± 5.4
$cAPA^{Flu}$	-YAPAEEGK(FAM)-	24	> 70	N/A

[a] Macrocycle length is given in number of atoms.

Errors are given as standard deviations of three experiments, each performed in triplicate.

2.6 Selectivity for C-terminal EH domain-containing proteins

The presence of negatively charged residues C-terminal to the NPF motif was reported to confer selective binding to C-terminal EH domain-containing proteins.[33, 60, 64] We incorporated the two glutamic acid residues in our peptides to promote selectivity for C-terminal EH-domain containing proteins, such as EHD1, over N-terminal EH-domain containing proteins.[28b, 60] As an initial test of selectivity, we measured the binding affinity of cNPF1^{Flu} and Lin^{Flu} for the second EH domain of Eps15 (Eps15-EH2), an N-terminal EH domain-containing protein (Figure 2.5). Even under low-salt conditions, these probes were unable to bind Eps15-EH2. We have reported the production of Eps15-EH2 before, and CD spectroscopy was used to confirm the protein was properly folded. (Figure 2.6). Thus, we concluded that the cyclic peptide was selective for EHD1-EH over Eps15-EH2.

We also demonstrated that the NPF motif was necessary for EHD1-EH binding. We synthesized the peptide cAPA^{Flu} to serve as a negative control for our direct binding experiments (Table 2.2, Figure 2.3). We altered the sequence to ensure that binding was due to the NPF motif, and not due to non-specific electrostatic interactions.[60, 64] When we tested this peptide in a direct binding assay with EHD1-EH, it showed no binding (Figure 2.3). Therefore, we concluded that the NPF motif was required for EH domain binding, and the detected interactions were likely to be specific to the NPF-binding pocket.

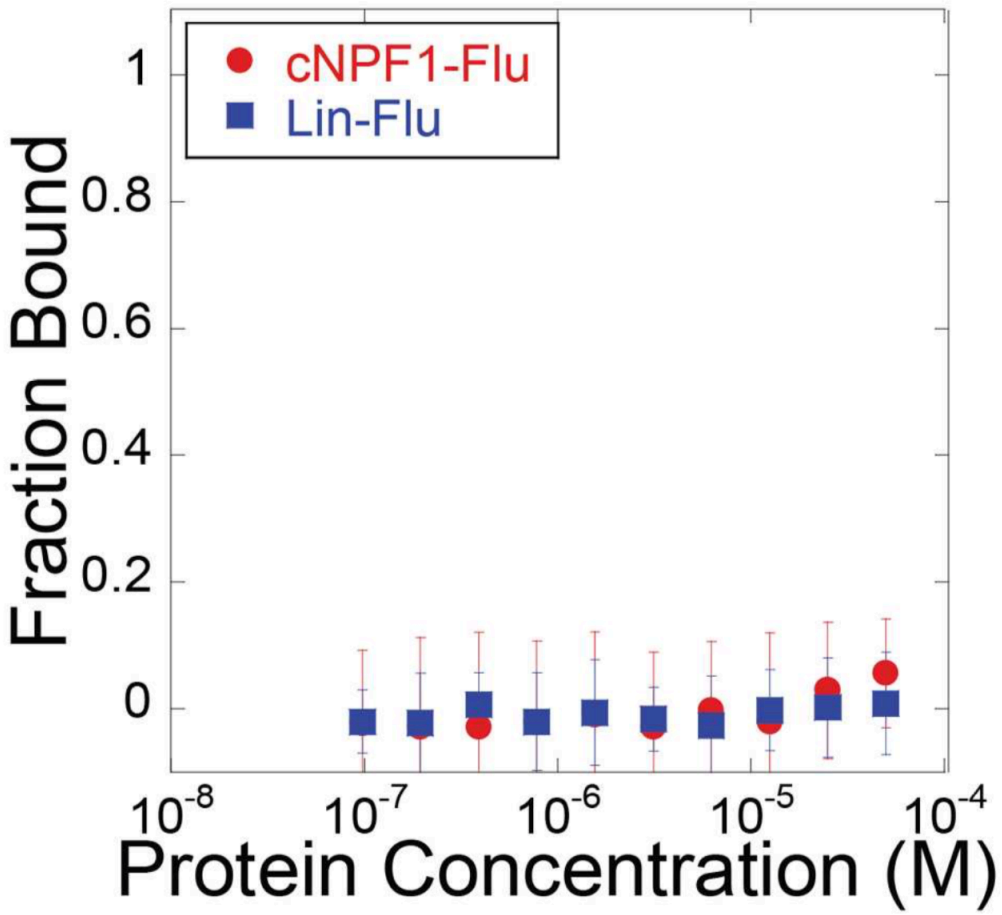

Figure 2.5. FP direct binding experiments of linear and cyclic peptides with Eps15-EH2 to measure selectivity. A 100 nM concentration of probe was used. The experiments were performed in 1 mM DL-dithiothreitol to ensure that Eps15-EH2 was properly folded, with all cysteine side chains reduced.

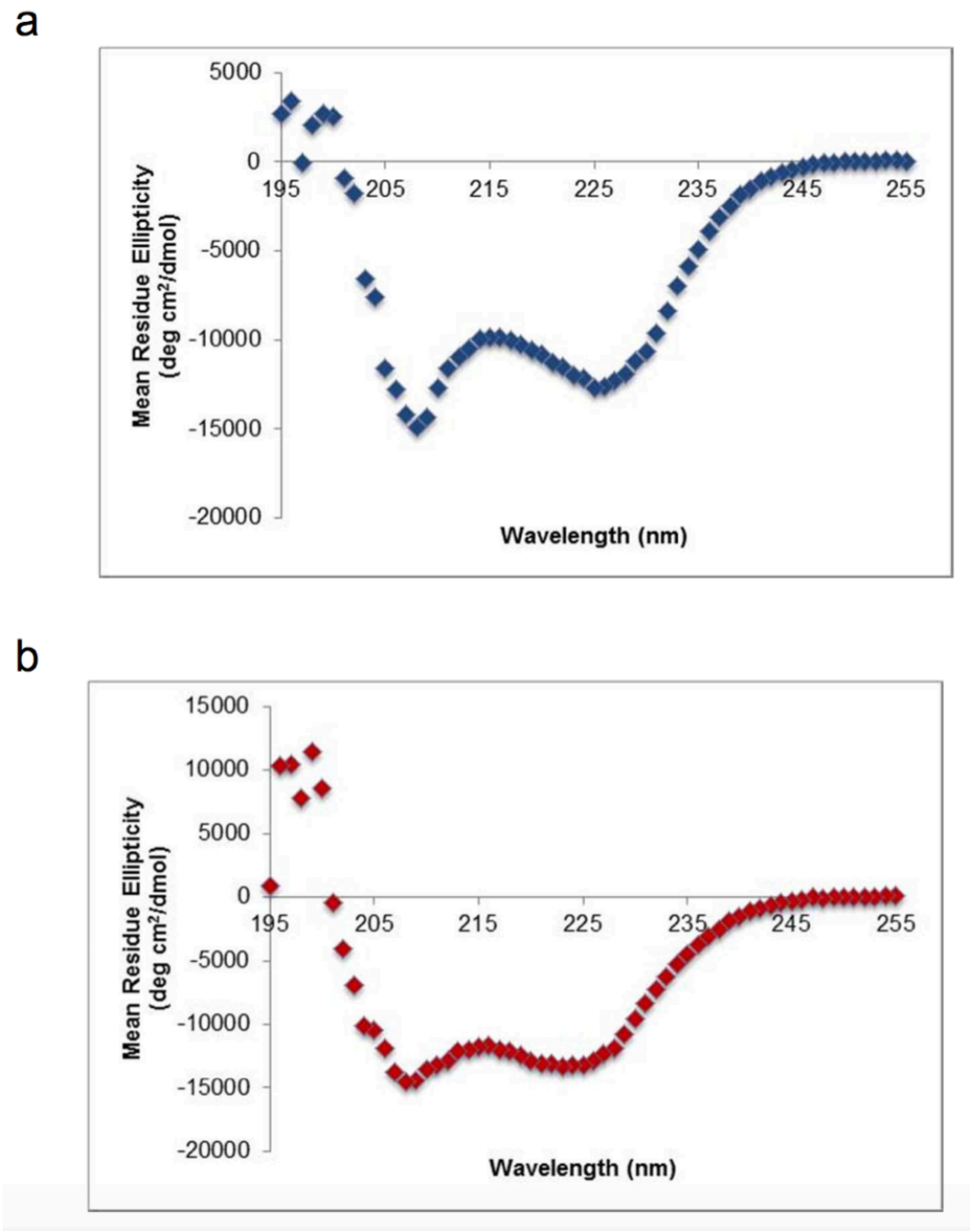

Figure 2.6. CD spectra of EHD1-EH (a) and Eps15-EH2 (b). The spectra for both proteins are consistent with predominantly alpha-helical secondary structure, as expected for EH domains. These results indicate that the proteins were properly folded, and that lack of binding affinity for Eps15-EH2 by cNPF1^{Flu} results from genuine selectivity among EH domains. These experiments were performed by Dr. Robyn Eisert.

2.7 The requirement for negatively charged residues

In the case of cNPF1^{Flu}, we were interested in probing the importance of each negatively charged residue, with the goal of pre-emptively improving the peptide's potential cell-penetrating capabilities. Replacement of either glutamate with alanine resulted in weaker affinity compared to cNPF1^{Flu}, especially replacement of the glutamate immediately adjacent to the NPF motif (Table 2.2, Figure 2.3). These effects matched trends observed for linear peptides.[60, 64]

Replacement of the second glutamate with glutamine (cNPF6^{Flu}) provided an uncharged side chain in this position while roughly maintaining the shape and size of the original residue. cNPF6^{Flu} displayed reduced binding affinity by roughly four-fold, a more dramatic change than replacement with alanine. Though cNPF1^{Flu} was the higher-affinity ligand, cNPF5^{Flu} and cNPF6^{Flu} were ligands with an affinity comparable to the linear NPF peptide, with less overall negative charge. We concluded that cNPF1^{Flu}, cNPF5^{Flu} and cNPF6^{Flu} could be useful starting points for the development of cell-penetrant EH domain inhibitors.

2.8 Implementation of the fluorescence polarization competitive binding assay

We then used the highest-affinity cyclic peptide probe, cNPF1^{Flu}, in a fluorescence polarization-based competitive binding assay to screen for better inhibitors of C-terminal EH domain-containing proteins. Notably, this was the first assay of its kind for an EH domain. The assay was tested with high- and low-affinity inhibitors to establish its suitability for future screens (Table 2.3).

The original cyclic peptide, cNPF1, was a stronger inhibitor in this FP competition assay than the linear control (Figure 2.7). This data corroborated with the binding affinities observed by ITC and direct binding FP experiments. We also tested an analog of cNPF1^{Flu} without the conjugated fluorescein (cNPF1B). This peptide was identical to cNPF1^{Flu}, except the lysine had been acetylated instead of fluoresceinated. This peptide was tested to determine the effect of incorporating an acylated lysine in this position. A twofold decrease in the half-maximal inhibitory concentration (IC_{50}) was observed in comparison to cNPF1. The different IC_{50} values of cNPF1 and cNPF1B explained the change in K_d value between cNPF1 and cNPF1^{Flu}; the altered linker used to attach the fluorophore reduced EH-domain binding affinity roughly two-fold. This implied that the affinity of cNPF1^{Flu} could be improved by altering the length and placement of the fluorescein. However, cNPF1^{Flu} had sufficient affinity for

competitive binding experiments, so we did not improve the affinity of cNPF1^{Flu} at this time.

In order to demonstrate the usefulness of the assay, we tested a few existing EHD1-EH lignds. We tested cNPF4^{Flu} without fluorescein (cNPF4) and cAPA as negative controls (Figure 2.7). cNPF4 displayed a weaker inhibition of EHD1-EH, in agreement with the relatively weaker binding of cNPF4^{Flu} in direct binding assays. No inhibition of EHD1-EH was detected with cAPA. The results of these experiments established that we had successfully developed an assay to search for better inhibitors of EHD1-EH.

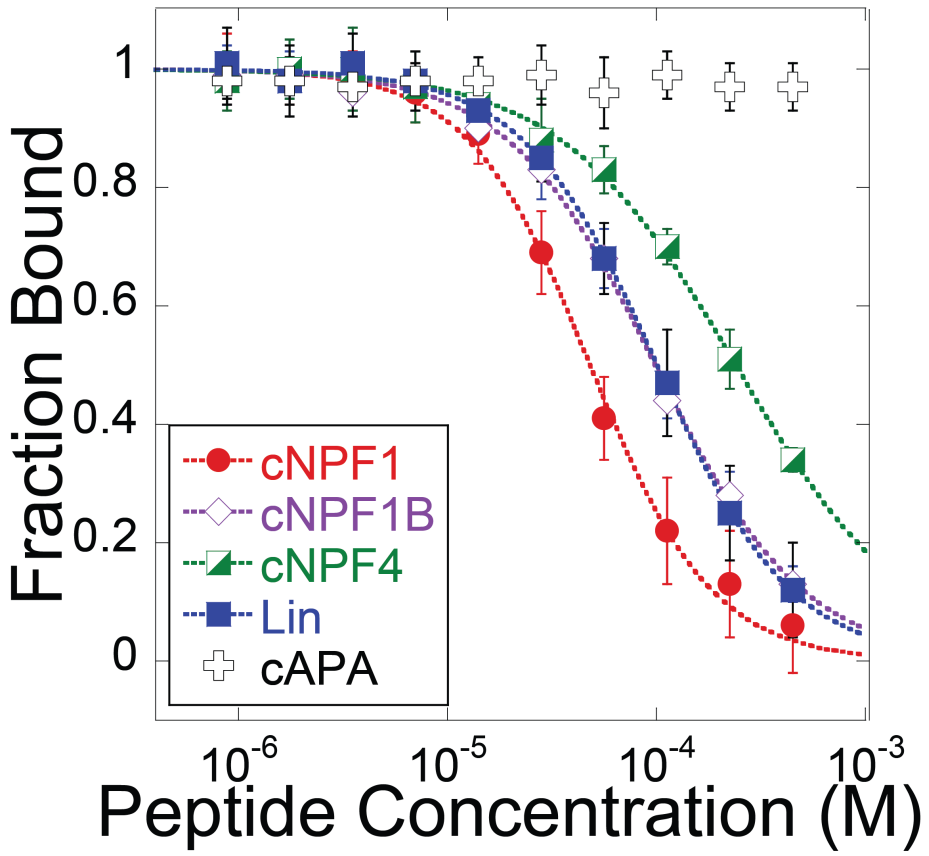

Figure 2.7. FP competitive binding assays of various peptides using cNPF1^{Flu} as a fluorescent probe. The experiments were done in 25 mM MOPS, pH = 6.8, with 15 mM NaCl, using 100 nM cNPF1^{Flu} and 20 μM EHD1-EH. The lower salt conditions were used to reduce the amount of material needed. cNPF1 showed the most potent inhibition, and cAPA served as a negative control. The lines represent curve fits to equation 2.3. Error bars represent standard deviation from three independent experiments, each of which was an average of three technical replicates.

Table 2.3. Competitive binding assay data using $cNPF1^{Flu}$ as a fluorescent probe.

Peptide	Sequence	IC_{50} (μM)
Linear	Ac-YNPFEEGG-$CONH_2$	107 ± 1
cNPF1	-YNPFEEGG-	49.2 ± 0.2
cNPF1B	-YNPFEEGK(Ac)-	100 ± 1
cNPF4	-YNPFAEGG-	240 ± 1
cAPA	-YAPAEEGG-	> 450

Error is standard deviation from three independent experiments, each of which was an average of three technical replicates. IC_{50} values were calculated from curve fits to equation 2.3.

2.9 Solution structure of cNPF1 ligand

Several structures of EH domains, some complexed to NPF-containing ligands, have been determined by NMR.[58-60] We sought to solve the structure of cNPF1 to ascertain whether the incorporation of the NPF motif into a cyclic peptide biased the structure towards the formation of the desired β-turn. We worked with Tiffany Corlin and Dr. Jim Baleja at the Tufts Sackler School to collect these data. The NMR spectra were taken on a Bruker Avance 600 MHz spectrometer. Spectra for each peptide were taken in 10% D_2O, 10 mM deuterated imidazole, 10 mM NaCl, 10 mM 4,4-dimethyl-4-silapentane-1-sulfonic acid and 0.02% NaN_3 adjusted to a pH between 5.6 and 5.9. The linear NPF peptide and cNPF1 were at a concentration of 1.2 mM and 4.9 mM, respectively. The concentrations were determined by absorbance at 274 nm with an extinction coefficient of 1280 $M^{-1}cm^{-1}$. Spectra were taken with a mixing time of 200 ms at 5°C. Assignment, simulated annealing, and structure refinement were performed by Tiffany Corlin and Dr. Jim Baleja, and are reported in the published work.[89]

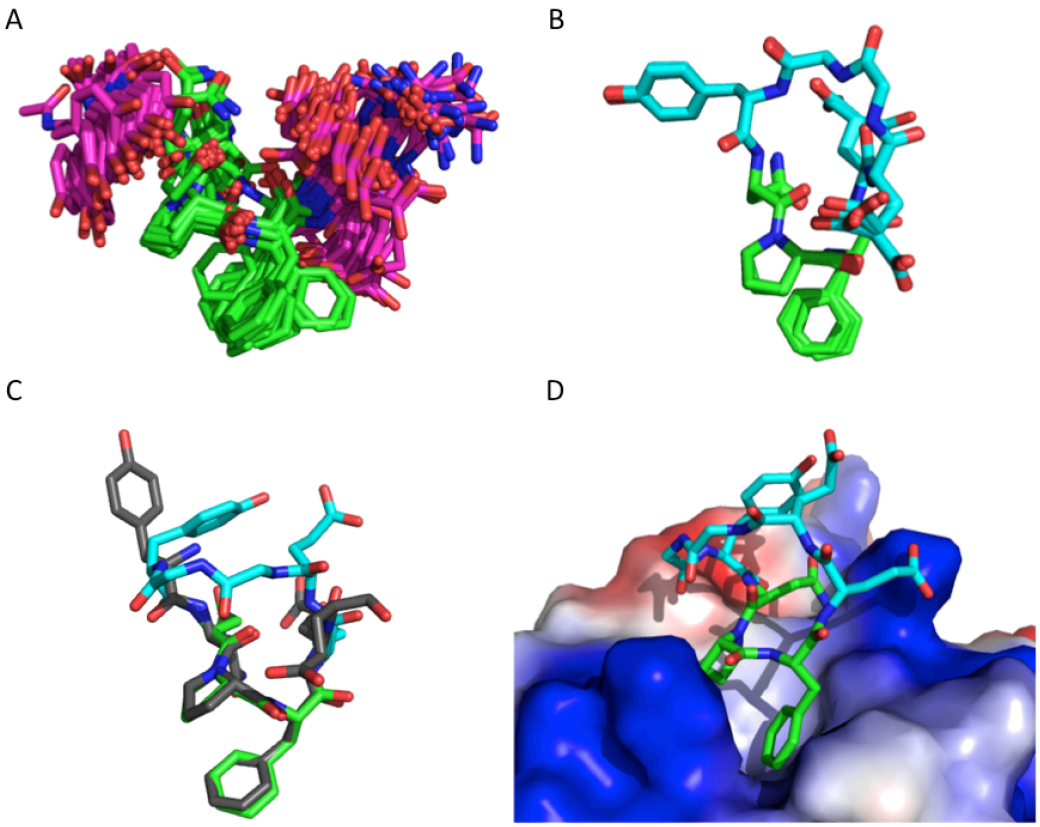

Figure 2.8. The solution structures of linear NPF (A) and cNPF1 (B). (C) The backbone of the NPFE of cNPF1 was pair-fitted using PyMOL to the corresponding atoms in the peptide YNPFEE, in its EHD1-EH-bound conformation (PDB ID : 2KSP).[60, 90] cNPF1 is shown in teal with a bright green NPF motif, while YNPFEE is shown in grey. The backbone atoms of the NPFE portion of the sequences had an RMSD of 0.333 Å. (D) cNPF1 overlaid with YNPFEE in the binding pocket of EHD1-EH (PDB ID : 2KSP).[60] All NMR spectra were taken by Tiffany Corlin.

Linear eight-residue peptides are rarely well-structured. As expected, the linear control was less structured in aqueous solution when in comparison with the cyclic peptide (Figure 2.8A). cNPF1 adopts a well-structured conformation in aqueous solution (Figure 2.8B). Strikingly, the NPF motif in cNPF1 forms a β-turn nearly identical to the turn observed in linear NPF peptides bound to EH domains.[60] When superimposed with a previously determined structure of an NPF/EHD1-EH complex, the backbone of cNPF1 overlays with the NPFE sequence of the ligand with a root mean squared deviation (RMSD) of 0.333 Å (Figure 2.8C).[60] We concluded that the NPFE region of cNPF1 adopts a structure similar to the corresponding motif of linear peptides bound to EH domains (Figure 7D).[60]

2.10 Conclusion

We applied our understanding of the NPF – EH domain interaction to the design of conformationally constrained, cyclic peptides as inhibitors. The improvements in binding associated with cyclization were enthalpy-driven, implying that cNPF1 makes more favorable contacts with EHD1-EH compared to the linear peptide. [60, 63b]

We also reported the first fluorescence-based assay for EH domain-ligand interactions. The K_d values obtained from these binding assays correlated with those obtained by ITC. Although the addition of the fluorophore slightly impeded

EH-domain binding, the target affinity of cNPF1^{Flu} was still strong enough to use it as a probe for a FP competition assay. We also established that the length of the linker for the backbone-cyclic peptide did not impact the probes' affinity for EHD1-EH within the macrocycles we explored. Cyclization overall improved the K_d value roughly two-fold. cNPF1^{Flu} was then used in a competition FP assay to demonstrate the first low-volume assay for EH domain inhibitors. When applied to a high-throughput screen, this new assay will enable the discovery of inhibitors of EHD1-EH and other EH domains.

Finally, we reported initial structure-activity relationships and a solution structure of the most promising cyclic peptide inhibitor, cNPF1. A model of cNPF1/EHD1-EH binding, informed by the solution structure of cNPF1, is shown in Figure 2.8D. These data will fuel additional rational design of EH domain inhibitors, including constrained peptides and peptidomimetics. Ultimately, the development of cell-penetrant analogs of cNPF1 would allow pharmacological investigation of EHD1's roles in vesicle trafficking and its importance in cancer invasion and metastasis.

2.11 Materials and methods

2.11.1 Preparation of EH-domain containing proteins

The EH domains were prepared from plasmids encoding the EH domains of EHD1 and Eps15, which were generous gifts from Dr. Jim Baleja (Sackler School of Graduate Biomedical Sciences, Tufts University, Boston, MA, USA). The EH domains were expressed in BL21 cells, using standard techniques, as glutathione S-transferase (GST) fusions for subsequent purification on a glutathione-agarose column (Gold Biotechnology).[64, 91] Protein expression was induced with 0.35 mM IPTG. A 4L culture of cells was lysed by sonication in 25 mM imidazole (pH 7.0), 150 mM NaCl, benzonase, and 100 μM $CaCl_2$. 1 mM DTT, 1 mM PMSF and an EDTA-free protease inhibitor pellet were added immediately prior to lysis. The cell lysate was then centrifuged at 14,000 rpm to remove excess material, and the clear cell lysate was added to the glutathione-agarose column and mixed for 2 hours at 4°C. Approximately 4 mL of glutathione agarose was used per liter of culture. Excess lysate was then washed away, and the column was equilibrated in thrombin cleavage buffer: 50 mM Tris HCl (pH 8.0), 150 mM CaCl, and 2.5 mM $CaCl_2$. The EH domains were cleaved from the GST, and the glutathione-agarose column with thrombin (Sigma Aldrich). 100 units of thrombin were added per liter of culture, and the thrombin cleavage proceeded overnight at 4°C. The elution volume was kept to ½ the volume of the column or less to increase the concentration of cleaved protein. The fractions eluted off of the glutathione

agarose were then run through a benzamidine agarose column (Sigma Aldrich) to remove thrombin. The protein was then dialyzed in buffer (25 mM MOPS, 1 mM $CaCl_2$, pH = 7.0) using 3.5 KDa MWCO dialyzers (Thermo-Scientific) at 4°C.[64] Concentrations were measured by absorbance at 280 nm, using an extinction coefficient of 13980 $M^{-1}cm^{-1}$. The procedure typically yielded roughly 18 mg of protein per liter of culture. The purity of each protein was estimated by SDS-PAGE using a 4-20% gradient gel (Bio Rad), and all proteins used were 95% pure or greater (Figure 2.9).

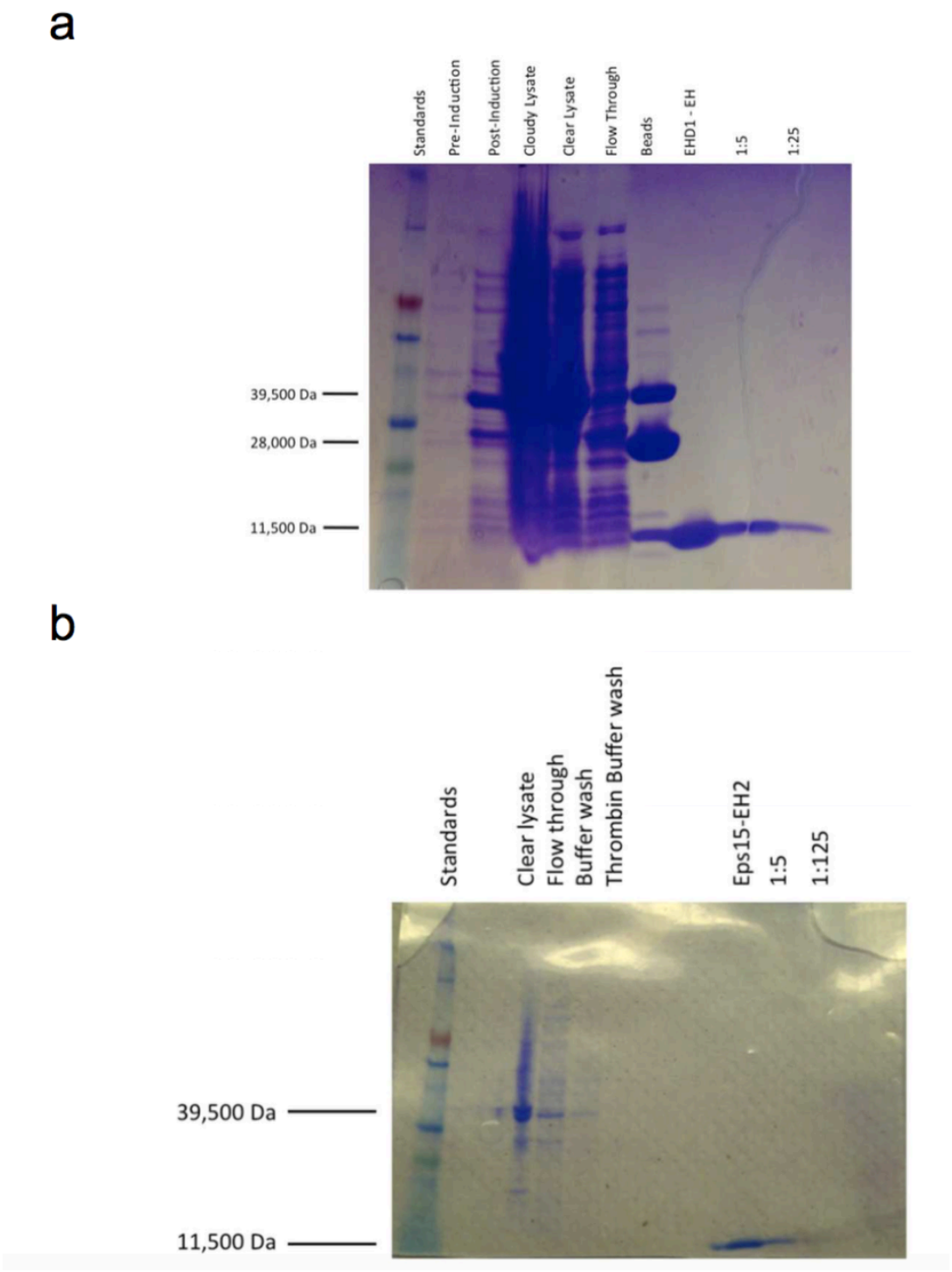

Figure 2.9. SDS-PAGE of protein preparations of EHD1-EH (A) and Eps15-EH2 (B). Samples from different points in the preparation were tested to monitor the quality of the process. The lanes are labeled with the samples of interest, and serial dilutions were performed to estimate protein purity.

2.11.2 Synthesis of linear and cyclic peptides

Materials were purchased from EMD Biosciences, Anaspec Advanced Chemtech, and Creosalis. All peptides were synthesized by solid-phase peptide synthesis (SPPS), using standard 9-fluoromethyloxycarbonyl (Fmoc) chemistry (Scheme 2.1). Linear peptides were synthesized in dimtheylformamide (DMF) with 5 equivalents of amino acid, 4.9 equivalents of 1-[bis(dimethylamino)methylene]-1*H*-1,2,3-triazolo[4,5-b]pyridinium 3-oxide hexafluorophosphate (HATU), 4.9 equivalents of hydroxybenzotriazole (HOBt), and 10 equivalents of diisopropylethylamine (DIPEA) for 30 minutes. The Fmoc deprotections were performed in 20% piperidine in DMF for 10 minutes and repeated. Between steps, the resin was washed with DMF and dichloromethane (DCM). To cyclize the peptides, both the Fmoc and the 4-{N-[1-(4.4-dimethyl-2,6-dioxocyclohexylidene)-3-methylbutyl]amino}benzyl ester (Dmab) protecting groups were removed in three 3-minute washes with 2 % hydrazine in DMF. The peptidyl resin was then washed extensively with DMF and DCM. The N and C termini were then cyclized with 5 equivalents of 6-chloro-benzotriazole-1-yloxy-tris-pyrrolidinophosphonium hexafluorophosphate (PyClock), 5 equivalents of 6-chloro-1-hydroxybenzotriazole (Cl-HOBt) and 10 equivalents of DIPEA (Scheme 2.1, Table 2.4).

The fluoresceinated cyclic peptides were synthesized on resin with standard Fmoc chemistry and orthogonal protecting groups, as described in Scheme 2.2. Unless

otherwise indicated, all fluoresceinated peptides were labeled on resin by coupling with 5(6)-carboxyfluorescein succinimidyl ester (Anaspec). 5 equivalents of the fluorophore were added with 10 equivalents of DIPEA in DMF, and the reaction proceeded overnight. Peptides were cleaved for 2 hours in 95 % trifluoroacetic acid (TFA), 2.5 % triisopropylsilane (TIS), and 2.5% H_2O.

All of the peptides were purified by reverse-phase HPLC on a C18 preparatory scale column and H_2O/CH_3CN with 0.1% trifluoroacetic acid. The peptides were then re-purified on a C18 analytical scale column as needed, until the final product was ≥95% pure. The lyophilized peptides were dissolved in dimethyl sulfoxide to prepare final stock solutions. Concentrations were determined by absorbance of the tyrosine at 274 nm with an extinction coefficient of 1280 $M^{-1}cm^{-1}$ or at 494 nm, with an extinction coefficient of 70,000 $M^{-1}cm^{-1}$, for fluorescein-labeled peptides.

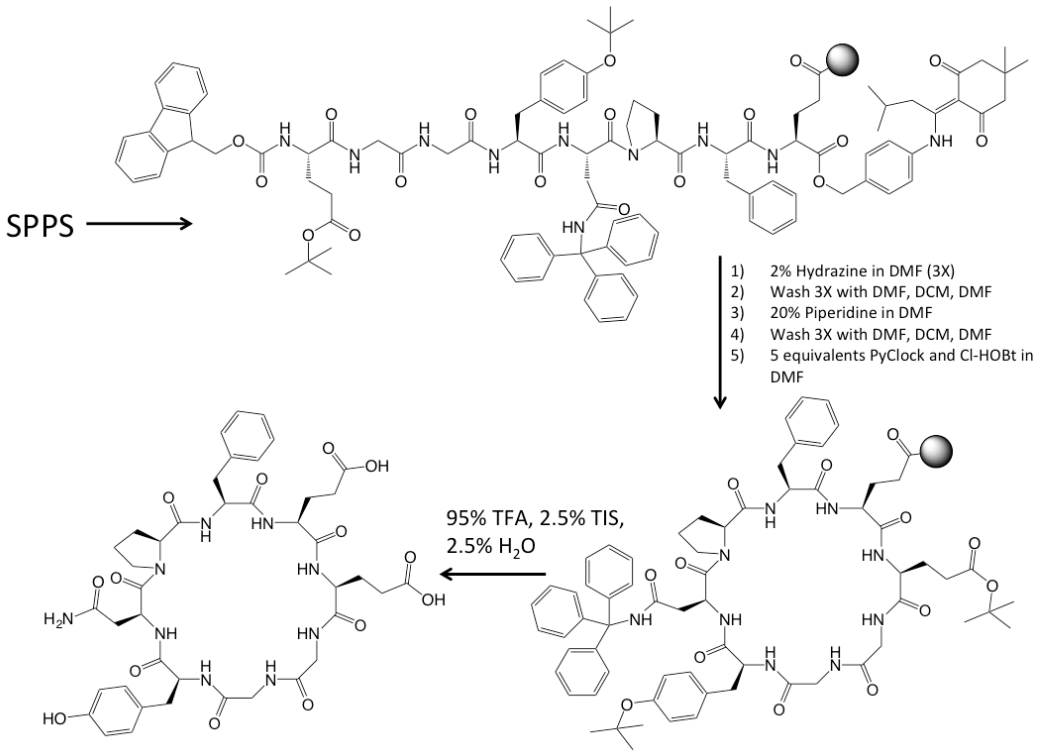

Scheme 2.1. Synthesis of backbone-cyclic, NPF-containing peptides. The linear peptide was synthesized using standard Fmoc chemistry, attached to Wang resin by its glutamic acid side chain. The C-terminus of the attached amino acid was orthogonally protected with a Dmab group. Following completion of the linear sequence, the C-terminal Dmab was removed in a solution of 2% hydrazine in DMF. The peptidyl-resin was also washed with 20% piperidine to ensure complete removal of the Fmoc group. The N-terminus was then coupled to the C-terminus with PyClock and Cl-HOBt as the coupling reagents. The peptide was then cleaved using standard techniques. The peptidyl resin was incubated at room temperature in 95 % trifluoroacetic acid (TFA), 2.5 % triisopropylsilane (TIS), and 2.5 % H_2O for 2 hours.

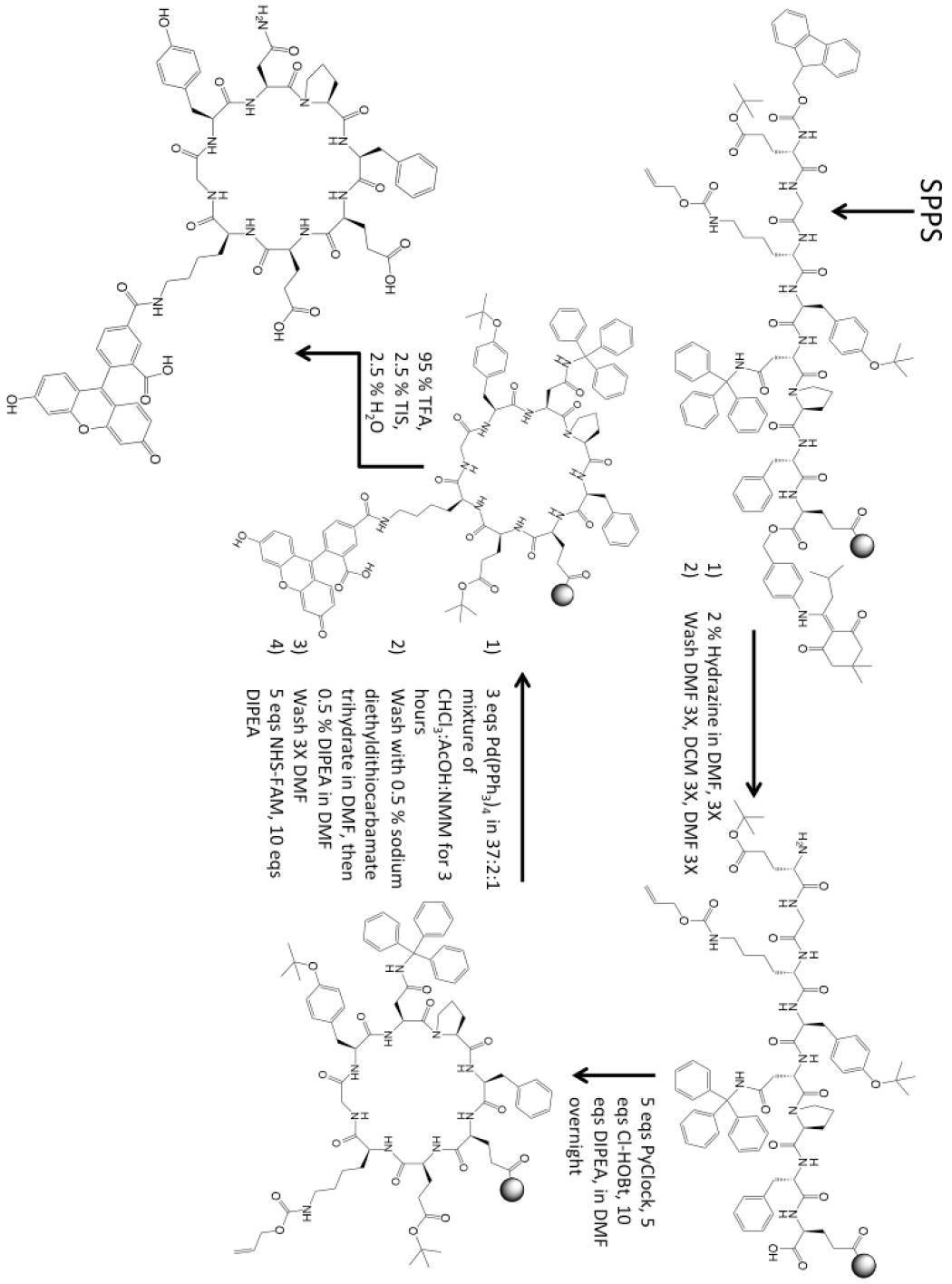

Scheme 2.2. Synthesis of fluoresceinated cyclic peptides. The linear peptides were synthesized on resin using standard Fmoc chemistry. The orthogonal Dmab and Alloc protecting groups were used to each amines at a particular point in the synthesis. The Alloc group was removed with palladium tetrakis ($Pd(PPh_3)_4$) in a 37:2:1 mixture of $CHCl_3$, acetic acid (AcOH), and N-methylmorpholine (NMM). The 5(6)-carboxyfluorescein NHS ester was added to fluorescently label the free lysine. Cyclic peptides were cleaved from the Wang resin for 2 hours.

Peptide	Sequence	Expected Mass (m/z)	Observed Mass (m/z)
Linear	Ac-YNPFEEGG-$CONH_2$	952.4	953.4
cNPF1	-YNPFEEGG-	893.4	894.4
Lin^{Flu}	(Flu)-ββYNPFEE-$CONH_2$	1296.5	1297.5
cNPF1^{Flu}	-YNPFEEGK(Flu)-	1322.5	1321.2
cNPF2^{Flu}	-YNPFEEγK(Flu)-	1349.5	1348.1
cNPF3^{Flu}	-YNPFEEK(Flu)-	1265.5	1263.3
cNPF4^{Flu}	-YNPFEAGK(Flu)-	1264.5	1262.6
cNPF5^{Flu}	-YNPFAEGK(Flu)-	1264.5	1262.9
cNPF6^{Flu}	-YNPFEQGK(Flu)-	1321.3	1320.4
cAPA^{Flu}	-YAPAEEGK(Flu)-	1203.5	1204.5
cNPF1B	-YNPFEEGK(Ac)-	1006.4	1004.9
cNPF5	-YNPFAEGG-	835.4	834.1
cAPA	-YAPAEEGG-	775.4	775.4

Table 2.4 The peptides synthesized as previously described. The masses of each product were determined by MALDI-TOF mass spectrometry or by ESI.

2.11.3 Isothermal titration calorimetry

The experiments were performed on a Microcal ITC200 system (GE Healthcare). All proteins and peptides were dialyzed together in 25 mM MOPS (pH 7.0), 1 mM $CaCl_2$, and either 15 mM or 150 mM NaCl at 4^{o}C prior to the experiments. The dialysis proceeded over 24 hours, with three buffer changes. The dialyzers had a molecular weight cut-off of 100-500 Da (Spectrum Labs, Micro Float-a-lyzer dialysis device) or 3,500 Da (Thermoscientific Slide-a-lyzer, 0.5-3 mL) for peptide and protein dialysis, respectively. The ITC experiments were performed at 20^{o}C with solutions of 20-50 μM protein, and peptide at tenfold higher concentration. While the buffer had a pH of 7.0 at 4^{o}C, the pH of MOPS is slightly dependent on temperature. Consequently, we determined that the buffer had a pH of 6.8 at the experimental temperature of 20^{o}C.

2.11.4 Protocol for fluorescence polarization direct binding assays

All experiments were performed in flat-bottom, black 384 well plates (Corning). The assay buffers (25 mM MOPS pH 7.0, 1 mM $CaCl_2$ at 4^{o}C) had a final sodium chloride concentration of either 15 or 150 mM as needed. Each well had a final concentration of 1.5% DMSO and 0.1% Tween-20, which were added with the fluorescent probes. As with the ITC experiments, the MOPS buffer was confirmed to have a pH of 6.8 at 20^{o}C. Each probe was incubated at a final concentration of 100 nM at room temperature with varying concentrations of

EHD1-EH or Eps15-EH2. To ensure that all liquid was at the bottom of the well, the plates were spun at 1,600 G at 20°C for 3 minutes. We measured the fluorescence polarization (Tecan F200 Pro) 1 hour after the addition of the probe, and a second time 4 hours after addition of the probe. We did not observe consistent differences in the data collected at the 1-hour and 4-hour time points. We used the data from the 1-hour time point for further analyses. Three or more independent trials were performed on each probe with each buffer condition. The K_d curve fits were derived from first principles (Equation 2.1), and fit using non-linear regression software (Kaleidagraph, Synergy Software). For the experiments performed in 150 mM NaCl, the data was fit to the upper bounds established by the data obtained from the experiments performed in 15 mM NaCl.

(Equation 2.1) $$P = P_F + (P_B - P_F) \times \frac{L_T + K_D + R_T - \sqrt{\{(L_T + K_D + R_T)^2 - 4L_T R_T}}{2}$$

(Equation 2.2) $$FB = \frac{(P - P_F)}{(P_B - P_F)}$$

P = experimental polarization value, P_F = polarization of free ligand, P_B = polarization of bound ligand, L_T = total ligand concentration, K_D = dissociation constant, R_T = total concentration of protein, and FB = fraction bound

2.11.5 Protocol for the fluorescence polarization competitive binding assays

All experiments were performed in flat-bottom, black 384 well plates (Corning). The assay buffers were prepared at 4°C with 25 mM MOPS, 1 mM $CaCl_2$, and 15 mM NaCl with a pH of 7.0. Each inhibitor was incubated at room temperature

with 20 μM EHD1-EH for 30 minutes. The fluorescent probes were then added to the mixture and the plates were incubated at room temperature for 1 hour. The IC_{50} curve fits were calculated using non-linear regression (Kaleidagraph, Synergy Software, Equation 2.3). Each well had a final concentration of 1.5% DMSO and 0.1% Tween-20, which were added with the fluorescent probes.

(Equation 2.3) $FB = 0 + \frac{1-0}{1+\frac{x}{IC_{50}}^{y}}$

IC_{50} = half-maximal inhibitory concentration, x = concentration of peptide, y = Hill Coefficient

2.11.6. Circular dichroism (CD) protocol

EHD1-EH and Eps15-EH2 were dialyzed at 4°C in 10 mM sodium phosphate buffer at pH = 7.0 with 1 mM $CaCl_2$ and 1 mM dithiothreitol. The CD experiments were performed at room temperature (Jasco J-715 circular dichroism spectropolarimeter) with EHD1-EH at 40.3 μM and Eps15-EH2 at 35.5 μM. The spectra were taken from 190 nm to 260 nm at 1 nm intervals. These experiments were performed by Dr. Robyn Eisert.

3 Chapter 3. The design, synthesis and screening of the next generation of EHD1-EH inhibitors.

3.1 Introduction

In our work to date, we had designed cNPF1, the highest affinity inhibitor of EHD1-EH reported at this time. However, its K_d value of 9.9 μM left us searching for a molecule that bound the target even more tightly.[89] In addition, we were looking to replace a portion of the peptide backbone and to reduce the overall charge of the peptides from the original design series in order to make the peptides more likely to be cell-penetrant. These goals led us to explore alternative chemical spaces.

The robust and modular peptide modification strategies established by Timmerman *et al.* presented an excellent opportunity to advance our strategy.[92] By flanking a peptide sequence with thiols, one can synthesize peptide macrocycles through a reaction with α,α'-dibromo xylenes.[92] Other commercially available linkers can be used in place of the dibromo xylenes, so that a variety of different linkers can be used to conformationally restrict a peptide and generate cyclic and bicyclic peptides.[92] This intramolecular reaction is robust and fairly quick, with most reactions reaching completion within 1 hour.[92]

The bis-alkylation strategy has been applied to the creation of peptide macrocycle libraries. Phage display libraries were used to generate cyclic and bicyclic peptide inhibitors specific to several target proteins. These libraries encoded peptides containing three cysteine residues that were then reacted with tris-(bromomethyl)benzene (TBMB), a linker with threefold symmetry.[93] This technique has been successfully used to target kallikrein, urokinase-type plasminogen activator, notch receptors, β-catenin, sortases, and the epidermal growth factor receptor Her2.[93-94] In related work, bis-alkylation was used to preserve helical secondary structure in phage display libraries. It had been previously established that cross-linking cysteine residues at positions *i* and *i+4* using bis-alkylation can stabilize α-helical structure.[95] Diderich *et al.* combined the bis-alkylation chemistry with phage display libraries to generate α-helical inhibitors of β-catenin.[96] The use of α,α'-dibromo-*m*-xylene, along with *trans*-1,4-dibromo-2-butene and *cis*-1,4-dichloro-2-butene allowed for the-synthesis of the desired peptides, which had single digit micromolar affinities for their designated targets.[96] This work provided an important example of the use of bis-alkylation chemistry to stabilize the secondary structure required for peptide activity.

For our next iteration of EHD1-EH inhibitors, we incorporated a thiol bis-alkylation strategy for cyclization (Figure 3.1). We placed thiol-containing amino acids N- and C-terminal to the NPF-containing binding epitopes. We then bis-alkylated these peptides with a variety of inexpensive, commercially available dibrominated linkers, generating small libraries of constrained cyclic peptides.

From a single sequence, we were able to investigate many different cyclic peptides, each sampling a different chemical space. We used a fluorescence polarization competitive binding assay to evaluate these molecules, and we identified multiple compounds with better inhibitory potency than cNPF1. Then, dye-labeled analogs of the best inhibitors were synthesized, and fluorescence polarization (FP) direct binding experiments identified five cyclic peptide inhibitors with single-digit micromolar affinities for EHD1-EH.

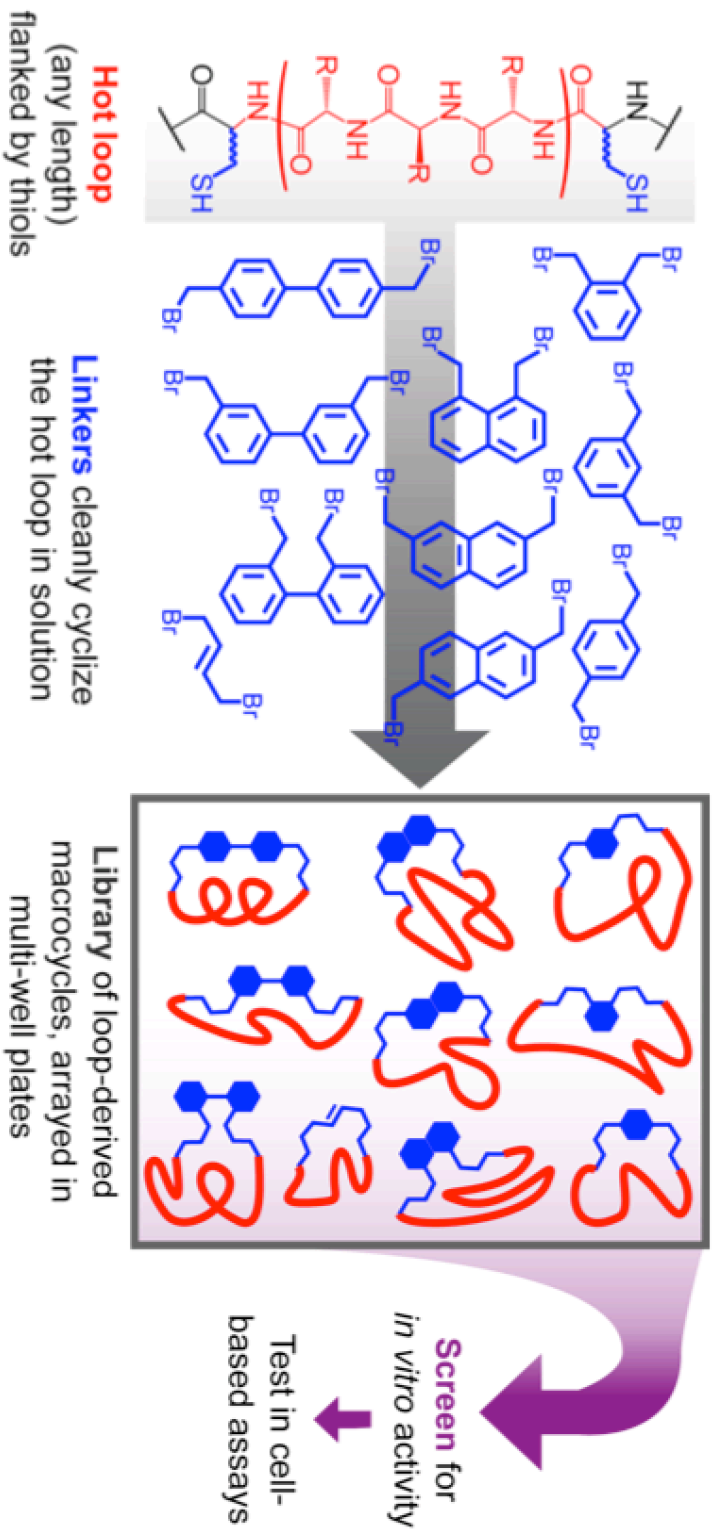

Figure 3.1. Diversity-oriented stapling strategy for finding cyclic peptide inhibitors of EHD1-EH. We flanked the binding sequence with thiols, then bis-alkylated to generate a small library of cyclic peptides that we tested *in vitro*.

3.2 Design of bis-alkylated macrocycles as EHD1-EH inhibitors

Our primary goal in applying bis-alkylation to EHD1-EH inhibitors was to search more widely for beneficial binding conformations, while perhaps promoting cell penetration through the incorporation of a hydrophobic linker.[27] The initial series of peptides were synthesized on cysteamine 2-chlorotrityl resin to afford a free thiol on the C-terminus, and a 4-pentynoic acid cap was incorporated on the N-terminus for potential cell-penetration experiments with click chemistry. We started with the binding epitopes YNPFEE, YNPFE, NPFE, and NPFEE (Table 3.1), and incorporated a cysteine residue N-terminal to each binding motif. The N-terminal cysteine and C-terminal cysteamine would provide two free thiols for bis-alkylation. Sequences 3 and 4 lacked the tyrosine, to produce a smaller molecule while exploring the relative importance of the tyrosine. Sequences 2 and 3 lacked the second glutamic acid, to reduce the number of charged residues while exploring the relative importance of the second negative charge.[76, 77c] While it had been shown for linear peptides that two or more negatively charged residues promote better affinity and selectivity for EHD1-EH binding,[60, 64] we hypothesized that conformational differences could compensate for the lack of a second negative charge, yielding a molecule that was both an effective inhibitor and more likely to be cell-penetrant.

3.3 Pilot Reactions to Optimize Bis-Alkylation Macrocyclization

Initially the bis-alkylation reaction (Scheme 3.1) was performed on crude peptides. However, these reactions yielded little cyclic peptide and required multiple HPLC passes to obtain only 1-2 % purified yield. Consequently, we synthesized and purified the linear peptides and ran pilot reactions with each linker to determine the best conditions for linker cyclization reactions (Figure 3.2). The pilot reactions for 4p-CNPFEE-(C*) (4-linear; C* denotes cysteamine) were run in a 20 μL volume. Two equivalents of tris(2-carboxyethyl)phosphine (TCEP) were added to a 1 mM solution of peptide and the mixture was incubated for 40 minutes to reduce any disulfide-linked byproducts. Then 1.5 equivalents of a dibromo-containing linker was added (the final reaction mixture was 5 % DMSO, 42.5 % acetonitrile, 42.5 % 20 mM aqueous NH_4HCO_3 pH = 8.0). The mixtures were incubated at room temperature for three hours and then quenched with acetonitrile with 0.1 % TFA. The reaction mixtures were then subjected to MALDI-TOF mass spectrometry to identify the products (Table 3.1). All of the reactions generated the desired cyclic peptide, most as the major product, as estimated by MALDI-TOF mass spectrometry. We detected a +144 m/z mass in several of the reaction mixtures, which corresponded to a TCEP salt or a TCEP adduct. Remaining linear peptide was detected in reactions with 1,8-Nap, 2,6-Nap, Tph, 2,2-BP, and 4,4-BP (Figure 3.2). We chose to move forward with the linkers that successfully produced the desired cyclic peptide product most robustly.

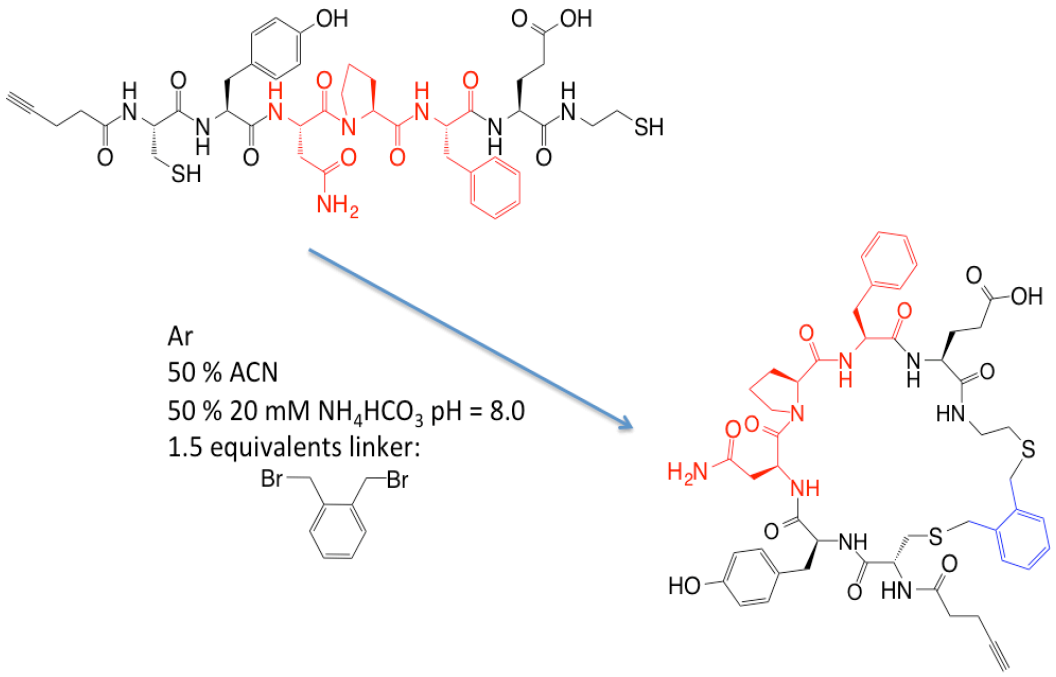

Scheme 3.1. Bis-alkylation synthesis of cyclic peptides. The NPF motif is shown in red, while the linker is shown in blue. The peptide represented is sequence 2 with the OX linker. Reactions were quenched with trifluoroacetic acid.

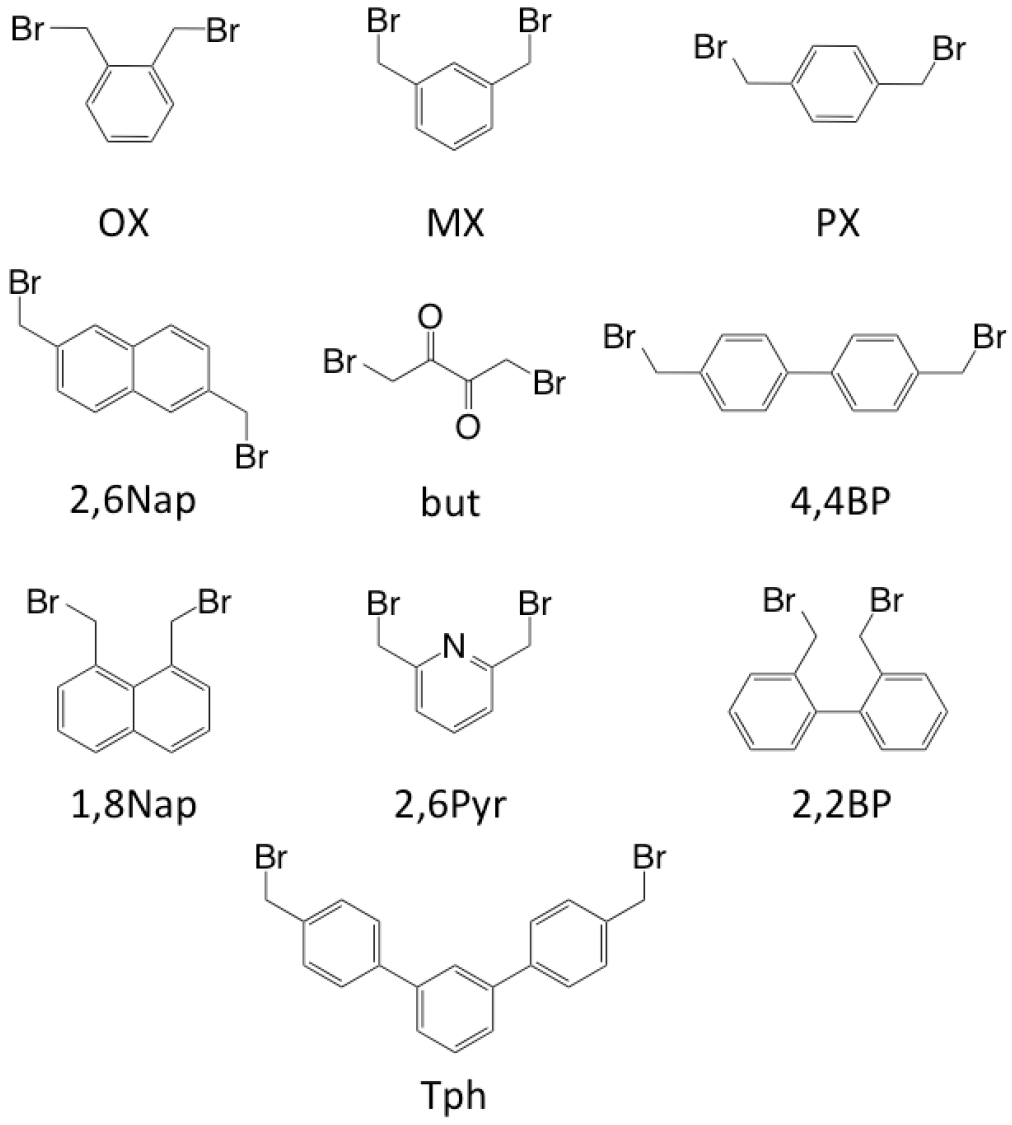

Figure 3.2. The linkers used in pilot cyclization reactions. Some cyclic peptide product was detected in each reaction, but only a selection of these linkers generated cyclic peptide in reasonable yields when synthesized on a larger scale.

Number	Sequence	OX	MX	PX	2,6Pyr	2,6Nap	1,8Nap	4,4BP	2,2BP	But	Tph
1	4p-CYNPFEE-(C*)-	=	+	+	=	+		=			
2	4p-CYNPFE-(C*)-	-	-	-	-	-		-		=	
3	4p-CNPFE-(C*)-	=	-	-	-	-		-	-		
4	4p-CNPFEE-(C*)-	=	=	=	=	=					

+ = better than cNPF1, = = similar, - = weaker

Table 3.1. A summary of the results from the initial 3-point competitive binding screen. Peptides marked with a green plus sign inhibited EHD1-EH with greater potency than cNPF1, which was used as a control. Peptides marked with a blue equal sign inhibited EHD1-EH with similar potency as cNPF1. Peptides marked with a red minus inhibited EHD1-EH with weaker potency than cNPF1. Peptides with no symbol were not synthesized in a large enough quantity to test due to poor yields of the bis-alkylation reaction. 4p denotes the 4-pentynoic acid cap, while C* represents cysteamine.

Linker	Expected mass (m/z)	Observed masses (m/z)
Linear	877.0	**877.2**, *899.1* (+ Na)
OX	979.1	***979.3***, 1001.5 (+ Na), 1017.5 (+ K), 1229.3 (+ TCEP)
MX	979.1	***979.5***, 1001.5 (+ Na), 1017.5 (+ K). 1230.5 (+ TCEP)
PX	979.1	***979.6***, 1001.5 (+ Na), 1017.5 (+ K), 1229.7 (+TCEP)
1,8 Nap	1029.2	*915.6* (linear + K), ***1029.4***, 1069.3 (+ K), 1279.4 (+ TCEP)
2,6 Nap	1029.2	915.8 (linear + K), ***1029.9***, 1051.9 (+ Na), 1072.7 (+ K), 1280.0 (+ TCEP)
Tph	1131.3	877.5 (linear), *1072.7* (linear + 195), **1132.0**, 1170.2 (+ K)
4,4 BP	1055.2	877.5 (linear), 899.6 (linear + Na), ***1055.6***, 1072.7 (linear + 195), 1305.8 (+ TCEP)
2,2 BP	1055.2	*1021.7* (linear + 144), **1055.6**
But	959.1	***959.5***, 981.5 (+ Na), 999.3 (+ K), 1072.2 (linear + 195)
2,6 Pyr	980.1	***980.5***, 1002.6 (+ Na), 1024.6 (+ K)

Table 3.2. Pilot reaction MALDI-TOF results for 4p-CNPFEE-(C*). Cyclic products are shown in bold, and the largest peaks are italicized.

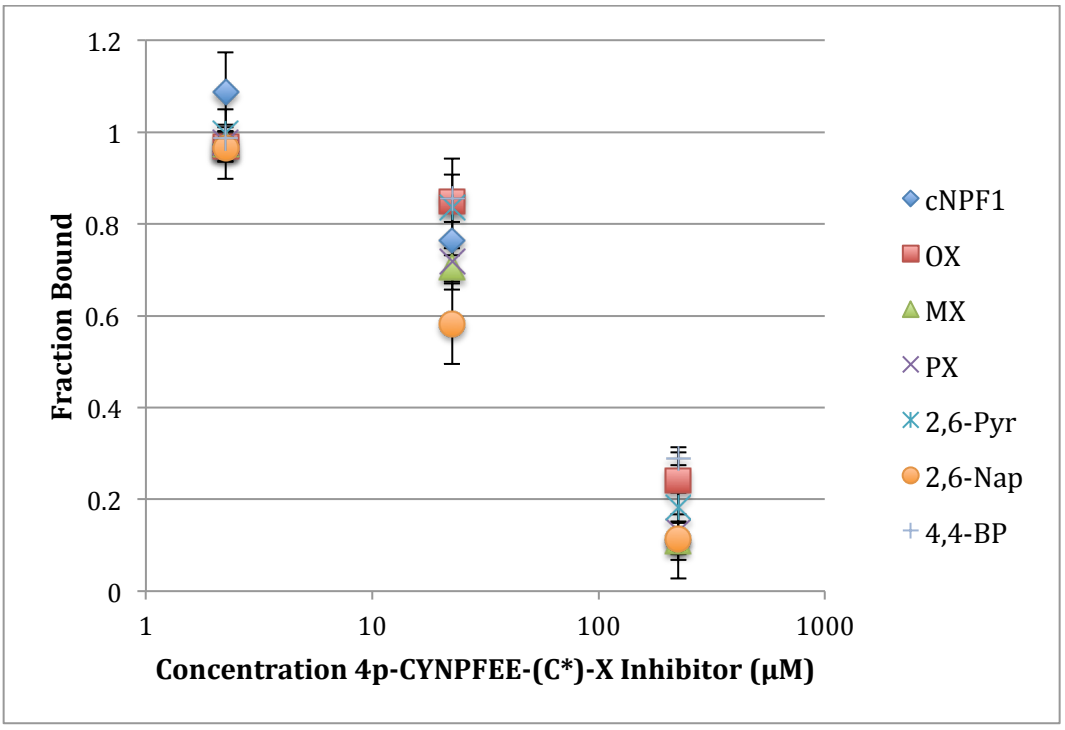

Figure 3.3. Data from the three-point screens for the cyclic peptide inhibitors with the sequence 4p-CYNPFEE-(C*) (Sequence 1). The error bars represent the standard deviation from three independent trials.

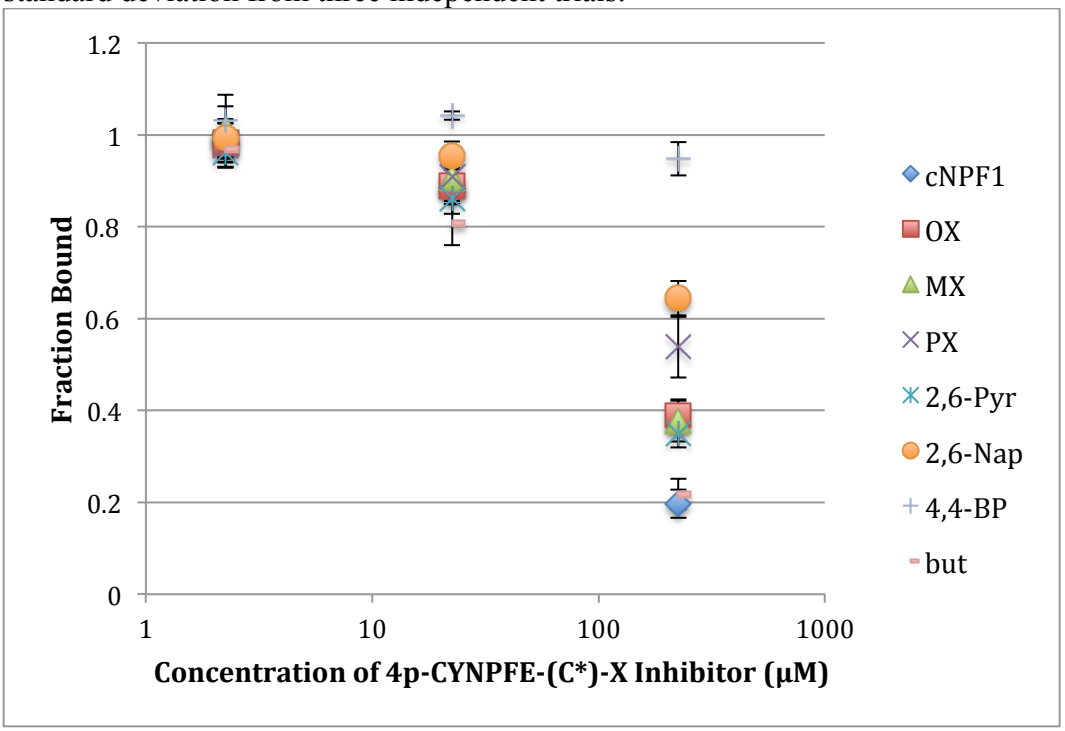

Figure 3.4. Data from the three-point screens for the cyclic peptide inhibitors with the sequence 4p-CYNPFE-(C*) (Sequence 2). The error bars represent the standard deviation from three independent trials.

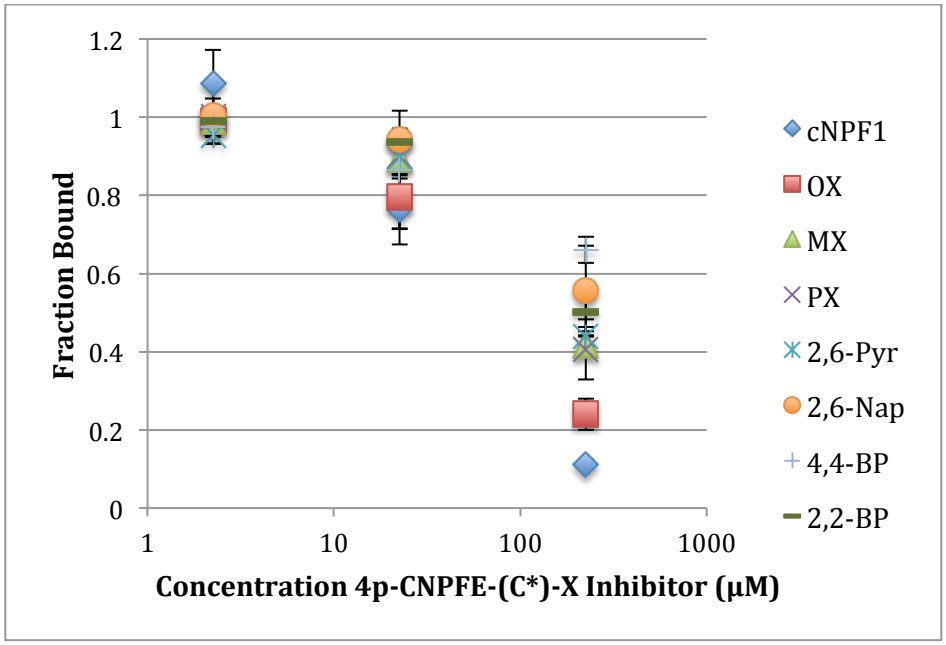

Figure 3.5. Data from the three-point screens for the cyclic peptide inhibitors with the sequence 4p-CNPFE-(C*) (Sequence 3). The error bars represent the standard deviation from three independent trials. Peptides with the 2,6-Nap and 4,4-BP linkers were only tested in two independent trials.

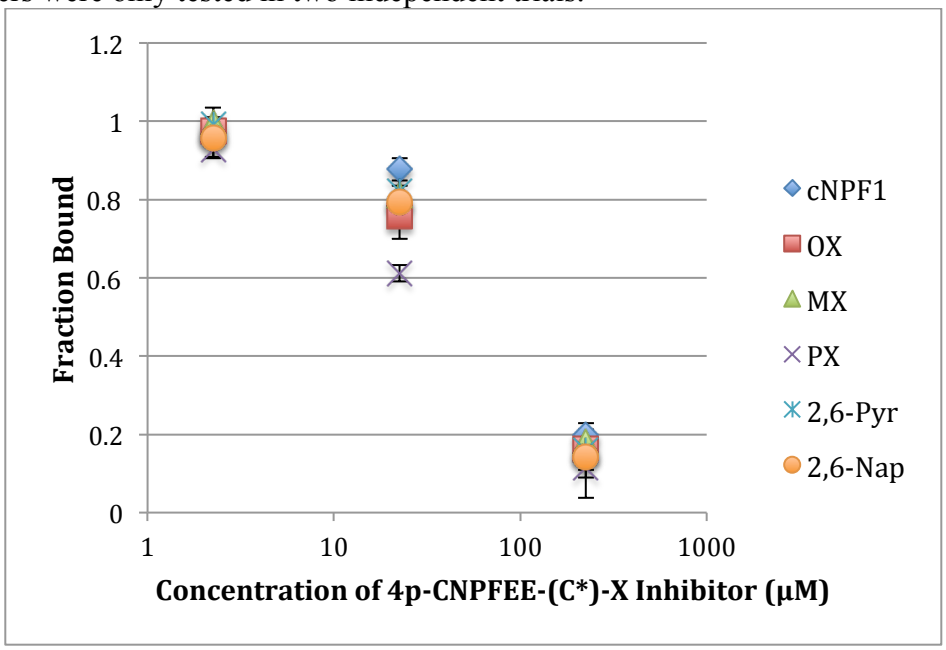

Figure 3.6. Data from the three-point screens for the cyclic peptide inhibitors with the sequence 4p-CNPFEE-(C*) (Sequence 4). The error bars represent the standard deviation from three independent trials. The peptide with the 2,6-Nap linker was only tested in two independent trials.

3.4 A measurement of the inhibitory potency of cyclic peptide inhibitors using fluorescence polarization competitive binding assays

We first tested the bis-alkylated peptides in a 3 point screen to identify peptides that had a greater inhibitory potency than cNPF1. The peptides were initially synthesized and tested on this smaller scale to save material (both peptide and protein). Any peptides identified as hits would then be tested more rigorously in a full 10 point competitive binding fluorescence polarization assay (Table 3.2). All of the inhibitors with two glutamic acids displayed an inhibitory potency for EHD1-EH similar to that of cNPF1 (Figure 3.3 and Figure 3.6), while the majority of the inhibitors stemming from the other sequences were not as effective (Figure 3.4 and Figure 3.5). Collectively, these results demonstrated that stabilization of the NPF motif structure was not enough to compensate for the requirement of two negative charges. The cyclic peptide with the best inhibitory potency that had only one negative charge was 4p-CNPFE-(C*)-OX. This result may be indicative of a conformation of the macrocycle that improved EH domain binding. The lead peptides from the CYNPFEE and CNPFE sequences were determined by Dr. Robyn Eisert, a post-doctoral associate who also worked on this project.

Peptides 4p-CYNPFEE-(C*)-PX (1-PX), 4p-CYNPFEE-(C*)-MX (1-MX), 4p-CYNPFEE-(C*)-2,6Nap (1-2,6Nap), 4p-CYNPFE-(C*)-but (2-but), 4p-CNPFEE-(C*)-OX (4-OX), 4p-CNPFEE-(C*)-MX (4-MX), 4p-CNPFEE-(C*)-PX (4-PX),

4p-CNPFEE-(C*)-2,6Pyr (4-2,6Pyr), 4p-CNPFEE-(C*)-2,6Nap (4-2,6Nap), and 4p-CNPFE-(C*)-OX (3-OX) were all advanced for further testing. The peptides were compared to cNPF1 within the context of their linear sequences. We were interested primarily in molecules with greater inhibitory potency than cNPF1, but if an inhibitor had a similar potency and possessed fewer charged side chains, we would pursue it further in the event that it had improved cell-penetrating capabilities.

For the 4p-CYNPFEE-(C*) sequence (sequence 1), peptides with the MX and 2,6-Nap linkers (peptides 1-MX and 1-2,6NAP) did not inhibit as strongly as the control. However, sequence 1 with the PX linker (1-PX) had an IC_{50} of 27.1 ± 3.6 μM, which was a twofold improvement over cNPF1. Almost all cyclic peptides derived from sequences 2 and 3, 4p-CYNPFE-(C*) and 4p-CNPFE-(C*) respectively, had poorer inhibitory potencies than cNPF1 (Figures 3.8 and 3.9). Peptide 2-but inhibited two-fold weaker than cNPF1, with an IC_{50} of 119.8 ± 1.6 μM. Peptide 3-OX had an IC_{50} of 76.5 ± 9.8 μM, and it was the only inhibitor with a single charged residue with an affinity close to that of cNPF1. Most of the cyclic peptides derived from 4p-CNPFEE-(C*) (sequence 4) had inhibitory potencies weaker than cNPF1, but two of the peptides showed a promising improvement (Figure 3.10). Peptide 4-2,6Pyr had an IC_{50} of 44.4 ± 3.2 μM, while 4-PX had an IC_{50} of 38.9 ± 16.0 μM. Among all the bis-alkylated peptides screened in competitive inhibition assays, 1-PX was the most potent EHD1-EH inhibitor.

This series had some patterns similar to our head-to-tail cyclic series. Most of the peptides tested inhibited with a similar potency as cNPF1 (Table 3.3). As with the backbone macrocyclic peptides, the majority of the inhibitors with two glutamic acids displayed an inhibitory potency comparable to that of cNPF1, while the inhibitors stemming from the other sequences were not as effective. We were able to find three peptides that inhibited more potently than cNPF1: 1-PX, 3-OX and 4-PX. Most of them have two glutamic acid residues. The peptide with a single negative charge that inhibited with the best potency was 3-OX, which we also advanced to further analysis.

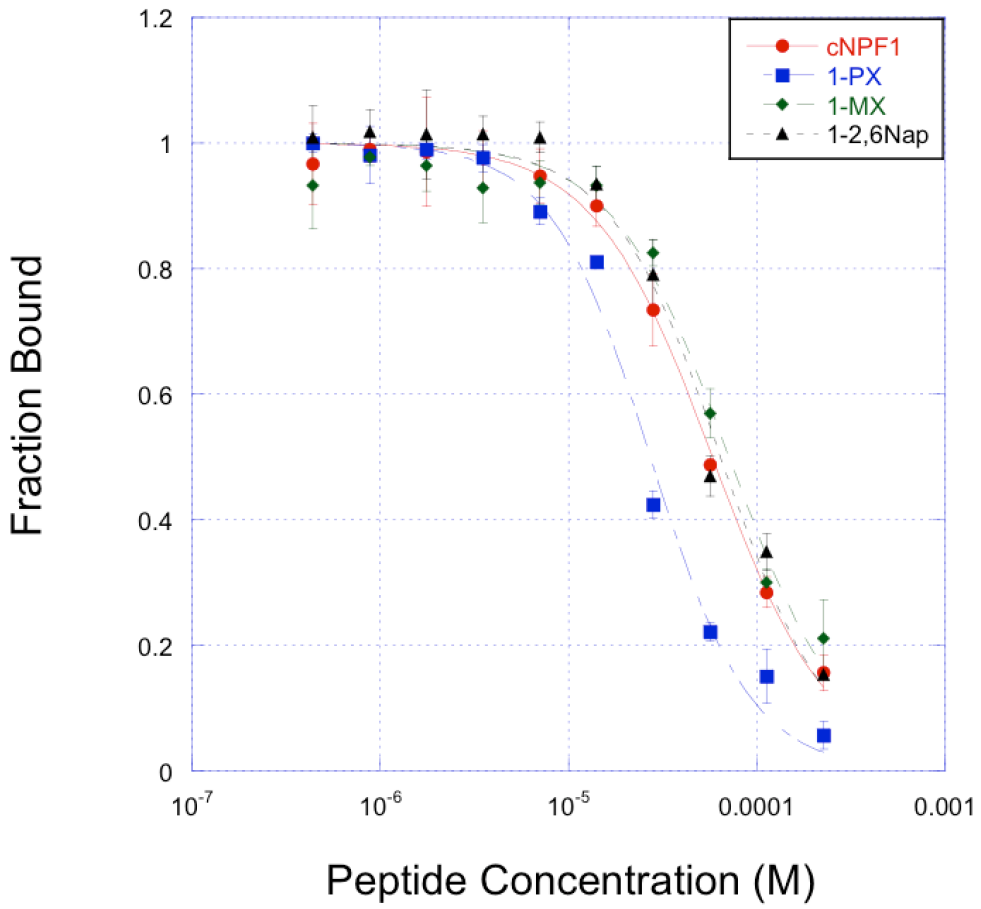

Figure 3.7. Competitive binding experiments with cyclic peptides generated from sequence 1. 10 nM cNPF1^{Flu} was used as the fluorescent probe. The experiments were done in 25 mM MOPS, pH = 6.8, with 15 mM NaCl. One representative trial for each peptide is shown, but reported IC_{50} values represent the average among three independent trials.

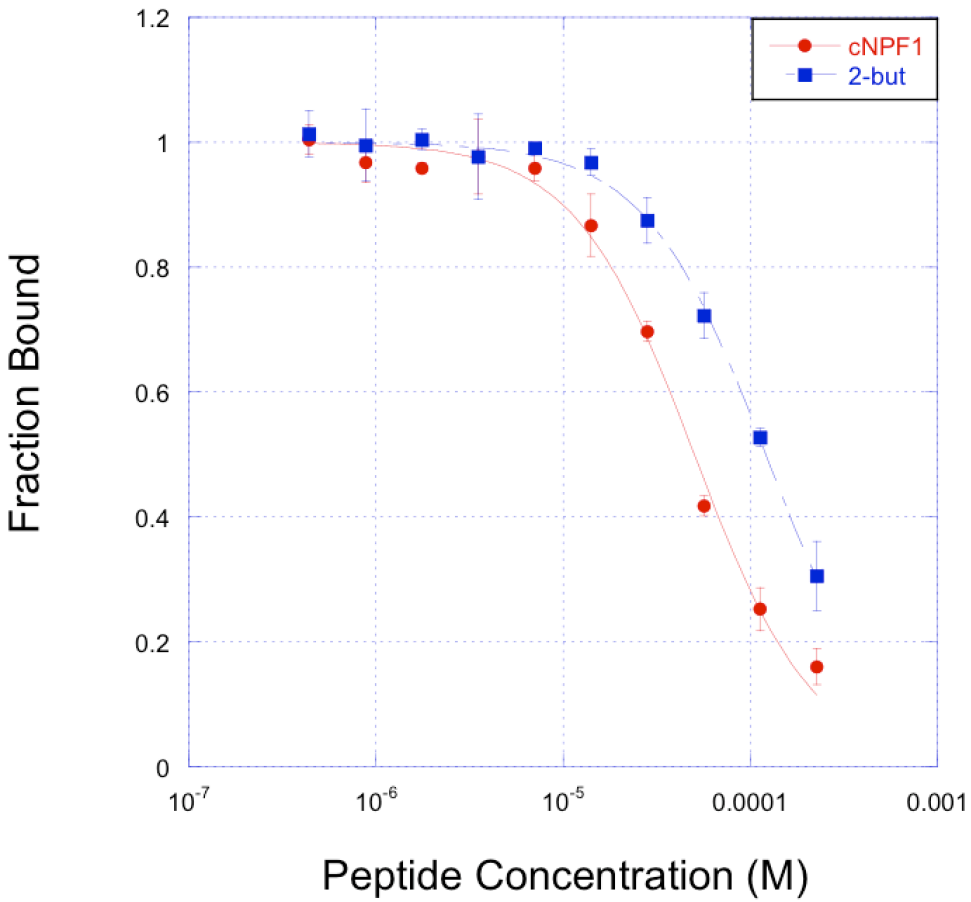

Figure 3.8. Competitive binding experiments with cyclic peptides generated from sequence 2. This peptide was identified as a hit in the initial three-point screen. 10 nM cNPF1^{Flu} was used as the fluorescent probe. The experiments were done in 25 mM MOPS, pH = 6.8, with 15 mM NaCl. One representative trial for each peptide is shown, but reported IC_{50} values represent the average among three independent trials.

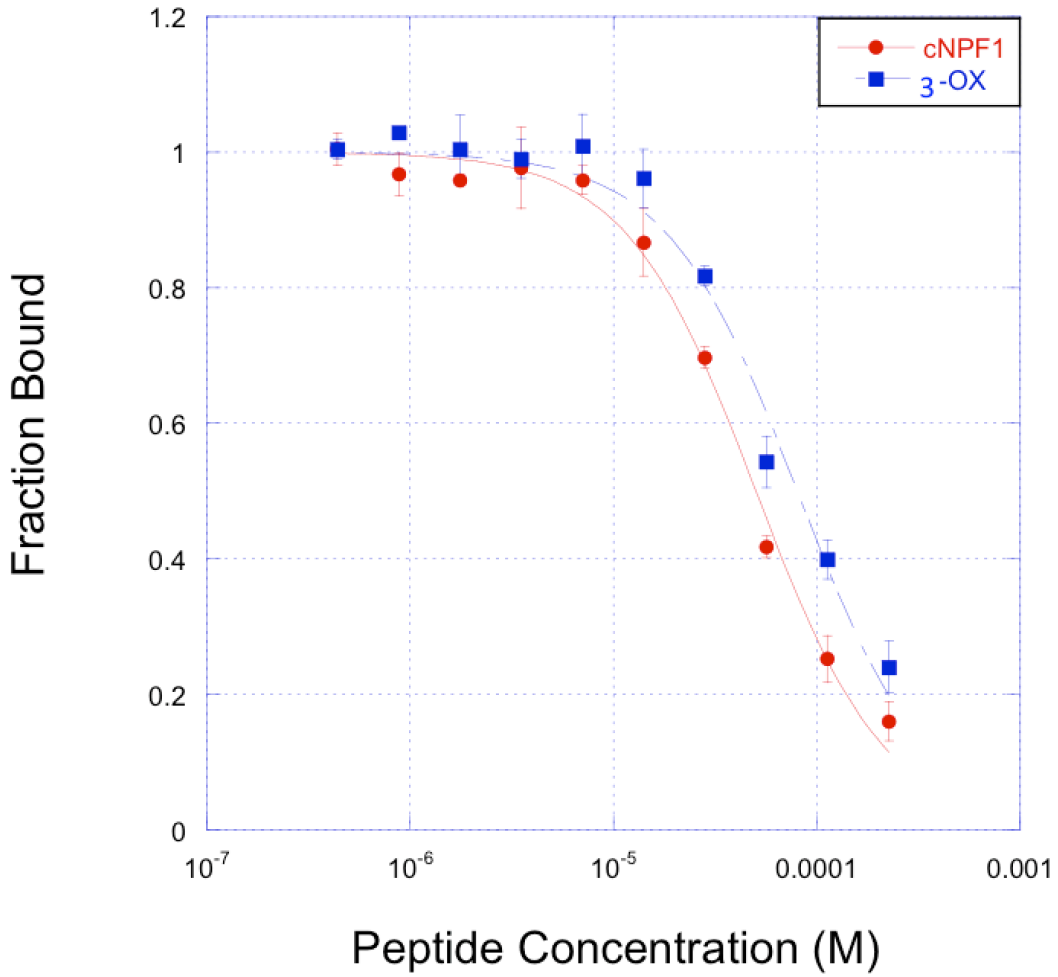

Figure 3.9. Competitive binding experiments with cyclic peptides generated from sequence 3. This peptide was identified as a hit in the initial three-point screen. 10 nM cNPF1^{Flu} was used as the fluorescent probe. The experiments were done in 25 mM MOPS, pH = 6.8, with 15 mM NaCl. One representative trial for each peptide is shown, but reported IC_{50} values represent the average among three independent trials.

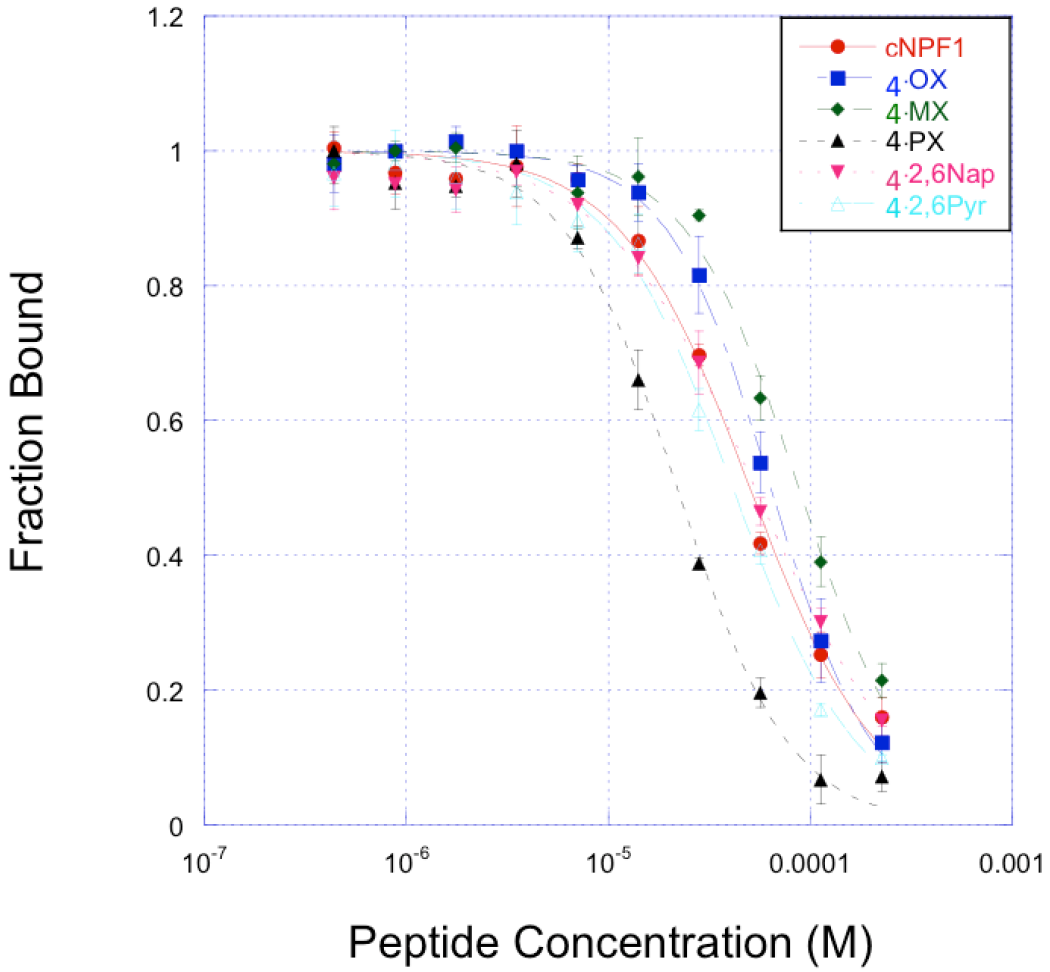

Figure 3.10. Competitive binding experiments with cyclic peptides generated from sequence 4. These peptides were identified as hits in the initial three-point screen. 10 nM $cNPF1^{Flu}$ was used as the fluorescent probe. The experiments were done in 25 mM MOPS, pH = 6.8, with 15 mM NaCl. One representative trial for each peptide is shown, but reported IC_{50} values represent the average among three independent trials.

Peptide	Sequence	Linker	IC_{50} (μM)
cNPF1	-YNPFEEGG-	backbone	48.8 ± 5.4
1	4p-CYNPFEE-(C*)-	MX	68.8 ± 5.7
		PX	27.1 ± 3.6
		2,6 Nap	67.1 ± 5.3
2	4p-CYNPFE-(C*)-	but	119.8 ± 1.6
3	4p-CNPFE-(C*)-	OX	76.5 ± 9.8
4	4p-CNPFEE-(C*)-	OX	62.8 ± 1.1
		MX	88.1 ± 3.2
		PX	38.9 ± 16.0
		2,6 Pyr	44.4 ± 3.2
		2,6 Nap	52.2 ± 0.9

Table 3.3. IC_{50} values from competitive binding assays with bis-alkylated cyclic peptides. Two peptides, 1-PX and 4-PX, had improved inhibitory potency over cNPF1. The IC_{50} values represent the average of IC_{50} values obtained from curve fits to three independent experiments, which were each performed with three technical replicates. The error represents the standard deviation of the three IC_{50} values.

3.5 Inhibitory potencies of di-cysteine-containing, bis-alkylated EHD1-EH inhibitors

1-PX and 4-PX had better inhibitory potency than cNPF1. Parallel to the development of 1-PX and 4-PX, Dr. Robyn Eisert designed an additional inhibitor series. These new peptides incorporated the minimum binding epitope NPFE (Table 3.4, sequence 5), but used cysteine residues at the N- and C-termini (instead of cysteamine at the C-terminus as for sequences 1-4). The peptide was produced with a free acid at its C-terminus, providing a second negative charge. Peptides were N-terminally capped with an acetyl group. Sequence 5 was bis-alkylated with the OX linker to generate the final product, termed 5-OX (Table 3.4). Dr. Eisert had also tested this peptide with the MX and PX linkers in previous screens, but the peptide with the OX linker was shown to be the most promising.

Once 5-OX was shown to have good inhibitory potency (see below), we further explored this sequence in several ways. For sequence 6, we replaced the C-terminal cysteine with a penicillamine. We introduced penicillamine in this position to create additional torsional constraints, which might better pre-organize the NPF motif in the binding conformation. We also synthesized sequence 6B, with penicillamine in place of the N-terminal cysteine to explore conformational constraint in the other linker position. Dr. Eisert examined the NPF-binding pocket on EHD1-EH, and observed that it was deeper than required to fit the

phenylalanine (Figure 3.11). Informed by this observation, we replaced the phenylalanine with 1-napthylalanine or 2-napthylalanine, sequences 7 and 8 respectively, to generate a binding epitope that might be able to make additional hydrophobic contacts.

We tested peptides 5-OX, 6-OX, 6B-OX, 7-OX, and 8-OX in the three-point competitive binding screen, using EHD1-EH and $cNPF1^{Flu}$ (Figure 3.12). 5-OX, 6-OX, and 7-OX had a similar or better inhibitory potency as cNPF1 in this assay. The poorer inhibitory potency of 8-OX could indicate that 2-napthylalanine is less compatible with the hydrophobic binding pocket compared to Phe or 1-naphthylalanine. 6B-OX had poorer inhibitory potency than 5-OX, implying that the N-terminally located penicillamine reduced EHD1-EH binding.

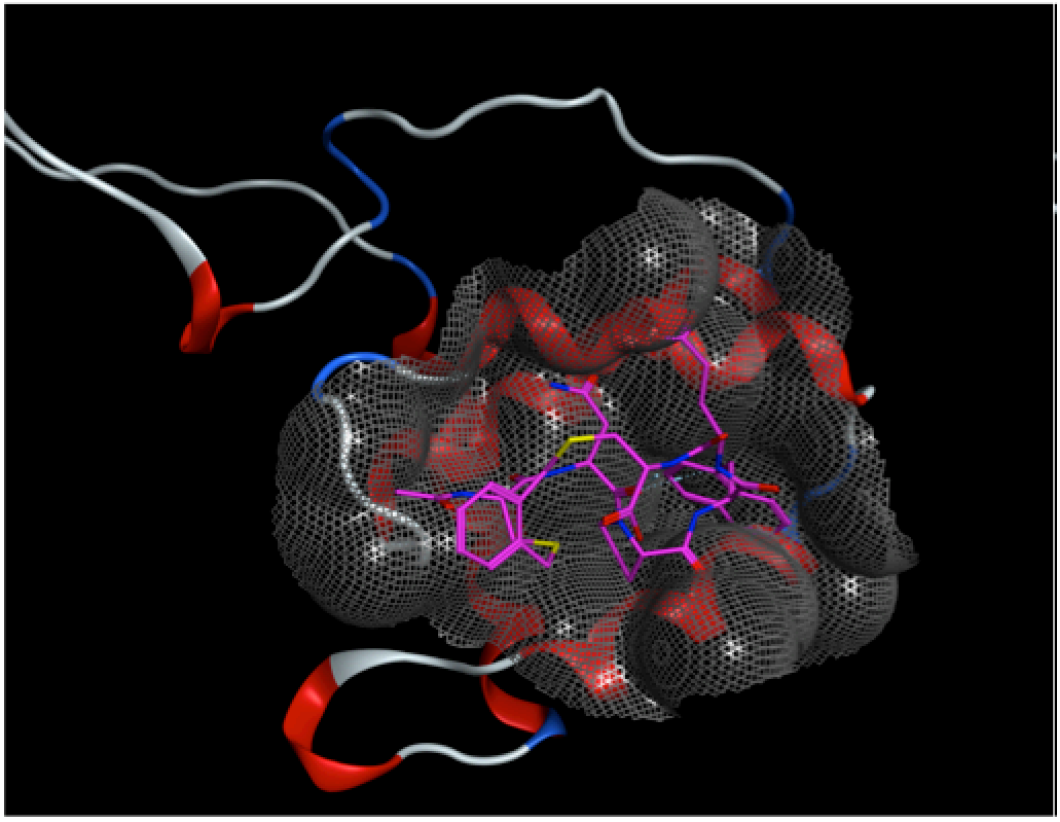

Figure 3.11. A model of the binding pocket of EHD1-EH in complex with 7-OX. The image was created with Molecular Operating Environment (MOE).[60, 97] The binding pocket was modeled with its ligand peptide, but with 1-napthylalanine substituted in place of phenylalanine. This image was generated by Dr. Robyn Eisert.

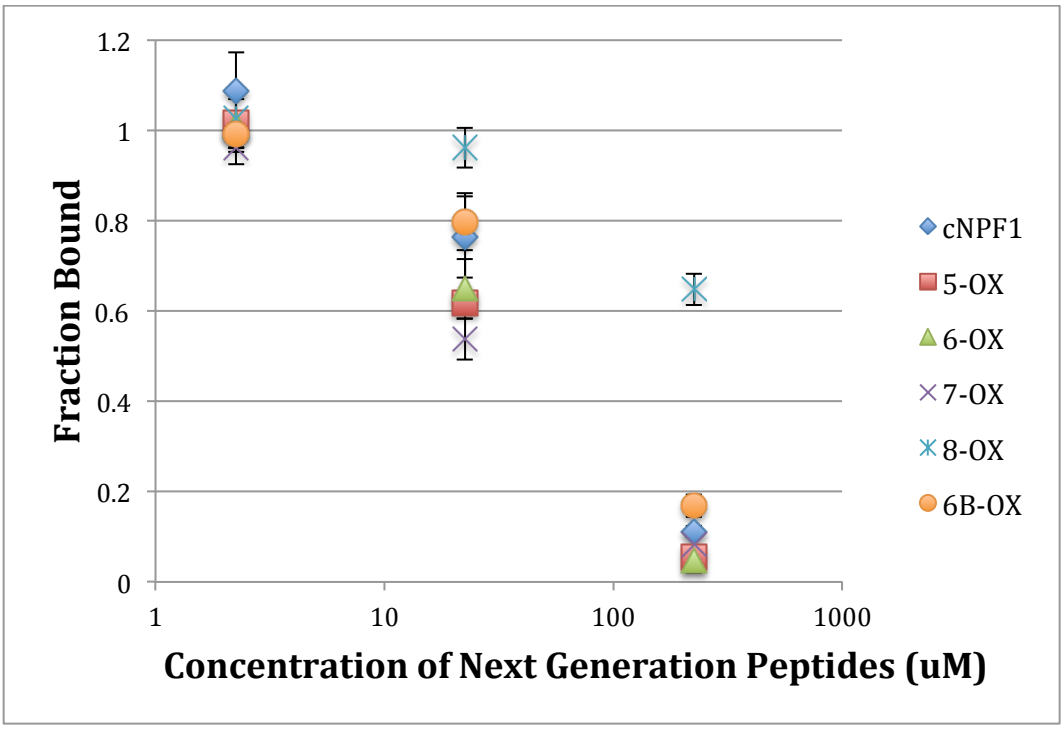

Figure 3.12. The data from the three-point screen of cyclic peptides derived from linear sequences 5-8. The error bars represent the standard deviation from three independent trials. Dr. Robyn Eisert contributed most of these data.

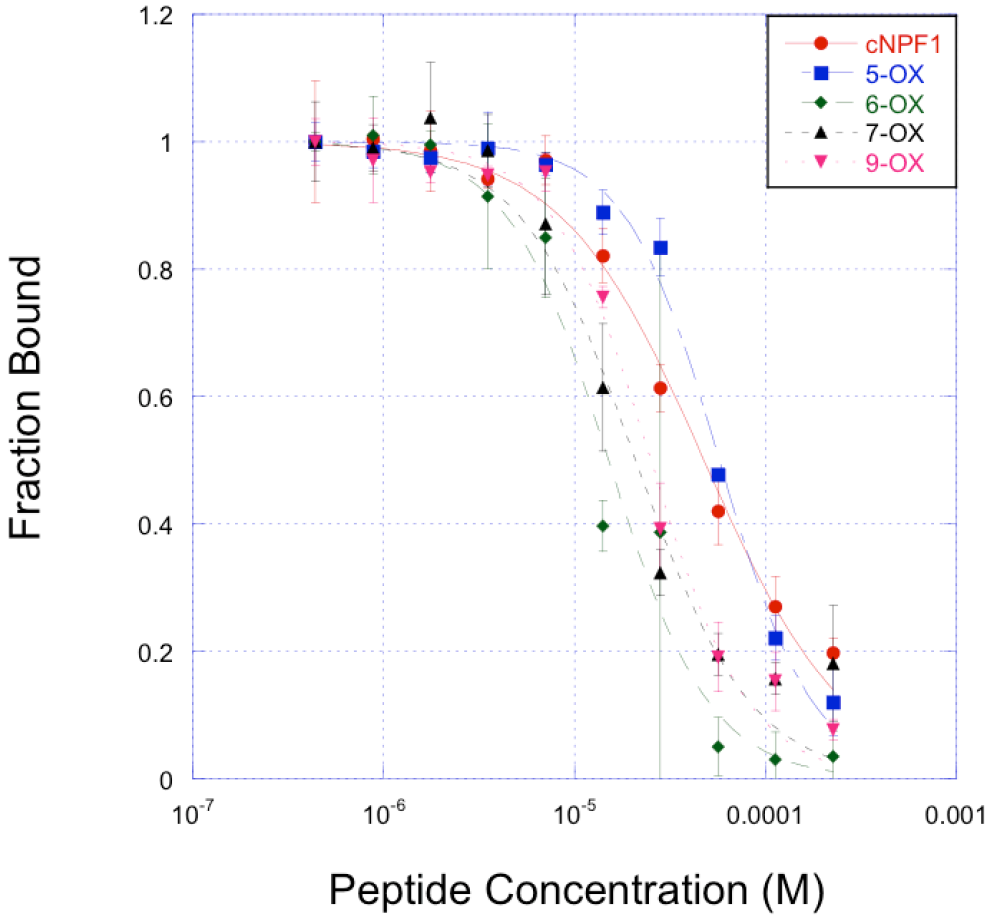

Figure 3.13. The inhibitory potency of the cyclic peptides derived from linear peptides 5-9. These competitive binding experiments were performed by Dr. Robyn Eisert. These peptides were identified as hits in the initial three-point screen. $cNPF1^{Flu}$ was used as the fluorescent probe. The experiments were done in 25 mM MOPS, pH = 6.8, with 15 mM NaCl. cNPF1-Flu had a final concentration of 10 nM while EHD1-EH had a final concentration of 20 μM. One representative trial for each peptide is shown, with error bars representing standard deviation of three technical replicates.

Peptide	Sequence	Linker	IC_{50} (μM)
cNPF1	-YNPFEEGG-	backbone	48.8 ± 5.4
5	Ac-CNPFEC-OH	OX	57.3 ± 0.3[a]
6	Ac-CNPFE(Pen)-OH	OX	12.8 ± 3.1[b]
7	Ac-CNP(1-Nal)EC-OH	OX	20.9 ± 0.3[a]
9	Ac-CNP(1-Nal)E(Pen)-OH	OX	25.1 ± 0.2[a]

Table 3.4. The IC_{50} values from the competitive binding assays of the peptides designed by Dr. Robyn Eisert. All peptides tested had similar or better inhibitory potency than the original cyclic peptide inhibitor, cNPF1. The IC_{50} reported is an average of the value from three independent experiments.

[a]This experiment has been performed once with three technical replicates, and will be repeated two independent times.

[b]This experiment has been performed in three technical replicates on two independent occasions, and will be repeated one more time.

Next, we tested 5-OX, 6-OX, 7-OX, and 9-OX in the full competitive binding assay. All four peptides inhibited EHD1-EH with a similar or greater potency than cNPF1 (Table 3.4). 5-OX, which has one glutamic acid and a free C-terminus, inhibited just as well as cNPF1, with an IC_{50} of 57.3 ± 0.3 μM. It seemed that keeping two negative charges C-terminal to the NPF motif was beneficial for inhibition. Replacement of the C-terminal cysteine residue with penicillamine, producing 6-OX, also proved to be beneficial. 6-OX had an IC_{50} of 12.8 ± 3.1 μM, the lowest value measured to date. Replacement of the phenylalanine of 5-OX with 1-Nal, a larger and more hydrophobic residue, also improved the affinity of the inhibitor. This peptide, 7-OX, had an IC_{50} of 20.9 ± 0.3 μM. We then combined the design improvements of 6-OX and 7-OX in a peptide with both 1-napthylalanine and a C-terminal penicillamine, sequence 9 (Table 3.4). 9-OX had an IC_{50} of 25.1 ± 0.2 μM, which was less potent than 6-OX or 7-OX. These individual changes did not appear to be additive. The most potent peptide of this series was thus 6-OX, which was roughly fourfold more potent than cNPF1.

3.6 Binding affinities of bis-alkylated EHD1-EH inhibitors

To further analyze our most promising cyclic peptides, we measured their direct binding affinity for EHD1-EH. To this end, an analog of each peptide was conjugated to 5(6) carboxyfluorescein succinimidyl ester (Table 3.4, Figure 3.14). A β-alanine residue was incorporated to serve as a linker between the cyclic

peptide and the fluorophore. Each fluorescently-labeled peptide was then used in an FP direct binding assay, and results were compared to cNPF1^{Flu}. The experiments were initially performed under low-salt conditions to ensure that the resulting binding curve fully saturated, to enable accurate K_d curve fits. Using the upper bounds established under low-salt conditions, we then repeated these experiments with 150 mM NaCl to measure the affinity under more physiologically relevant conditions.[89]

The trends observed for direct binding experiments matched the trends observed for competitive binding assays. Under low-salt conditions, Flu-1-PX and Flu-4-PX bound approximately twofold more tightly than cNPF1^{Flu}, with K_d's of 1.3 ± 0.1 μM and 2.0 ± 0.3 μM respectively (Figure 3.15, Table 3.5). Flu-3-OX had a similar or weaker affinity for EHD1-EH than the original cNPF1^{Flu} probe, with a K_d of 4.2 ± 0.5 μM. The weaker binding of Flu-3-OX was likely due to the fact that this peptide only contained one glutamic acid residue. Meanwhile, Flu-5-OX and Flu-7-OX bound with K_d values three-fold lower than cNPF1 (1.3 ± 0.1 μM and 0.90 ± 0.07 μM respectively, Figure 3.16). Flu-6-OX had the greatest target affinity of all the peptides tested. Under low salt conditions, it had a K_d of 0.55 ± 0.08 μM: a five-fold improvement over cNPF1^{Flu}.

We were then able to obtain saturated binding curves for the experiments at 150 mM NaCl (Figure 3.17-3.18). Flu-1-PX and Flu-4-PX had K_d values of 6.0 ± 0.5 μM and 8.1 ± 0.4 μM respectively (Table 3.5). Flu-3-OX bound EHD1-EH with

a K_d of 14.7 ± 1.3 μM, which was similar to the affinity of $cNPF1^{Flu}$. The highest affinity ligands under physiological salt conditions were those that had highest inhibitory potency in competitive binding experiments (Figures 3.16-3.17). Flu-5-OX, Flu-6-OX, and Flu-7-OX had K_d values of 7.2 ± 1.6 μM, 3.1 ± 0.2 μM, and 5.4 ± 0.5 μM respectively (Table 3.5). Based on our binding model, we hypothesize that the incorporation of penicillamine (6-OX) and the substitution of phenylalanine with 1-napthylalanine (7-OX) either produces peptides with more extensive binding contacts or generates favorable changes in the macrocycle conformation.

For the most part, the observed binding patterns for each cyclic peptide remained the same under both salt conditions tested. However, the affinities measured for Flu-3-OX did vary slightly when comparing the high and low salt assays. In 15 mM NaCl, Flu-3-OX had the lowest affinity for EHD1-EH out of all the peptides tested in this design iteration. Flu-3-OX's comparatively stronger affinity for the target under higher salt conditions was less surprising because this inhibitor only had one charged residue and was therefore less affected by the higher salt concentration. As a result, Flu-3-OX was also worth pursuing in cell-based experiments.

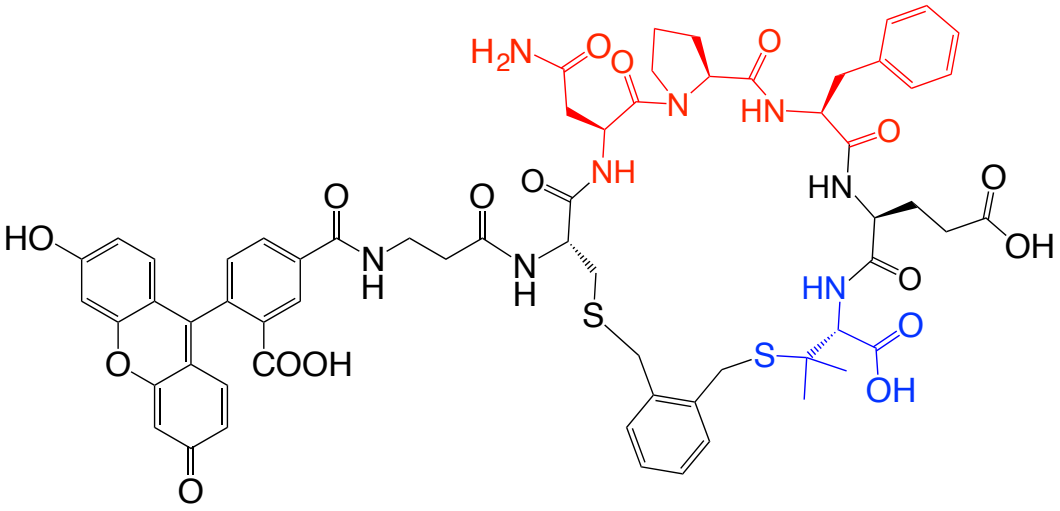

Figure 3.14. The structure of a representative bis-alkylated, fluorescently-labeled cyclic peptide. Flu-6-OX has been depicted, with a sequence of (FAM)-β-CNPFE(Pen)-OX. The NPF motif is shown in red, and the penicillamine has been highlighted in blue.

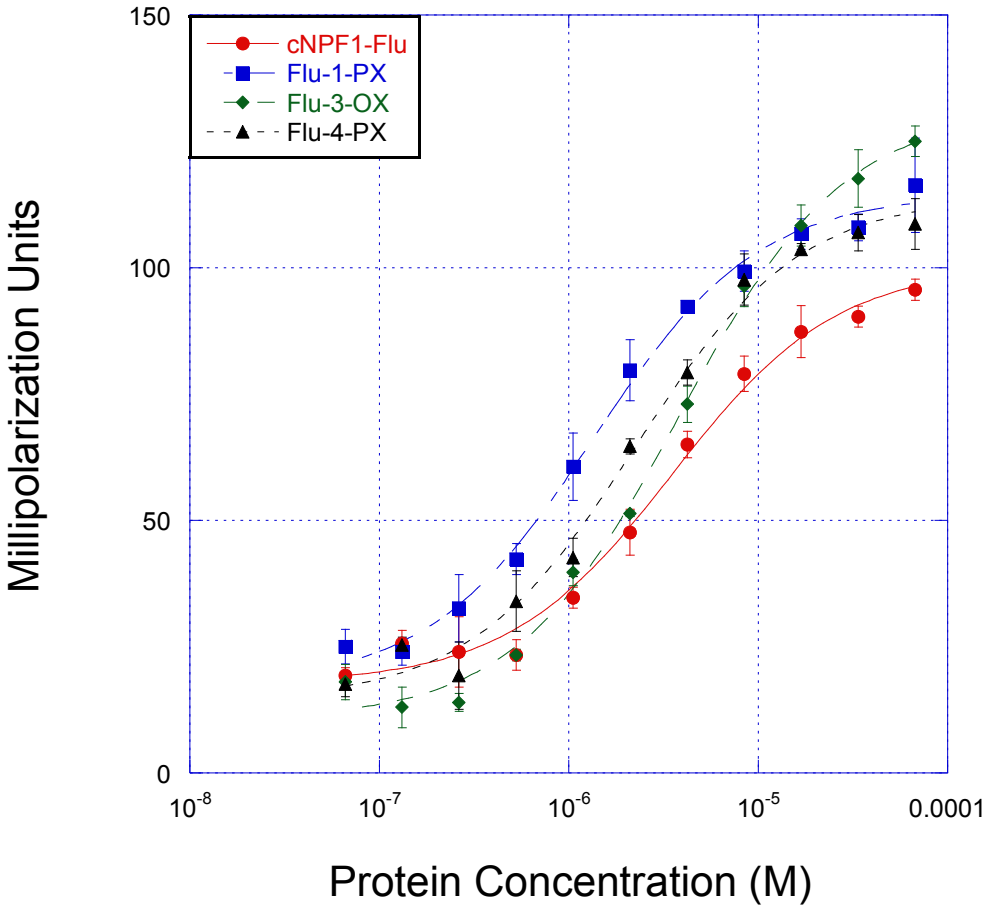

Figure 3.15. FP Direct binding experiments with Flu-1-PX, Flu-3-OX, and Flu-4-PX under low-salt (15 mM NaCl) conditions. The experiments were done in 25 mM MOPS, pH = 6.8, with 15 mM NaCl. The fluorescence polarization was measured 1 hour after addition of the probe, and then checked at the 4 hour time point to ensure equilibrium had been reached. One representative trial for each peptide is shown here, with error bars showing standard deviation among three technical replicates. Reported K_d values represent the average between two independent trials.

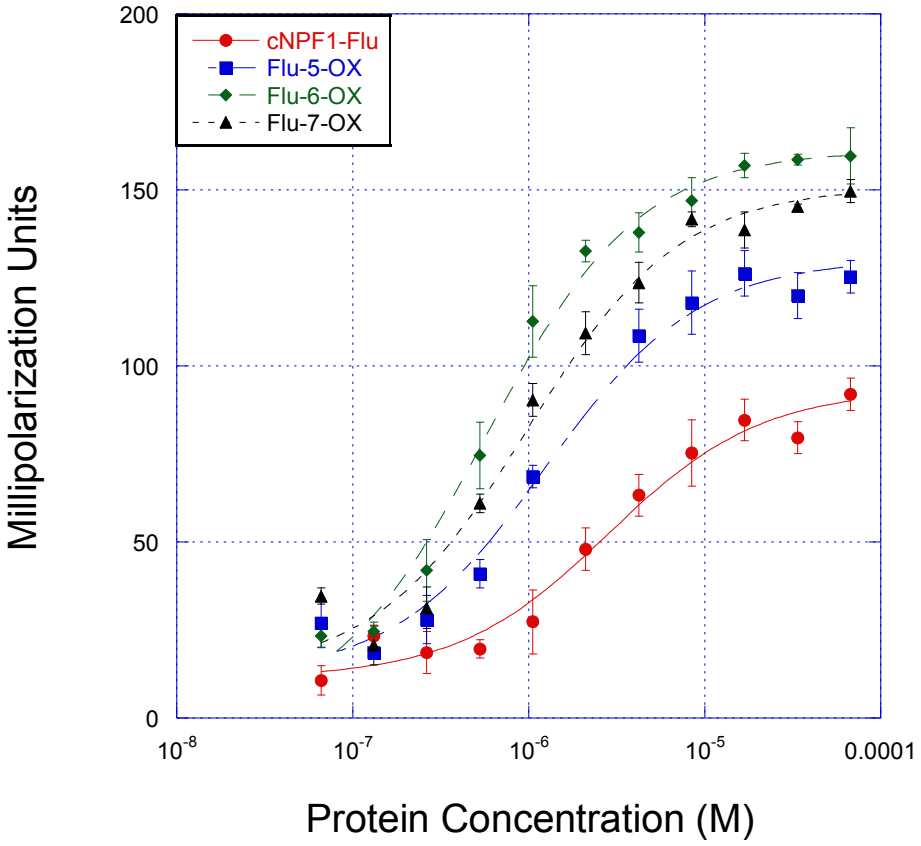

Figure 3.16. FP Direct binding experiments with Flu-5-OX, Flu-6-OX and Flu-7-OX under low-salt (15 mM NaCl) conditions. The experiments were done in 25 mM MOPS, pH = 6.8, with 15 mM NaCl. The fluorescence polarization was measured 1 hour after addition of the probe, and then checked at the 4 hour time point to ensure that equilibrium had been reached. One representative trial for each peptide is shown, with error bars showing standard deviation among three technical replicates. Reported K_d values represent the average among three independent trials.

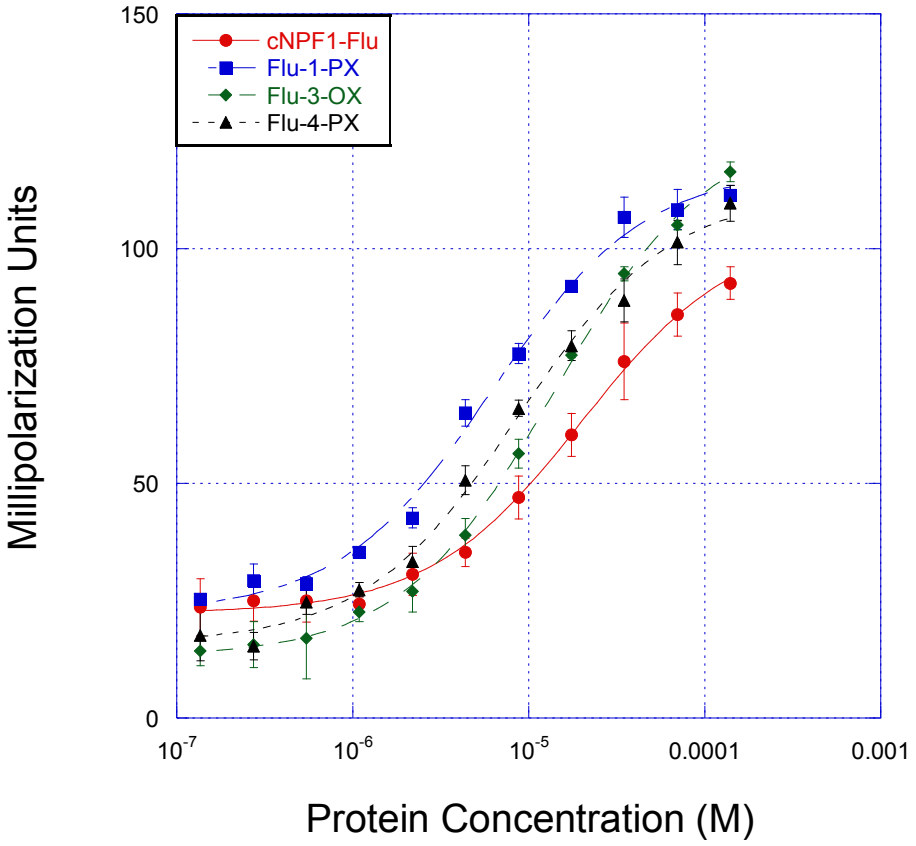

Figure 3.17. FP Direct binding experiments with Flu-1-PX, Flu-3-OX, and Flu-4-PX under physiological salt (150 mM NaCl) conditions. The experiments were done in 25 mM MOPS, pH = 6.8, with 150 mM NaCl. The fluorescence polarization was measured 1 hour after addition of the probe, and then checked at the 4 hour time point to ensure that equilibrium had been reached. One representative trial for each peptide is shown, with error bars showing standard deviation among three technical replicates. Reported K_d values represent the average among three independent trials.

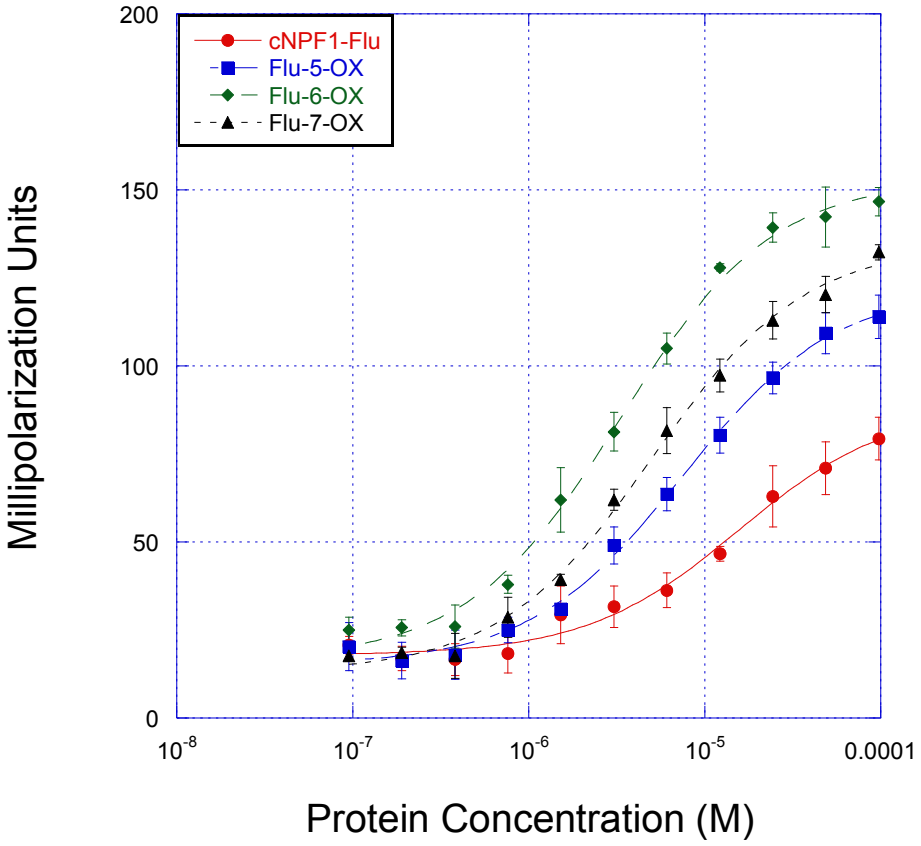

Figure 3.18. FP Direct binding experiments with Flu-5-OX, Flu-6-OX and Flu-7-OX under physiological salt (150 mM NaCl) conditions. The experiments were done in 25 mM MOPS, pH = 6.8, with 150 mM NaCl. The fluorescence polarization was measured 1 hour after addition of the probe, and then checked at the 4 hour time point to ensure that equilibrium had been reached. One representative trial for each peptide is shown, with error bars showing standard deviation among three technical replicates. Reported K_d values represent the average among three independent trials.

Peptide	Sequence	Linker	K_d (μM) 15 mM NaCl	K_d (μM) 150 mM NaCl
cNPF1^{Flu}	-YNPFEEGK(Flu)-	N/A	3.1 ± 0.6	15.2 ± 2.8
Flu-1-PX	Flu-β-CYNPFEE-(C*)	PX	1.3 ± 0.1[a]	6.0 ± 0.5
Flu-3-OX	Flu-β-CNPFE-(C*)	OX	4.2 ± 0.5[a]	14.7 ± 1.3
Flu-4-PX	Flu-β-CNPFEE-(C*)	PX	2.0 ± 0.3[a]	8.1 ± 0.4
Flu-5-OX	Flu-β-CNPFEC-OH	OX	1.3 ± 0.1	7.2 ± 1.6
Flu-6-OX	Flu-β-CNPFE(Pen)-OH	OX	0.55 ± 0.03	3.1 ± 0.2
Flu-7-OX	Flu-β-CNP(1-Nal)EC-OH	OX	0.90 ± 0.07	5.4 ± 0.5

Table 3.5. The sequences and direct binding data for bis-alkylated cyclic peptides. All peptides were tested alongside cNPF1^{Flu} as a control. The K_d value reported was an average of independent curve fits for each of three independent experiments. The error reported was the standard deviation of the three K_d values.

[a]Errors represent standard deviation from two independent experiments, each of which was an average of three technical replicates..

3.7 Conclusion

We first set out to develop cyclic peptide inhibitors of EHD1-EH, with the hypothesis that we could use cyclization to pre-organize the bound conformation of the NPF motif.[89] In this chapter, we applied a new synthetic strategy to allow for greater exploration of conformational space. The synthetic techniques adapted by Timmerman and Heinis were applied to the synthesis of cyclic peptides based on the YNPFEE motif.[92-93] This approach allowed us to explore multiple conformations and chemical spaces within the context of a single peptide sequence. Furthermore, the linkers were inexpensive and commercially available, which gave us the opportunity to incorporate linkers with varying shapes, sizes, and hydrophobicity. We were able to test this chemistry with four different NPF-containing peptide sequences to generate and test a small library of inhibitors.

We started with sequences that explored the necessity of the tyrosine and the necessity of the two glutamic acids. After testing the synthetic strategy with one of our sequences with a variety of linkers, we used the best-yielding linkers and reaction concentrations to synthesize larger quantities the more promising peptides. We synthesized a small library of cyclic NPF peptides and tested them in a three-point screen. Each of the four original sequences yielded at least one cyclic peptide worth testing further.

The results of the fluorescence polarization competitive binding assays confirmed structure-activity relationships for bis-alkylated peptides that were similar to those observed previously for head-to-tail cyclic peptides.[89] The presence or absence of a tyrosine residue did little to alter the peptides' affinities for the EH domain, but two negative charges were still required for highest inhibitory potency. One notable outlier was 4p-CNPFE-(C*)-OX (3-OX). This inhibitor was the only peptide containing a single negative charge that had an inhibitory potency close to that of cNPF1. 3-OX provided us with a unique opportunity to generate an EHD1-EH inhibitor with fewer charges, which is anticipated to be desirable in the long-term to promote eventual cell penetration. Meanwhile, most of the peptides that contained two charges bound with an affinity similar to that of cNPF1. However, we did identify three peptides that bound significantly more tightly than cNPF1. 4p-CNPFEE-(C*)-PX (4-PX) and 4p-CNPFEE-(C*)-2,6Pyr (4-2,6Pyr) had IC_{50} values more potent than cNPF1. 4p-CYNPFEE-(C*)-PX (1-PX) bound EHD1-EH twofold more tightly than cNPF1, making it our most effective peptide in this design iteration.

Although we had identified inhibitors more effective than cNPF1, we still sought molecules with a greater affinity for our target protein. The peptide series designed by Dr. Robyn Eisert provided another opportunity to develop additional inhibitors. In these peptides the C-terminus was left as a free acid to compensate for the charge usually provided by the second glutamic acid residue. These alterations alone were an excellent starting point to improve EHD1-EH affinity

over cNPF1, therefore we turned to other modifications. The replacement of the C-terminal cysteine with a penicillamine yielded a twofold improvement in binding affinity. We suspect that the introduction of the penicillamine in this position further stabilized the β-turn of the NPF motif. The substitution of phenylalanine with 1-napthylalanine (7-OX) improved the potency twofold over 5-OX. However, the combination of the penicillamine and the 1-napthylalanine replacements did not improve efficacy.

In the end, we used dye-labeled analogs to measure K_d values for our most promising EHD1-EH inhibitors. Flu-5-OX, Flu-6-OX, and Flu-7-OX had the greatest improvement over the original backbone cyclic NPF peptides, with K_d values in the single-digit micromolar range. Dynasore, an inhibitor of endocytosis, has an IC_{50} value of 15 μM in *in vitro* experiments, and this molecule is potent enough to elicit phenotypic effects in cell-based assays.[14] Since our inhibitors have similar potencies that are similar or better, we proceeded to test these inhibitors in mammalian culture to ascertain whether they selectively inhibit the long-loop recycling pathway. Such inhibitors would be useful for exploring the importance of this pathway in cancer cell motility and invasiveness.

3.8 Materials and methods

3.8.1 Synthesis of bis-alkylated cyclic peptides

The linear peptides were synthesized by standard Fmoc solid-phase peptide synthesis, and purified by reversed-phase HPLC on either a C8 or a C18 column (Chapter 2). Once the linear peptides were determined to be greater than 75% pure by analytical HPLC (C18), they were cyclized using the bis-alkylation techniques previously established in the literature (Scheme 3.1).[92-93, 94e] Synthesis of the cyclized peptides was attempted with dibromo-o-xylene (OX), dibromo-m-xylene (MX), dibromo-p-xylene (PX), 1,8 bis(bromomethyl)naphthalene (1,8-Nap), 2,6-bis(bromomethyl)naphthalene (2,6-Nap), 4,4-bis(bromomethyl-(1,1':3',1")terphenyl (Tph), 4,4- bis(bromomethyl)-biphenyl (4,4-BP), 2,2-bis(bromomethyl)-1,1'-biphenyl (2,2-BP), 1,4-dibromo-2,3-butanedione (but), and 2,6-bis(bromomethyl)pyridine (2,6-Pyr) as linkers. The reactions were quenched after 2 hours with the addition of trifluoroacetic acid until the buffer solution had a pH of 4.0, as determined with pH paper. The quenched mixture was then lyophilized to reduce the volume prior to purification. The bis-alkylated peptides were then purified by reversed-phase HPLC on either a C8 or a C18 column, and their purity was measured by reinjection on an analytical C18 column. Unless otherwise indicated, the yield of linear and cyclic peptides were determined by weight, due to the fact that many of them did not contain a UV active side chain.

Peptide	Sequence	Linker	Expected Molecular Weight (m/z)	Observed Molecular Weight (m/z)
cNPF1	-YNPFEEGG-	Backbone	893.4	894.4
cNPF1^{Flu}	-YNPFEEGK(FAM)-	Backbone	1322.5	1321.2
1	4p-CYNPFEE-(cysteamine)	OX	1142.3	1142.6
		MX	1142.3	1143.2
		PX	1142.3	1143.2
		2,6Pyr	1143.3	1143.6
		2,6Nap	1192.3	1192
		4,4BP	1218.4	See Robyn
2	4p-CYNPFE-(cysteamine)	OX	1013.2	1013.6
		MX	1013.2	1013.6
		PX	1013.2	1013.6
		2,6Pyr	1014.2	1014.6
		2,6Nap	1063.2	1063.9
		4,4BP	1089.3	1089.7
		But	993.1	993
3	4p-CNPFE-(cysteamine)	OX	850.0	850
		MX	850.0	851.0
		PX	850.0	850.5
		2,6Pyr	851.0	851.8
		2,6Nap	900.1	See Robyn
		4,4BP	926.1	926.6
		2,2BP	926.1	926.1
4	4p-CNPFEE-(cysteamine)	OX	979.1	979.3
		MX	979.1	979.5
		PX	979.1	979.6
		2,6Pyr	980.1	980.5
		2,6Nap	1029.2	1029.9
5	Ac-CNPFEC-OH	OX	856.0	856.4
6	Ac-CNPFE(Pen)-OH	OX	884.0	884.5
6B	Ac-(Pen)NPFEC-OH	OX	884.0	883.8
7	Ac-CNP(1-Nal)EC-OH	OX	906.0	906.7
8	Ac-CNP(2-Nal)EC-OH	OX	906.0	910
9	Ac-CNP(1-Nal)E(Pen)-OH	OX	934.1	934.1
Flu-1	(FAM)-β-CYNPFEE-(cysteamine)	PX	1491.6	1492.4
Flu-3	(FAM)-β-CNPFE-(cysteamine)	OX	1199.3	1199.4
Flu-4	(FAM)-β-CNPFEE-(cysteamine)	PX	1328.4	1328
		2,6Pyr	1329	1329

Flu-5	(FAM)-β-CNPFEC-OH	OX	1243.3	1244.0
Flu-6	(FAM)-β-CNPFE(Pen)-OH	OX	1271.4	1271.4
Flu-7	(FAM)-β-CNP(1-Nal)EC-OH	OX	1293.4	1294.4
Flu-9	(FAM)-β-CNP(1-Nal)E(Pen)-OH	OX	1321.4	1321.3

Table 3.6. The peptides synthesized as previously described. The masses of each product were determined by MALDI-TOF mass spectrometry or by ESI.

3.8.2 Protocol for the three-point screen of cyclic peptide inhibitors

The peptides were first tested in a three-point fluorescence competition assay. These peptides were assayed alongside cNPF1, as a control, using $cNPF1^{Flu}$ as a probe. The experiments were performed in 384 well black plates (Corning) in 25 mM MOPS, 1 mM $CaCl_2$, and 15 mM NaCl at a pH of 7.0 at 4°C.[89] The inhibitors were incubated with 20 μM EHD1-EH for 30 minutes at 20 °C, after which 10 nM $cNPF1^{Flu}$ was added. Fluorescence polarization was measured 1 hour after the addition of the probe (Tecan F200 Pro). The fluorescence polarization readings were taken at a final inhibitor concentrations of 225 μM, 25 μM, 2.5 μM, and 0 μM. The measurements were normalized to the values obtained for no inhibitor added (100% bound).

3.8.3 Fluorescence polarization competitive binding assay protocol

The concentration of each peptide had previously been determined by mass because half of the sequences did not contain tyrosine, and therefore could not have their concentrations measured by UV-Vis spectrometry. Consequently, the peptides identified from the three-point screens were subjected to amino acid analysis to obtain more precise concentrations. Using these more accurate concentrations, each peptide was tested under low-salt (25 mM MOPS pH = 6.8, 1 mM $CaCl_2$, 15 mM NaCl) conditions with $cNPF1^{Flu}$ as a probe and cNPF1 as a control. As with the three-point screen, the inhibitors were added to 20 μM EHD1-EH and incubated at room temperature for 30 minutes. Then the $cNPF1^{Flu}$ fluorescent probe was added to a final concentration of 10 nM, and the entire

mixture was incubated at room temperature. Fluorescence polarization was measured on a Tecan F200 Pro 1 hour after the addition of the probe, and repeat readings were taken 4 hours after probe addition to verify that binding had reached equilibrium. The IC_{50} curve fits were calculated with Kaleidagraph Synergy Software. Three independent experiments were performed, each of which was an average of three technical replicates.

3.8.4 Synthesis of fluorescently-labeled EHD1-EH probes

We synthesized variants of our cyclic peptides linked to a fluorophore, NHS-fluorescein, on the N-terminus (Table 3.5). A β-alanine was added between the N-terminal cysteine and the fluorescein to serve as a spacer between the binding sequence and the fluorophore. We synthesized the linear peptides and conjugated them to fluorescein on resin using standard techniques (Chapter 2.11.2). We then cleaved the linear peptides from the resin and purified them prior to cyclization using the conditions described in section 3.8.1. The purified linear peptides were bis-alkylated with the previously described protocols (3.8.1). The peptides were then purified by reversed-phase HPLC before being stored as a DMSO stock.

3.8.5 Protocol for the direct binding assays with bis-alkylated fluorescent probes

All experiments were performed in flat-bottom, black 384 well plates (Corning). The assay buffers (25 mM MOPS pH 7.0, 1 mM $CaCl_2$ at 4^{o}C) had a final sodium

chloride concentration of either 15 or 150 mM as needed. Each well had a final concentration of 1.5% DMSO and 0.1% Tween-20, which were added with the fluorescent probes. The MOPS buffer was confirmed to have a pH of 6.8 at 20^{o}C. Each probe was incubated at a final concentration of 10 nM at room temperature with varying concentrations of EHD1-EH. To ensure that all liquid was at the bottom of the well, the plates were spun at 1,600 G at 20^{o}C for 3 minutes. We measured the fluorescence polarization (Tecan F200 Pro) 1 hour after the addition of the probe, and a second time 4 hours after addition of the probe. We did not detect a difference in the data collected at the 1-hour and 4-hour time points. We used the data from the 1-hour time point for further analyses. Three or more independent trials were performed on each probe with each buffer condition. The K_d curve fits were derived from first principles (Equation 2.1), and calculated using non-linear regression software (Kaleidagraph, Synergy Software).

4 Chapter 4: The optimization and testing of bis-alkylated cyclic EHD1-EH inhibitors in mammalian culture.

4.1 Introduction

The development of an inhibitor specific to the long-loop recycling pathway would be helpful for studying vesicle trafficking in invasive cancers.[1, 70] We have selected a protein known to be involved in this pathway, EHD1, as a target for inhibition.[38] The inhibitors were based on known EHD1 binding partners containing the NPF motif.[62] By incorporating the NPF sequence into a cyclic peptide, we hypothesized that we could stabilize the binding epitope in its binding conformation, improving affinity of the resulting inhibitor.[89] Executing this strategy with head-to-tail cyclic peptides and, later, bis-alkylated cyclic peptides, we identified several peptides with single-digit micromolar affinity for EHD1.[92-93] While we had successfully identified inhibitors for this protein, we had yet to ascertain their effects on cells.

Cancerous cells adhere to the extracellular matrix (ECM) with focal adhesion complexes containing integrins.[1] Integrins are transmembrane proteins that link the cell to the ECM or neighboring cells.[1, 7d] Upon the disassembly of focal adhesion complexes, integrins are taken up by the cell and are either degraded in the lysosome or recycled back to the cell membrane.[1, 7d] During short-loop recycling, integrins are sorted to the early endosome (EE) and are trafficked back

to the cell surface within two minutes.[4, 8, 10] Long-loop recycling requires the integrins to be sent from the EE to the perinuclear recycling compartment (PNRC), where they remain until they are sorted back to the plasma membrane.[12, 98] The long-loop recycling process occurs over 15-20 minutes.[1, 7d] The disruption of long-loop recycling greatly inhibits cancer motility due to its involvement in polarized endocytic pathways in cancerous cells.[1, 38] The endosomal transport systems responsible for long-loop recycling also facilitate the movement of integrins to the advancing lamellipodium, the protruding portion of the cell surface that leads the cell's migration.[6] This polarization of endocytosis improves cancer cell motility by allowing these cells to advance in a specific direction.[6-7] Since vesicle trafficking and recycling pathways are clearly important for cell motility and invasiveness, inhibitors of these pathways can serve as a tool for improved understanding and control of these processes.

Another protein known to be recycled through the long-loop recycling pathway is transferrin, a protein responsible for iron transport and storage.[99] Upon binding the transferrin receptor, transferrin is internalized via endocytosis.[99] The bound transferrin then releases iron within the endosome, after which the receptor is recycled back to the cell surface.[99] Fluorescently-labeled transferrin has been used to track movement through endocytic pathways.[100] Indeed, fluorescently-labeled transferrin has been utilized to study the relative importance of EHD1 in the context of recycling from the PNRC.[100]

We chose to use the trafficking of transferrin as a model system to measure the effects of our inhibitors on the long-loop recycling pathway. This takes advantage of the well-understood trafficking of transferrin through the various vesicle trafficking pathways. In this chapter, we describe the optimization of an experiment to monitor the trafficking of fluorescently-labeled transferrin by flow cytometry and fluorescence microscopy. This experiment allowed us to evaluate the effects of our inhibitors by observing the location and amount of intracellular transferrin.

4.2 Mammalian culture studies of intracellular trafficking

In mammalian culture, vesicle trafficking experiments often involve pulse-chase experiments. First the cells are incubated with a labeled protein for a defined period of time, the "pulse."[101] The cells are then incubated with the same protein, but unlabeled, during the "chase" incubation.[101] This experiment allows one to directly observe a protein as it passes through a specific pathway during a specific time period. In the context of vesicle trafficking, one can monitor the passage of a labeled protein throughout its trafficking throughout the cell. Radiolabeled or fluorescently-labeled proteins are typically used for these experiments.[35a, 101] Pulse-chase experiments were used to examine the role of EHD1 in vesicle trafficking, using fluorescently-labeled transferrin and fluorescently-labeled antibodies to β1-integrins.[35a, 38, 42] In EHD1 knock-down HeLa cells and in EHD1 knock-out MEF cells, pulse-chase experiments demonstrated that EHD1 was

important to the process of the long-loop recycling of these proteins.[35a, 38, 42] We have adapted these protocols to test the effects of our cyclic peptide inhibitors in mammalian culture.

Several non-specific inhibitors have been explored in the context of endocytic recycling. Ionophores and weak bases, such as monensin, chloroquine, and primaquine have been used to inhibit the recycling pathways.[19b, 102] Many of these lysosomotropic agents, agents which prevent endosomal acidification, are weak bases that alter the pH within the endosome.[19b, 102] While they have been demonstrated to impede the recycling of labeled transferrin, they are not specific to the long-loop recycling pathway.[25a, 102] Indeed, primaquine is known to affect the secretory pathway, while monensin impacts the transport between endosomes and lysosomes.[23a, 25b] We used primaquine as a control to validate the pulse-chase assay, and as a basis of comparison for cyclic peptide EHD1 inhibitors.

4.3 Monitoring fluorescently-labeled transferrin by flow cytometry

We tested our peptides in HeLa cells, adapting previously established protocols to monitor effects on the long-loop recycling pathway (Figure 4.1).[25d, 38, 40a] We adopted the pulse-chase methodology for fluorescently-labeled transferrin, and monitored the cells with and without EHD1-EH inhibitor. The experiment was designed to measure the efficacy of an inhibitor by measuring the amount of intracellular fluorescently-labeled transferrin that remained at the end of the

procedure. An effective inhibitor would impede the long-loop recycling pathway, and prevent trafficking from the perinuclear recycling compartment back to the surface of the cell. As a result, the amount of intracellular fluorescently-labeled transferrin would build up in the PNRC, resulting in higher mean fluorescence of cells relative to the untreated cells. As a negative control, we included a short, 3 minute "mini-chase" with unlabeled transferrin. This step was included so that the unlabeled transferrin would outcompete any surface-bound, fluorescently-labeled transferrin. Consequently, any fluorescence detected was assumed to be intracellular.

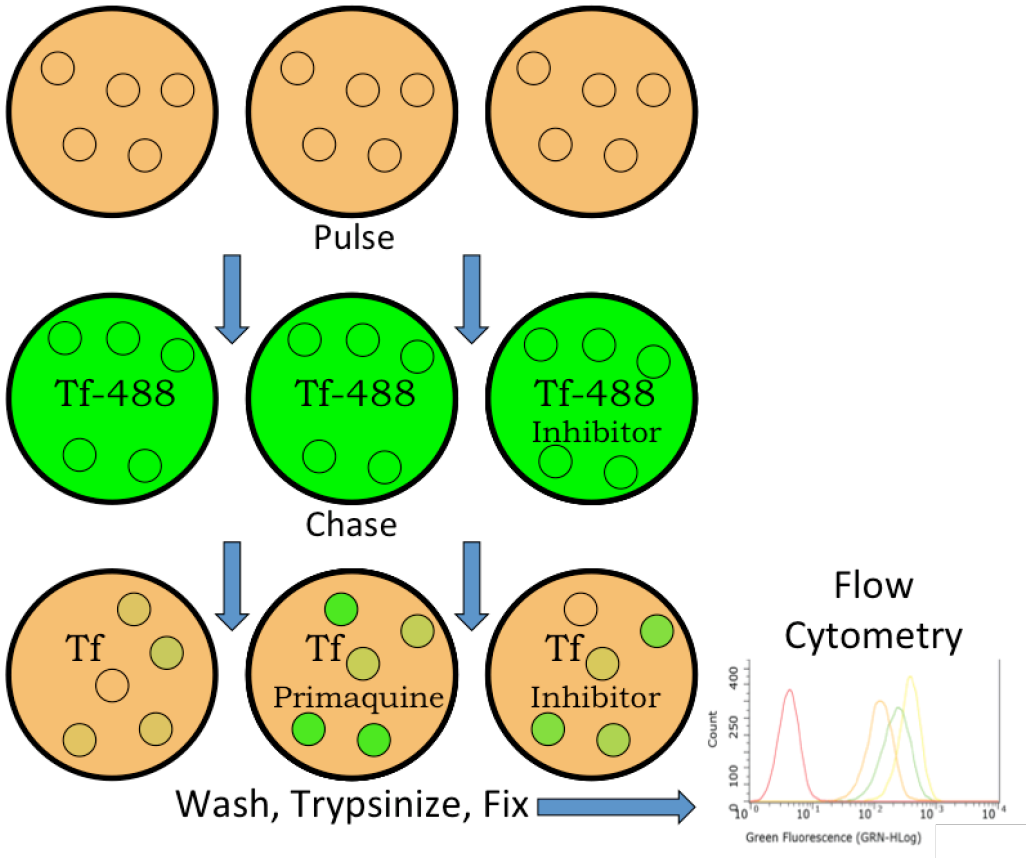

Figure 4.1. Pulse-chase experiments for analyzing effects on long-loop recycling. The incubation times and media components were optimized in conjunction with Jenna Walz and Dr. Robyn Eisert. Each large circle represents a well in the plate. The smaller circles represent the cells within the well.

The experiment used several controls (Figure 4.2). The autofluorescence of the control cells, which were only exposed to DMSO, is represented by the red histogram. The cells exposed to fluorescently-labeled transferrin and the "mini-chase" were represented by the yellow histogram. This yellow histogram illustrated the maximum amount of fluorescently-labeled transferrin that was able to enter the cell. The orange histogram corresponded to the negative control, in which the cells were pulsed and chased with no inhibitor. This histogram showed the amount of intracellular Tf-488 left at the end of the experiment. Lastly, the green histogram denoted the positive control, the cells pulsed and then chased with primaquine. The positive control demonstrated how the cells behave in the presence of an inhibitor; when recycling was impeded, the cells retained a larger amount of intracellular Tf-488. A successful inhibitor, like the positive control, would produce a histogram with greater fluorescence than the negative control, approaching the histogram representing the greatest amount of internalized Tf-488.

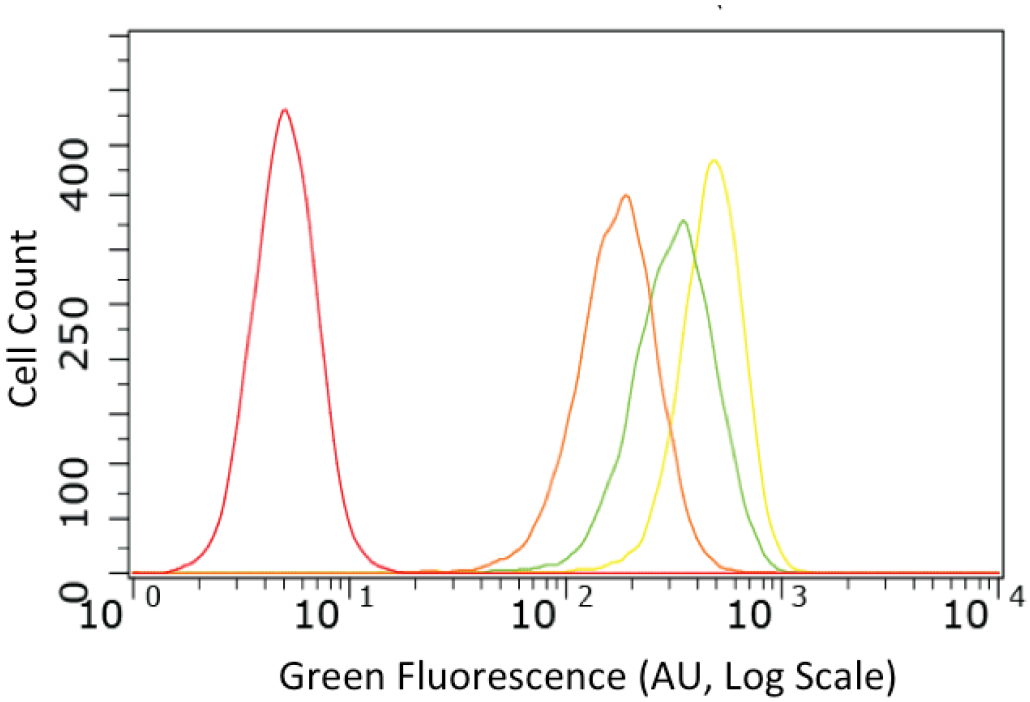

Figure 4.2. Flow cytometry data for the experimental controls. The red histogram is data from cells not treated with labeled transferrin, and thus represents the autofluorescence of the HeLa cells. The yellow histogram is data from cells pulsed with Tf-488 followed by the "mini-chase." The orange histogram is data from cells pulsed with Tf-488 followed by the 30-minute chase with unlabeled transferrin. The green histogram is data from cells treated with primaquine in the pulse and chase steps. This represents a positive control for the assay. 10,000 cells were counted for each histogram.

4.4 Optimization of the protocol for the flow cytometry experiments

When adapting the pulse-chase experiments, we focused on several factors to optimize the protocol.[25a, 38, 42] The pulse incubation was kept at 60 minutes to allow enough time for the fluorescently labeled transferrin to saturate the relevant vesicle trafficking pathways. We explored 30-minute and 60-minute times for the chase incubation (Figure 4.3). While the longer chase time allowed for a better separation between peaks, the separation obtained after the 30-minute chase allowed for more of the Tf-488 to remain intracellular as a point of comparison.

We next varied the concentration of fluorescently labeled transferrin added during the pulse step (Figure 4.4). We tested concentrations of Tf-488 ranging from 1 to 25 μg/mL.[38] At 1 μg/mL, we achieved a significant separation between untreated, chased cells and cells chased with primaquine. We saw similar separation between cells chased with primaquine and cells subject to a "mini-chase" (cells incubated with unlabeled transferrin for three minutes to remove surface-bound Tf-488). All three assay conditions achieved similar peak separations, but the signal was much greater with the higher Tf-488 concentration. As a result, we chose to pursue the remaining experiments with a Tf-488 concentration of 25 μg/mL.

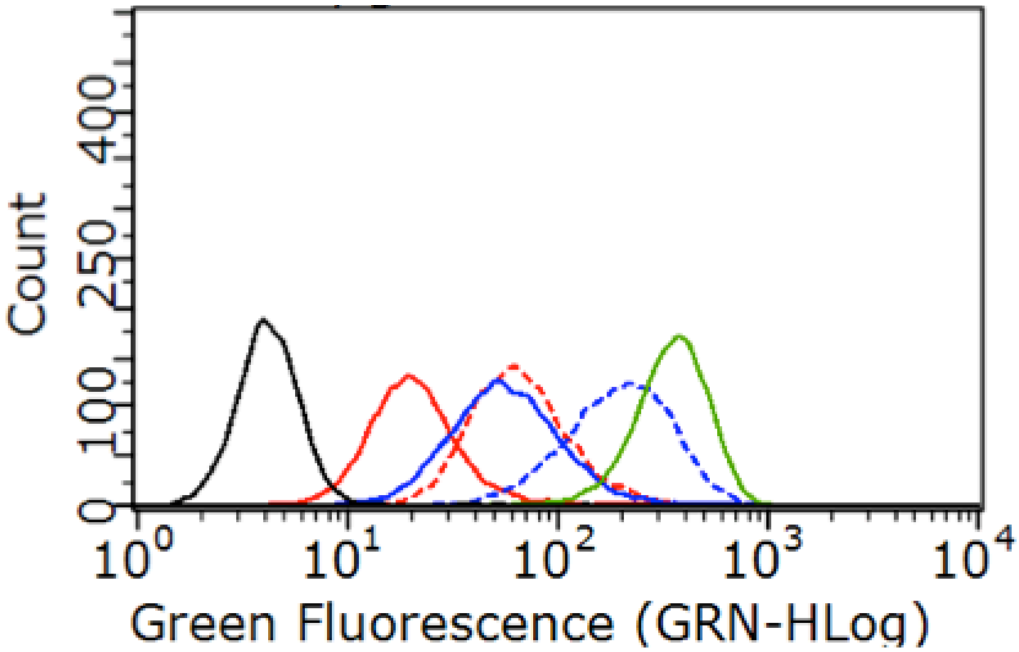

Figure 4.3. Optimization of the length of time for the chase incubation. This experiment was performed by Dr. Robyn Eisert. Lines represent histograms, for which 10,000 cells were counted. The black line shows the autofluorescence of the HeLa cells. The green line shows HeLa cells pulsed with Tf-488, but without the full chase incubation. The red solid line shows cells pulsed with Tf-488, followed by a 60-minute chase with unlabeled Tf. The red dotted line shows cells pulsed with Tf-488, followed by a 60-minute chase with unlabeled Tf and 60 μM primaquine., The blue solid line shows cells pulsed with Tf-488, followed by a 30-minute chase with unlabeled Tf. The red dotted line shows cells pulsed with Tf-488, followed by a 30-minute chase unlabeled Tf and 60 μM primaquine.

We next optimized the concentration of primaquine to establish a good positive control. For these experiments, we teamed up with the Mace laboratory to take advantage of the cell culture expertise of graduate student Jenna Walz. We ran the experiments with 40 μM, 50 μM, 60 μM, and 70 μM primaquine during the chase incubations (Figure 4.5). Each of these concentrations impeded recycling of the Tf-488 out of the cell, as evidenced by the histograms with increased fluorescence relative to untreated cells. Imaging of the cells on a Leica DMi8 microscope indicated that higher concentrations of primaquine were toxic to the cells (Figure 4.6). As a result, we chose to work at primaquine concentrations of 50 μM to maximize the efficacy of the inhibitor and minimizing toxicity. To promote cell viability, we incorporated 0.5% w/v BSA during the serum starvation and the pulse incubation steps.[38]

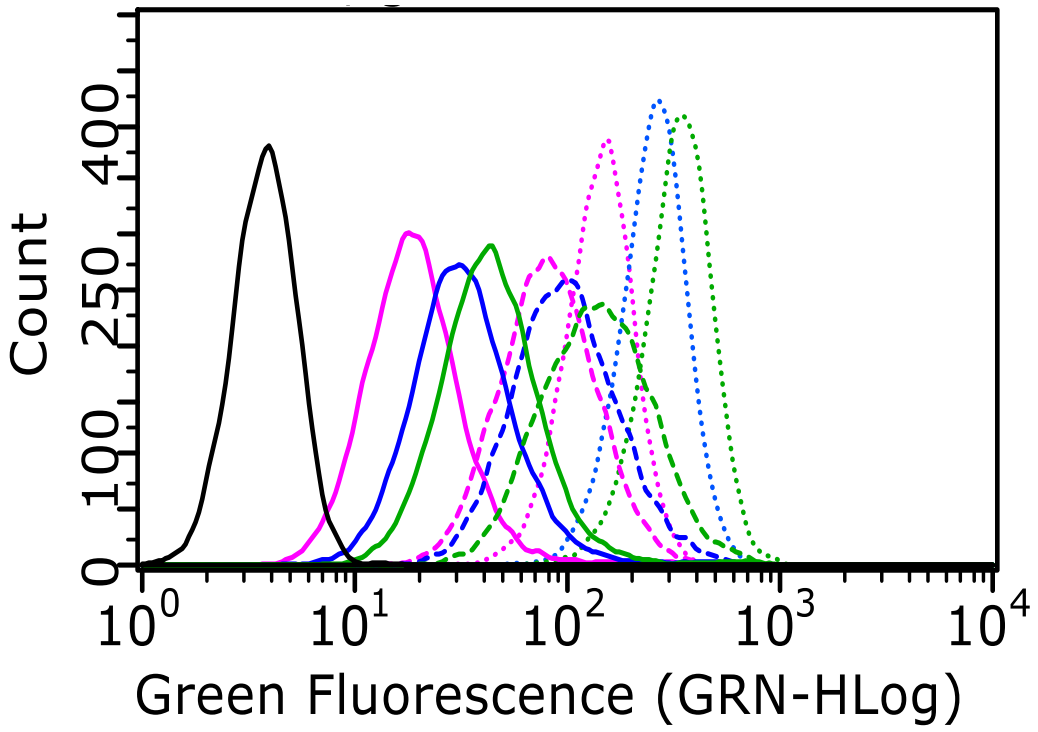

Figure 4.4. Optimization of the concentration of fluorescently-labeled transferrin (Tf-488) in the cell-based assays. Each experiment counted 10,000 cells. The magenta histograms corresponded to the cells incubated with Tf-488 at 1 μg/mL. The blue histograms denoted the cells pulsed with 5 μg/mL Tf-488. The green histograms represented the cells pulsed with 25 μg/mL Tf-488. The magenta, blue, and green solid-lined histograms represented the cells pulsed with Tf-488 and chased with unlabeled transferrin only. The histograms shown in the dashed lines denoted the cells pulsed with Tf-488 and chased with unlabeled transferrin and primaquine. Lastly, the histograms with the dotted lines were for the cells subject to the pulse and the "mini-chase." Each experiment was set to count 10,000 cells. Primaquine concentrations were 60 μM in each chase.

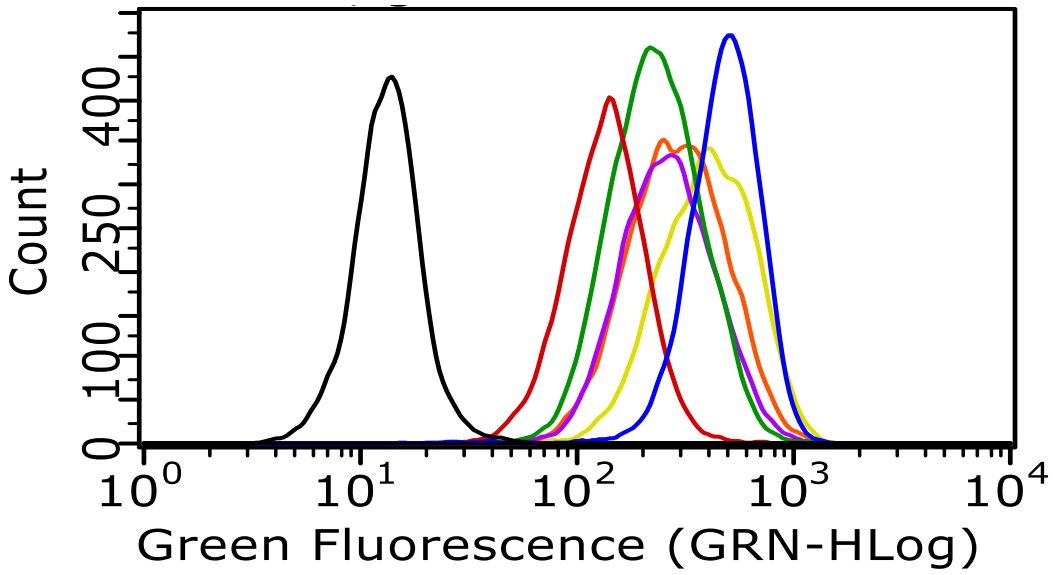

Figure 4.5. Optimization of the concentration of primaquine used as a positive control. Each experiment counted 10,000 cells. The black histogram denoted the autofluorescence of the HeLa cells, while the blue histogram represented the total internalized Tf-488 after the pulse and a "mini-chase." The red histogram was the signal obtained from the cells pulsed and chased with no inhibitor. The green histogram represented the cells chased with 40 μM primaquine. The purple histogram displayed the results from the cells incubated with 50 μM primaquine. The signal from the cells subject to 60 μM primaquine and 70 μM primaquine were shown in orange and yellow respectively. This experiment was performed with Jenna Walz.

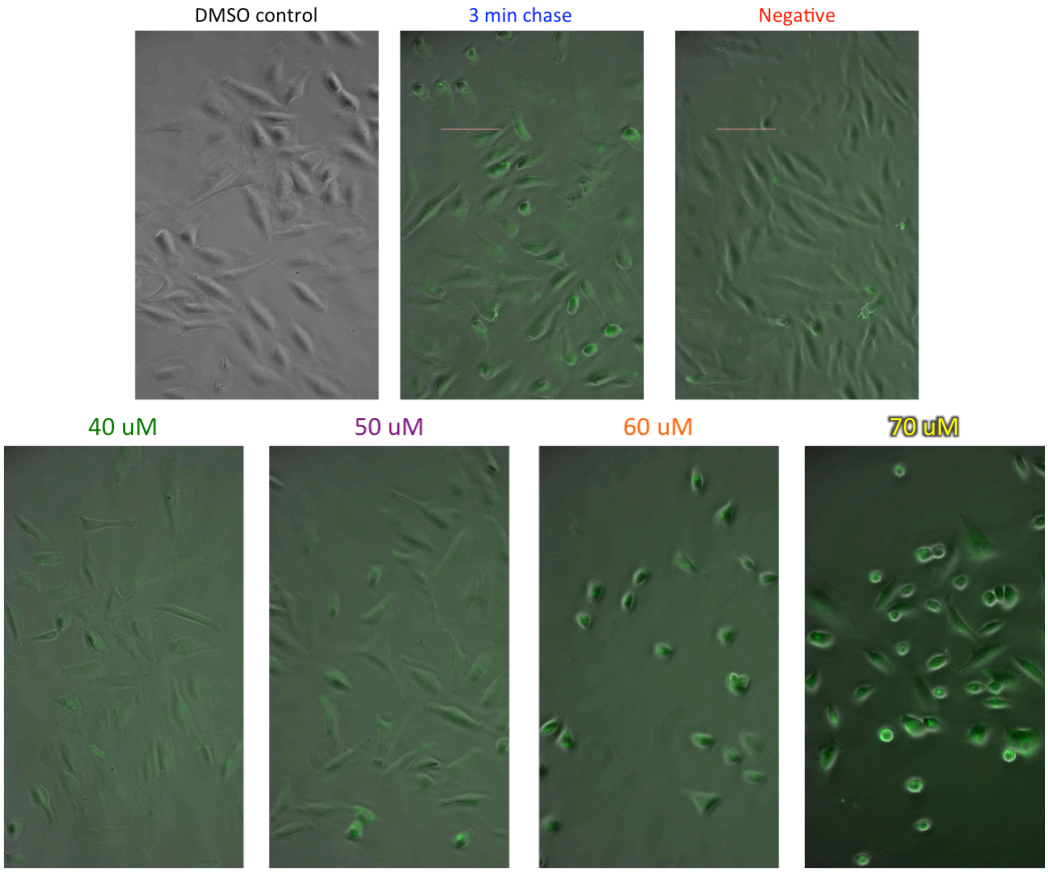

Figure 4.6. Fluorescence microscopy of cells from transferrin recycling experiments with increasing concentrations of primaquine. The experiments were performed with 25 µg/mL Tf-488. The images were taken on a Leica DMi8 microscope at a magnification of 20X. The cells were chased with 40 to 70 µM primaquine, as labeled. This experiment was performed by Jenna Walz.

4.5 Cyclic peptides had no effect on HeLa cells

Next, we tested our cyclic peptide EHD1-EH inhibitors in the optimized HeLa cell assay to determine their effects on long-loop recycling. We incubated the cells with 50 μM peptide during both the pulse and the chase. We added the peptide during both of these incubations to maximize the amount of time the inhibitors had to enter the cell, bind EHD1, and elicit an effect on vesicle trafficking. We tested the cells with cNPF1, 1-PX, and 5-OX (Figures 4.7 – 4.8, Table 4.1). These peptides represented some of the tightest-binding EHD1-EH inhibitors, with K_d values that ranged from 6 to 19 μM. While each of the peptides was tested at a concentration higher than their target affinity, they did not affect the trafficking of Tf-488. If anything, 1-PX slightly increased TF-488 recycling. However, the difference between the mean fluorescence of cells with and without 1-PX is small (Figure 4.8). It is likely that the peptides were ineffective because they were unable to penetrate the plasma membrane to interact with the target protein, which is cytosolic. Consequently, we needed to find a means of making these peptides more cell-penetrant.

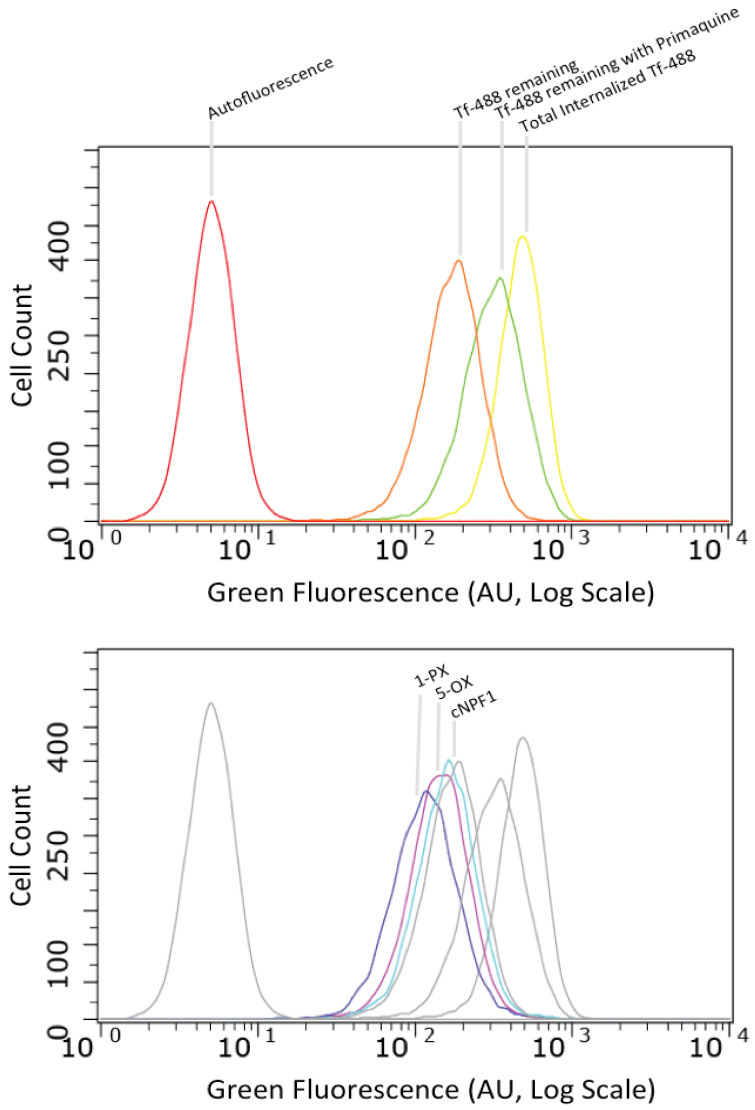

Figure 4.7. Cell-based experiments testing 50 μM of 1-PX, 5-OX, and cNPF1. (Top) The experimental controls for the flow cytometry experiments. The red histogram represented the autofluorescence of the HeLa cells. The yellow histogram denoted the total internalized Tf-488 after a pulse incubation, but without a chase. The orange histogram corresponded to the cells subject to a pulse and chase with no inhibitor, and represented the remaining internalized Tf-488 without perturbation as a negative control. As a positive control, shown in green, cells were pulsed and then chased with primaquine (60 μM), a non-specific recycling inhibitor. (Bottom) The respective controls established in the top image were shown in gray. The navy histogram represented the fluorescence from the cells incubated with 1-PX. The purple histogram corresponded to the fluorescence from the cells tested with 5-OX. Lastly, the light blue histogram was the signal from the cells incubated with cNPF1. These experiments were done in duplicate on two different days. One representative experiment is shown for each.

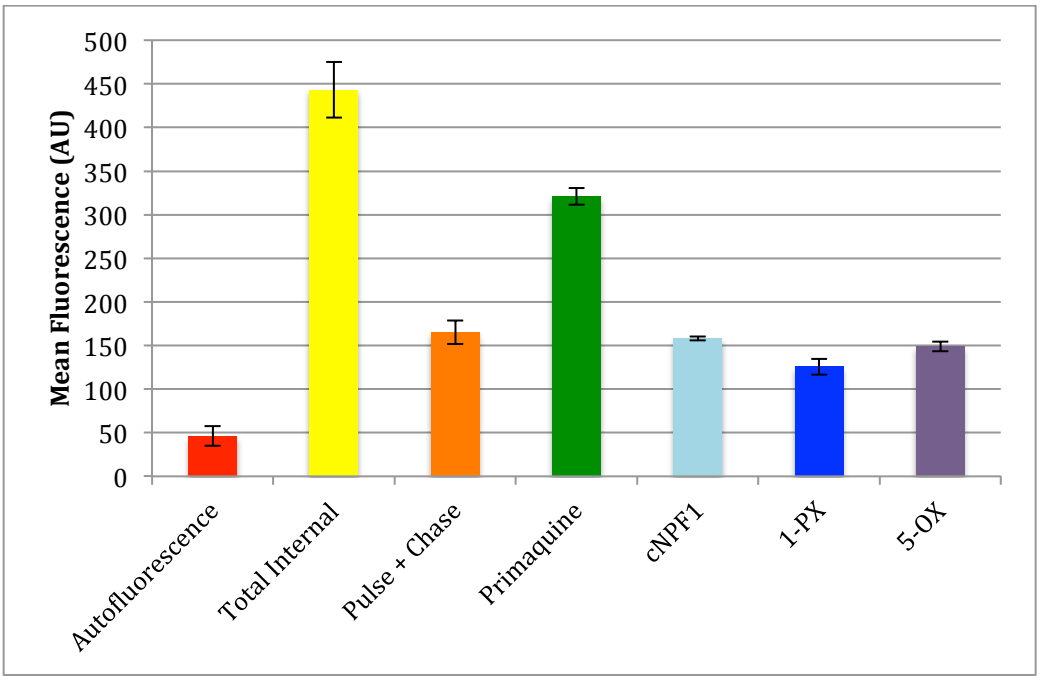

Figure 4.8. Bar graph representation of the mean fluorescence obtained from the flow cytometry experiments with cyclic peptides. The colors match the corresponding histograms of Figure 4.7. The experiments were completed in technical duplicates on two independent occasions. The error bars represented the standard deviation from these two trials.

Peptide	Sequence	Linker
cNPF1	-YNPFEEGG-	backbone
1-PX	4p-CYNPFEE-(C*)	PX
5-OX	Ac-CNPFEC	OX
6-OX	Ac-CNPFE(Pen)	OX
TAT-1-PX	YRGKKRRQRRR-ββ-CYNPFEE-(C*)	PX
TAT-6-OX	YRGKKRRQRRR-ββ-CNPFE(Pen)	OX
TAT-6scr-OX	YRGKKRRQRRR-ββ-CFPNE(Pen)	OX
TAT-7-OX	YRGKKRRQRRR-ββ-CNP(1-Nal)EC	OX
TAT-9-OX	YRGKKRRQRRR-ββ-CNP(1-Nal)E(Pen)	OX

Table 4.1.The names and sequences of the peptides used in cell-based experiments. The C* denoted the cysteamine on the C-terminus. Unless otherwise indicated, the linear peptides had a free C-terminus. 4p denotes 4-pentynoic acid, and Ac denotes the acetyl cap on the N-terminus.

4.6 Improving the cell penetration of cyclic peptide inhibitors

We hypothesized that the failure to impede transferrin recycling was a consequence of the peptides' inabilities to enter the cell.[75a-c, 78, 103] Cyclization has been used to promote the cell-penetrating capabilities of peptides due to the removal of additional charged groups and its potential to promote additional internal hydrogen bonds.[75a-c, 78, 103] However, in this design series, cyclization did not appear to generate a cell-penetrant EHD1 inhibitor. As a result, we turned to other strategies.

Cell-penetrating peptides (CPPs) are a class of peptides with the unique ability to deliver conjugated cargo to the interior of cells.[104] CPPs typically contain several positively-charged amino acids, particularly arginine due to the capacity of its guanidinium group to interact with the surface of the plasma membrane.[104] These peptides are capable of participating in both active and passive transport, entering the cell via endocytic mechanisms as well as passively permeating the cell membrane.[104] The HIV-1 transactivator of transcription (TAT, sequence YGRKKRRQRRR) provided the first and most well-studied CPP.[105] This CPP has been used to transport small molecules, peptides, and larger proteins to the interior of cells.[105] Therefore, we conjugated TAT to our best EHD1 ligands. We synthesized the peptides with the TAT sequence on the N-terminus, with two β-alanine residues separating the binding sequence from the cell-penetrating sequence (Table 4.1). This linker was included to minimize the effects of TAT

on the inhibitors' activities, and to minimize effects of the peptides on TAT's cell-penetrating capabilities.

4.7 TAT-linked bis-alkylated cyclic peptides do not impede the long-loop recycling of Tf-488.

With the transferrin recycling protocol optimized, we were ready to test our TAT-linked peptides in mammalian culture (Table 4.1). We incubated the HeLa cells in media with 5 μM of TAT-6-OX, TAT-7-OX, or TAT-9-OX during both the pulse and the chase. We also tested a scrambled version of the TAT-linked cyclic peptide, TAT-6scr-OX, as an additional control. The cells incubated with TAT-6scr-OX did not have any effects on Tf-488 recycling (Figure 4.9). Thus, we concluded that the TAT sequence alone did not affect transferrin trafficking. Fluorescence micrographs of the cells incubated with TAT-7-OX also suggest that this peptide did not impact vesicle trafficking. The cells exposed to TAT-6-OX and TAT-9-OX appeared to have accumulated a marginally greater amount of visible fluorescently-labeled transferrin compared to the cells of the negative control (Figures 4.9-4.11). Qualitatively, it appeared that more Tf-488 remained endosomally localized, resulting in more fluorescent puncta.

Meanwhile, the quantitative data produced by the flow cytometry experiments demonstrated that any detected change by microscopy was insignificant. No effects on Tf-488 recycling were observed at 5 or 10 μM TAT-6-OX, TAT-6scr-

OX, TAT-7-OX, or TAT-9-OX. We also tested TAT-1-PX (Figures 4.12-4.13) under identical conditions, and this peptide did not affect transferrin recycling. These results might indicate that the peptides did not efficiently enter the cells, that the TAT peptide was altering the peptides' activities or trapping them within the endosome, that they did not have strong or specific enough binding to EHD1, or that EHD1-EH binding did not have the anticipated effect on long-loop recycling.

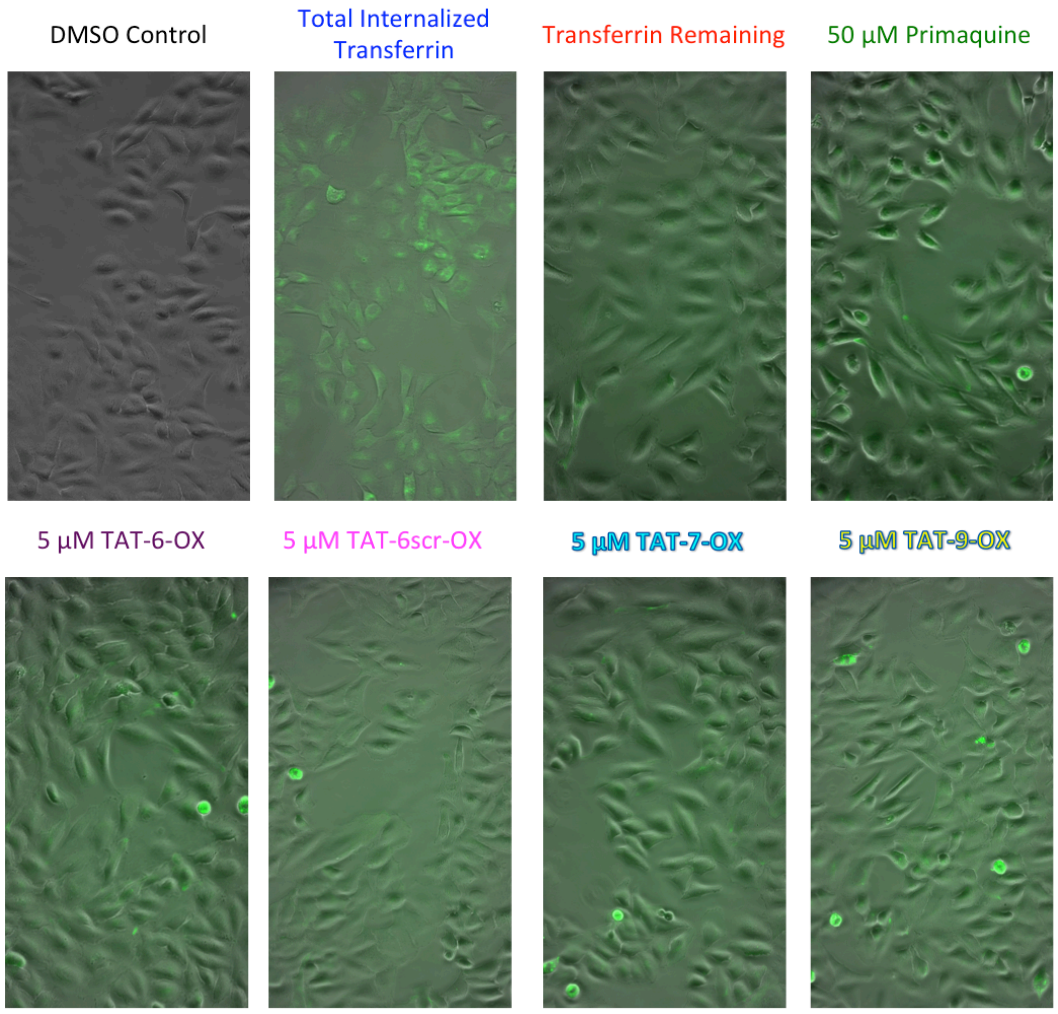

Figure 4.9. Fluorescence micrographs of transferrin recycling experiments with TAT-linked cyclic peptides. The experimental controls are shown in the top row, while the cells incubated with peptide are shown in the bottom row as labeled. The images were taken on a Leica DMi8 microscope at a magnification of 20X. The images were taken by Jenna Walz.

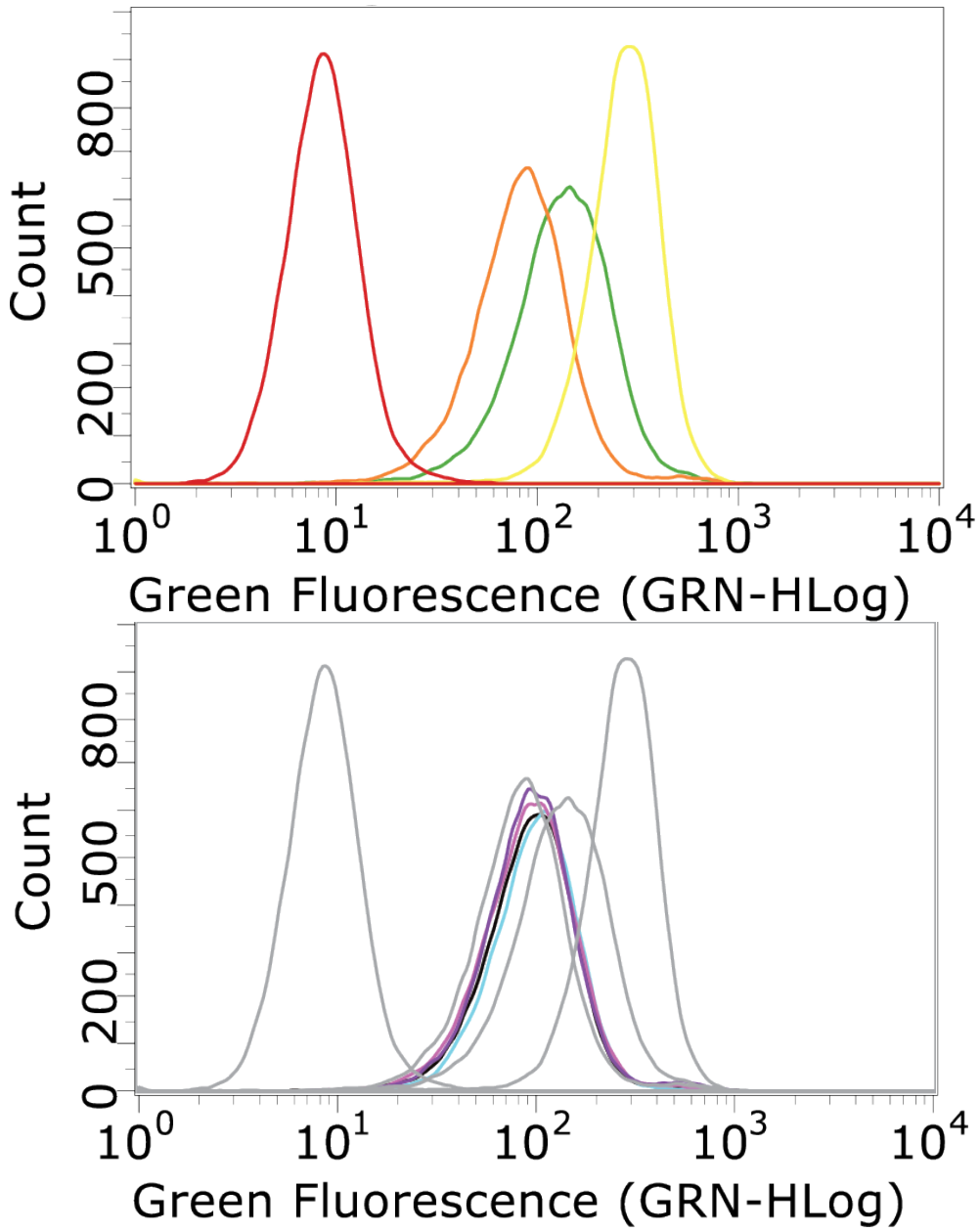

Figure 4.10. Flow cytometry analysis of transferrin recycling experiments with TAT-linked cyclic peptides. These experiments were performed by Jenna Walz. (Top) Controls used for the flow cytometry experiments. The red histogram represented the autofluorescence of the HeLa cells. The yellow histogram denoted the cells exposed to the shorter 3-minute chase, which demonstrated the maximum amount of internalized Tf-488. The cells pulsed and chased with unlabeled transferrin were shown in orange, while the cells pulsed and then chased with primaquine were represented by the green histogram. (Bottom) The controls, shown in grey, have been displayed alongside the experiments of the peptides in mammalian culture. The purple, pink, black, and dark green histograms represented the cells tested with TAT-6-OX, TAT-6scr-OX, TAT-7-OX, and TAT-9-OX respectively.

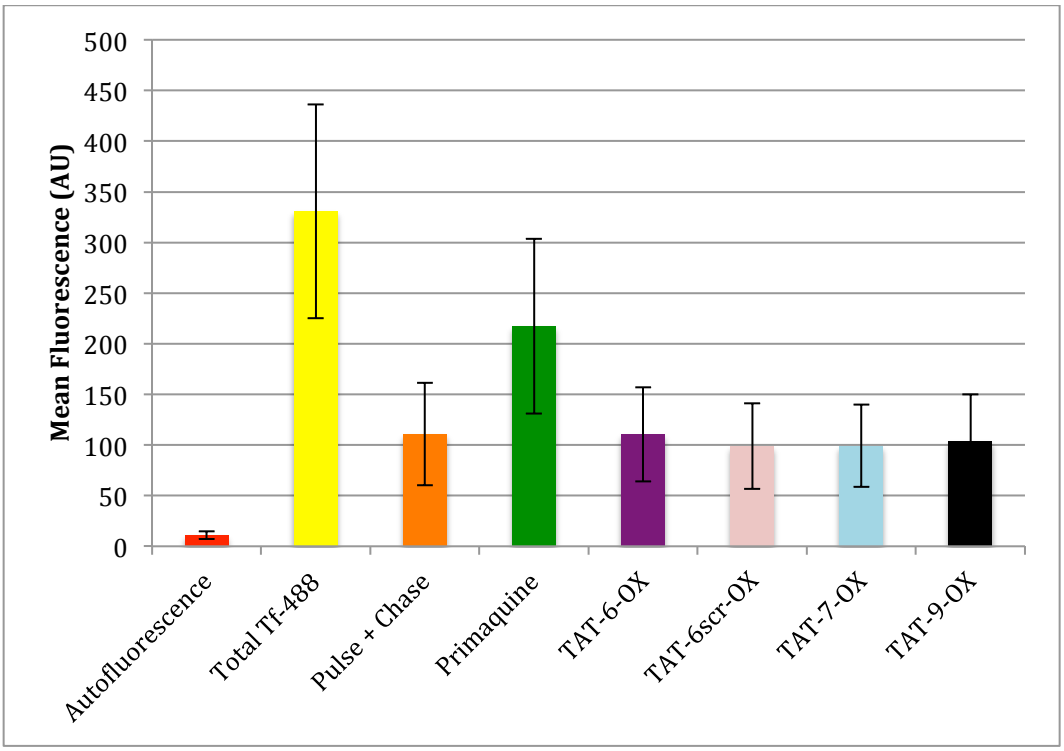

Figure 4.11. Bar graph representation of the mean fluorescence obtained from the flow cytometry experiments with TAT-linked cyclic peptides. The colors match the corresponding histograms of Figure 4.10. The error bars represented the standard deviation of 10,000 cells.

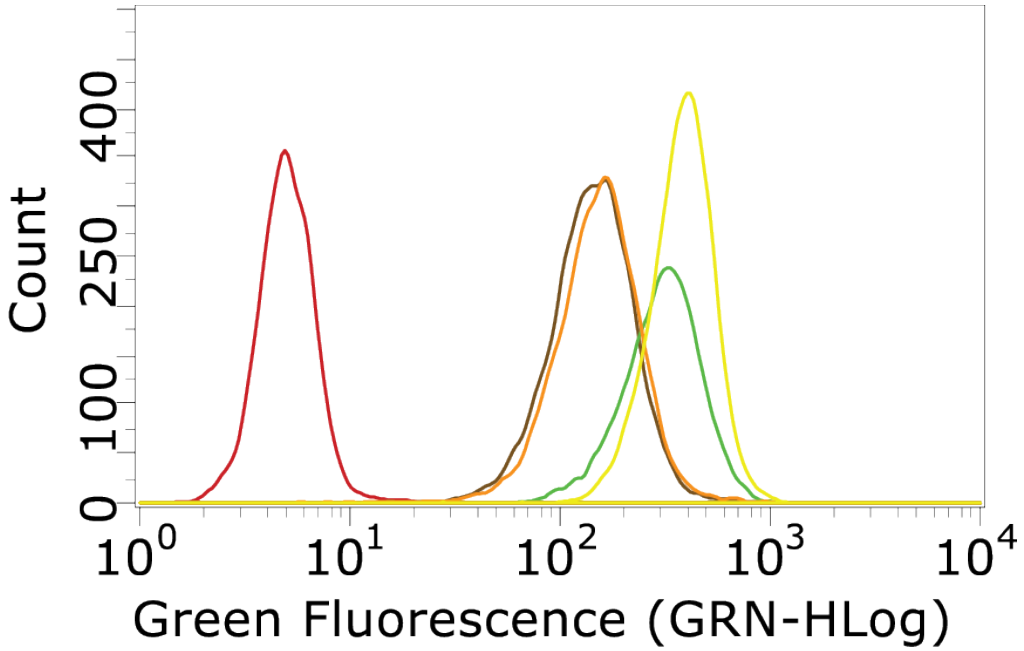

Figure 4.12. Flow cytometry experiments with TAT-1-PX. These experiments were performed by Jenna Walz. The red histogram represented the autofluorescence of the HeLa cells. The yellow histogram denoted the cells exposed to the shorter 3-minute chase, which demonstrated the maximum amount of internalized Tf-488. The cells pulsed and chased with unlabeled transferrin were shown in orange, while the cells pulsed and then chased with primaquine were represented by the green histogram. The brown histogram represented the cells incubated with 10 μM TAT-1-PX.

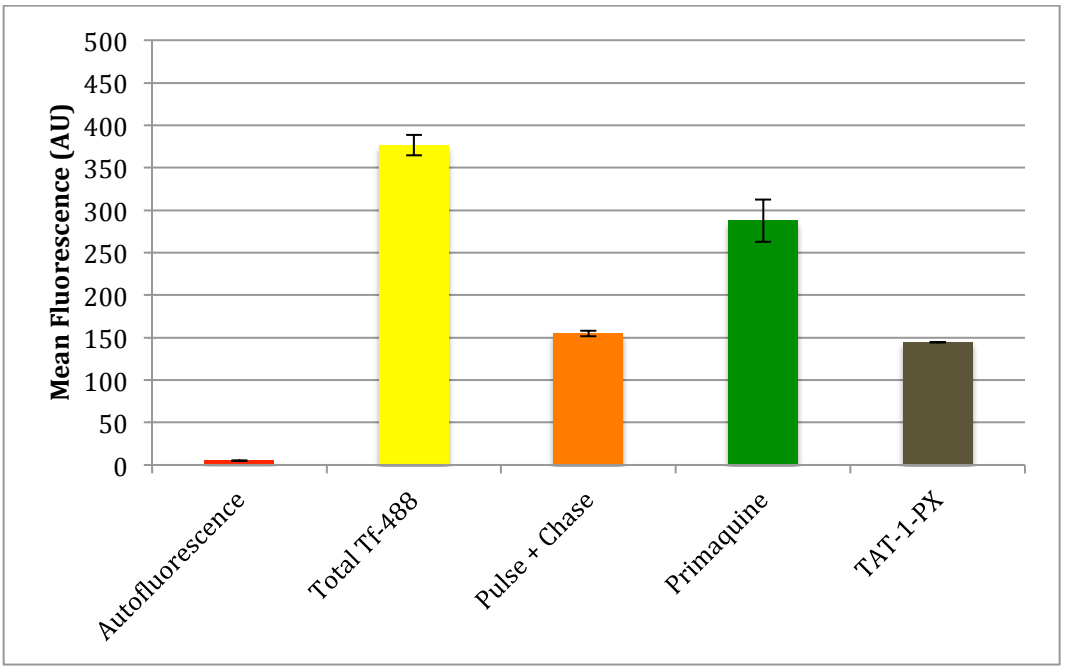

Figure 4.13. Bar graph representation of the mean fluorescence obtained from the flow cytometry experiments with TAT-1-PX. The colors match the corresponding histograms of Figure 4.12. Error bars represent standard deviation from two independent experiments.

4.8 Alternative methods for promoting cell penetration of the cyclic, bis-alkylated EHD1 inhibitors

The TAT-linked peptides did not work in mammalian culture, and this can be explained by several possible factors. First, the target affinity of the TAT-linked cyclic peptides could be significantly less than the original cyclic peptides. Dr. Robyn Eisert set up competitive binding experiments with the TAT-linked cyclic peptides, but the results were inconclusive since the inhibitor appeared to affect the cNPF1^{Flu} probe in the absence of protein. In the future, isothermal titration calorimetry (ITC) experiments could be conducted to measure binding affinities for the TAT-linked peptides. These K_d values would reveal whether the presence of the TAT sequence affected the binding affinity of the cyclic peptide ligands.

Poor endosomal escape provided another possibility for the ineffectiveness of the TAT-linked inhibitors in cell culture.[104] Cell-penetrating peptides are known to carry cargo into the cell, but only a small amount ends up in the cytosol. The overwhelming majority of the peptide, as well as its cargo, remains trapped in the endosome, unable to interact with proteins and vesicle trafficking machinery outside.[104] If the TAT-linked cyclic peptides were trapped within the endosome, than they would be unable to bind to their cytosolic target protein.

Esterification of the free acids represents an alternative strategy to improve the cell-penetrating capabilities of our inhibitors.[106] Our highest-affinity inhibitors

contained two free carboxylic acids, which would be deprotonated under physiological conditions. Consequently, the presence of these negatively charged groups would be expected to reduce cell penetration.[75a-c, 78, 103] By masking the negatively charged residues or C-termini with esters, we could reduce the negative charge of our cyclic peptides, potentially making them more cell-penetrant.[106] Once inside the cytosol, the negatively charged side chains would be unmasked by esterases,[106] freeing the negative charges for interaction with the target protein. The esterification of side chains has already been demonstrated to be successful in improving the cell-penetrating capabilities of peptidic prodrugs.[106] In the near future, we will apply this strategy to generate inhibitors that are more likely to be cell-penetrant.

4.9 Cyclic peptide inhibitors of EHD1: next steps

We sought to develop cyclic peptide inhibitors of EHD1 as tools to better understand EHD1's role in endocytic recycling. After identifying multiple cyclic peptides with affinity for the EH domain of EHD1, the project requires a study of target specificity. First, we will test the specificity of our inhibitors against the homologous family of N-terminal EH-domain containing proteins. We will run FP direct binding experiments with fluorescently-labeled peptides (Table 3.5) and both Eps15-EH2 and Reps1-EH. We expect to detect little or no binding to these EH domains due to the negative charges on the designed cyclic peptides. Prior work with linear peptides has shown that these residues are critical for selectivity

for C-terminal EH domains over N-terminal EH domains.[60, 64] We will then examine specificity for the EHD1-EH over the other members of the C-terminal EH domain family. To do this, we will perform FP direct binding experiments with fluorescently-labeled peptides (Table 3.5) and the EH domains of EHD2, EHD3, and EHD4. The high degree of sequence identity between all four C-terminal EH domains renders these results of particular interest.[36a] While the selective inhibition of EHD1 would be the most promising step in targeting long-loop recycling, the inhibition of the other C-terminal EH domains may prove beneficial due to their ability to compensate for one another.[36a, 38, 42]

When one or more peptides have been determined to bind selectively with the EH domain of EHD1, it will be important to discern whether they can interact specifically with the full-length EHD1 protein. A pull-down assay will be used to monitor the binding of EH domain ligands to EHD1 in the context of a cell lysate. Biotinylated peptides will be synthesized, and these will be incubated with HeLa cell lysate. Streptavidin-conjugated magnetic beads will be added, and the biotinylated peptide and any interacting proteins will be immobilized to the beads and separated from the lysate during wash steps. Proteins eluted from the beads can then be analyzed by SDS-PAGE, and a western blot with EHD1 antibodies will determine whether the peptides were able to specifically bind the target protein in the cell lysate.[107] The results of these experiments will reveal which peptides are able to bind to their targets, regardless of their abilities to penetrate the cell membrane.

Another important experiment will be to evaluate the half-life of our inhibitors in the presence of serum-containing media.[108] This will be a useful first indication of the peptide's resistance to degradation *in vivo*. The cyclic peptides with the highest EHD1-EH affinities (Table 3.5) will be incubated in fetal calf and human serum, and samples of each mixture will be taken at various time points.[108] The corresponding linear sequence of each peptide will also be tested to serve as a control to establish the effects of cyclization on proteolytic stability. Each sample will be analyzed by HPLC to monitor the degradation of the inhibitors.[108] The decrease in the peak areas that correspond to the peptide will reflect the peptide's survival in serum over time.[108] Previous research has indicated that backbone cyclic peptides are more protease-resistant than their linear counterparts; therefore, the cyclic peptides are anticipated to be more stable than any linear control.[109]

To more directly examine the cell penetration of our EHD1-EH inhibitors, the inhibitors will be directly labeled with 5(6) carboxyfluorescein. We will use the previously synthesized fluorescent probes (Table 3.5), or synthesize fluorescently-labeled analogs of any future design iterations. This fluorescent tag will enable the peptide to be detected in cultured HeLa cells via confocal fluorescence microscopy.[110] Once the remaining extracellular peptide has been washed away, the live cells will be imaged by confocal microscopy to observe the extent to which peptides were taken up by the cells.[110] Confocal microscopy examines one

focal plane of the cell at a time; therefore, this technique has the capacity to distinguish between peptides that adhere to the cell membrane and peptides that have truly been internalized.[110]

The overarching goal of this project was to develop inhibitors capable of perturbing the long-loop recycling pathway. We also explored an alternative cell-based experiment to determine whether our ligands could affect cell motility, which depends on long-loop recycling.[6-7, 111] We conducted these cell-based assays with H-2K^d-Ecad-II-4 (Ecad-II-4) SCC tumor cells. This Ecad-II-4 cell line expresses a dominant negative fusion protein (H-2K^d-E-cad) that suppresses E-cadherin expression by 80%.[111-112] The E-cadherin-suppressed cells poorly maintain cell-cell adhesions and spread easily in cultures.[111-112]

Preliminary experiments were performed with cNPF1, cNPF5, and 5-OX (Table 2.2 and 3.4) with the aid of Prof. Addy Alt-Holland. Each peptide was added at 50 μM to either E-cadherin-competent or E-cadherin-suppressed cells (generous gifts from Prof. Addy Alt-Holland at the Tufts School of Dental Medicine). Every 24 hours, the media was changed and fresh peptide was added. Wells with DMSO-free and DMSO-containing controls were also included. Each day the cells were imaged after the media change until, after 72 hours, the cells reached 100 % confluence. The cell growth and spreading was examined with slightly different methods for each cell line. The E-cadherin competent cells were monitored in terms of confluence because they formed easily identifiable

colonies, while the E-cadherin suppressed cells were measured by cell count (Table 4.2). The cells were quantified using specialized software. After 48 hours, many of the cells incubated with peptides were less confluent than the controls; therefore, it was possible that they were producing non-specific toxic effects. Ultimately, further experiments with these cell lines would be necessary to ascertain whether the peptides elicited any specific effects on cell motility.

Peptide	Sequence	Linker	E-Cadherin Competent (% Confluence)		E-Cadherin Suppressed (Number of Cells)	
			24 hours	48 hours	24 hours	48 hours
Control	N/A	N/A	31.3 ± 12.3	48.2 ± 4.4	607 ± 75	683 ± 269
DMSO	N/A	N/A	31.7 ± 4.9	55.4 ± 8.6	531 ± 53	770 ± 37
cNPF1	-YNPFEEGG-	backbone	28.7 ± 5.6	39.9 ± 4.0	402 ± 160	570 ± 71
cNPF5	-YNPFEAGG-	backbone	26.9 ± 3.1	48.3 ± 5.5	411 ± 50	636 ± 152
5	Ac-CNPFEC-OH	OX	33.7 ± 12.4	57.7 ± 9.3	431 ± 77	622 ± 98

Table 4.2. Effects of peptides on the growth of squamous cell carcinoma (SCC) cells. The E-Cadherin competent cells were measured by the amount of surface area covered by cells due to their numerous cell-cell adhesions. The cells were too close together to count individually. The E-cadherin suppressed cells were measured in terms of the number of total cells. These cells were further apart and more easily distinguished due to the lack of cell-cell adhesions. These cells were distributed throughout the plate, and they covered a larger surface area. As a result, it was more difficult to determine the amount of surface area covered by cells.

4.10 Conclusion

Our highest-affinity EHD1-EH inhibitor to date is 6-OX, which had a K_d of 3.1 ± 0.2 μM under physiological salt conditions. Existing inhibitors of vesicle trafficking pathways have similar affinities for their target proteins; therefore, we tested the effects of 6-OX and other peptides in mammalian cell culture.[16] While none of the peptides had any effects on transferrin recycling, this may have been the result poor cell penetration. We also conjugated our most promising inhibitors to the TAT sequence, but these TAT-linked peptides also had no effect on the long-loop recycling pathway.

There are a few experiments required to answer some remaining questions. Regarding target specificity, we will test 6-OX and other higher-affinity EHD1-EH inhibitors against N-terminal EH domains and the EH domains of the other proteins in the EHD family. We also plan to perform pull-down experiments to investigate the specificity of our peptides in cell lysates. We will study the inhibitors' cell-penetrating capabilities by testing esterified analogs, and by conducting confocal microscopy experiments with fluorescently-labeled peptides. Lastly, we plan to do serum-stability studies to compare the protease stability of the various cyclic compounds.

Over the course of this project, we have made great progress in the development of cyclic peptide inhibitors of EHD1. After demonstrating that cyclization of the

NPF motif improves affinity for the EH domain, we developed a fluorescence polarization based assay to screen for better EHD1-EH inhibitors.[89] We used this assay to screen a small library of cyclic peptides, the development of which was a separate achievement that required the adaptation and optimization of the bis-alkylation chemistry.[92-93] The development of these libraries resulted in the discovery of multiple peptides, including 6-OX, with a single-digit micromolar affinity for EHD1-EH under physiological salt conditions. Although none of our peptides altered the long-loop recycling of transferrin, we are investigating alternative methods to improve the cell-penetrating capabilities of our inhibitors to generate a phenotypic effect. Ultimately, these inhibitors will help us gather a better understanding of the effects of EHD1 in the context of cancer cell invasion.

4.11 Materials and methods

4.11.1 The final optimized protocol for the cell-based transferrin recycling assay

All serum and media were purchased from Life Technologies. Cells were seeded in Dulbecco's Modified Eagle's Medium (DMEM) with 10 % Fetal Bovine Serum (FBS), and grown in twelve-well plates at 37°C with an atmosphere of 5 % CO_2. Once the cells reached 80% confluence, they were starved for 30 minutes in DMEM with 0.5 % w/v bovine serum albumen (BSA). The cells were then subject to the pulse incubation with the fluorescently labeled transferrin (25 μg/mL, TF-488, from Life Technologies) to allow the TF-488 to enter the cell and

saturate the long-loop recycling pathway. This step utilized DMEM with 0.5% w/v BSA. When testing inhibitors, we also included them during this step to allow for more time to penetrate the cell.

Following the pulse, a 30 minute chase was conducted in 10% FBS in DMEM and unlabeled transferrin at a concentration of 2 mg/mL. The inhibitors were also included at the relevant concentrations. The peptides were stored as DMSO stocks, and the final DMSO concentration of each well was 0.2 % v/v. The unlabeled transferrin was added to saturate all trafficking within the cell. In the case of the positive control, the chase also contained 50 μM primaquine, a small molecule known to non-specifically inhibit vesicle recycling.[25a, 25b, 25d] The cells were then washed with cold phosphate buffer saline (PBS), trypsinized and fixed for subsequent analysis by flow cytometry. The cold PBS wash was included to halt vesicle trafficking prior to cell fixation. The flow cytometer (Guava easyCyte HT) was gated to count 10,000 live cells. The gating was guided by a previous experiment to determine where live cells stained with propidium iodide appeared.

4.11.2 The design and synthesis of TAT-linked cyclic peptides

The TAT-linked peptides were synthesized on 2-Chlorotrityl resin using standard Fmoc chemistry on a Tribute-UV IR peptide synthesizer from Protein Technologies (Table 4.1, Scheme 4.1, Chapter 3.8.1). The linear sequence was

then cleaved and purified by reversed-phase HPLC. After the pure linear product was lyophilized, it was dissolved in reaction buffer (50 % acetonitrile, 50 % NH_4HCO_3 pH = 8.0) at a 0.2 mM concentration. The peptides were then bis-alkylated using the previously optimized reaction technique, and the reaction was quenched after two hours by bringing the pH down to 4.0 with trifluoroacetic acid (Chapter 3.8.10). The cyclic peptide was then purified by reversed-phase HPLC. The peptides were stored in stock solutions of DMSO. The concentrations of the TAT-linked bis-alkylated peptides were determined by UV-Vis spectrometry by measuring the absorbance at 280 nm of the tyrosine side chain (extinction coefficient = 1490 $M^{-1}cm^{-1}$).

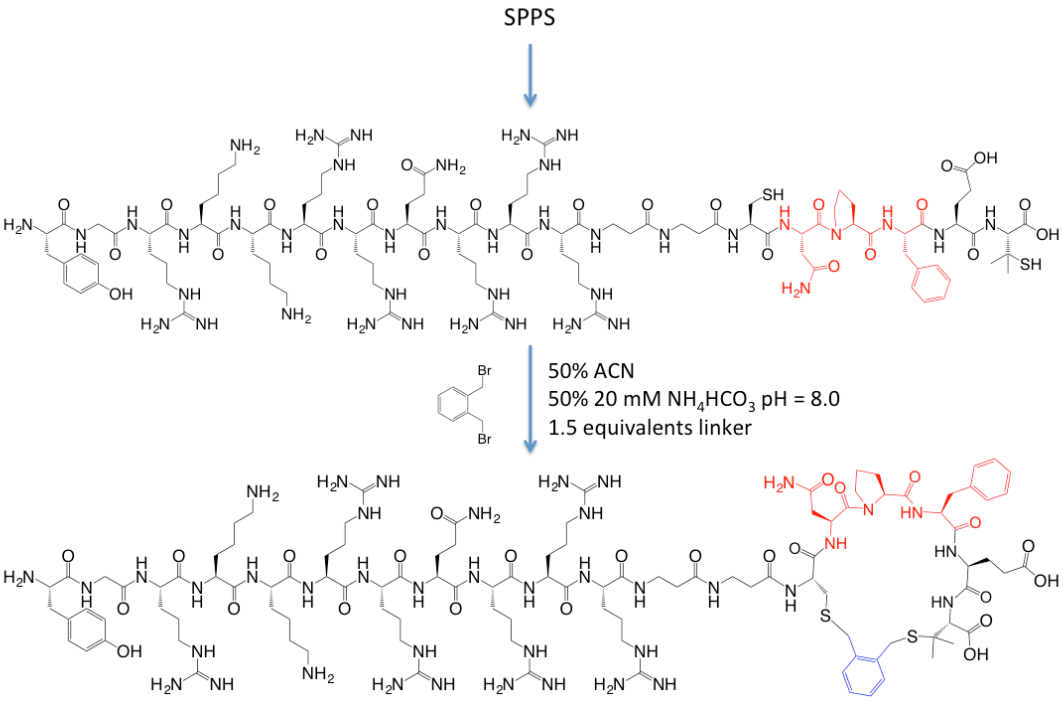

Scheme 4.11.1. Synthesis of bis-alkylated, TAT-linked cyclic peptides. TAT-6-OX is depicted. The NPF sequence is shown in red, while the linker is shown in blue.

TAT-1	YGRKKRRQRRR-ββ-CYNPFEE-(cysteamine)	PX	2746.2	2747.1
TAT-4	YGRKKRRQRRR-ββ-CNPFEE-(cysteamine)	PX	2583.5	2585.0
TAT-5	YGRKKRRQRRR-ββ-CNPFEC-OH	OX	2469.9	
TAT-6	YGRKKRRQRRR-ββ-CNPFE(Pen)-OH	OX	2526.0	2527
TAT-6scr	YGRKKRRQRRR-ββ-CFPNE(Pen)-OH	OX	2526.0	2528
TAT-7	YGRKKRRQRRR-ββ-CNP(1-Nal)EC-OH	OX	2548.0	2546.2
TAT-9	YGRKKRRQRRR-ββ-CNP(1-Nal)EC-OH	OX	2576.1	2575.1

Table 4.3. e peptides synthesized as previously described. The masses of each product were determined by MALDI-TOF mass spectrometry or by ESI.

References

1. Mosesson, Y.; Mills, G. B.; Yarden, Y., Derailed endocytosis: an emerging feature of cancer. *Nature Reviews Cancer* **2008,** *8* (11), 835-850.
2. Mellman, I.; Yarden, Y., Endocytosis and cancer. *Cold Spring Harb Perspect Biol* **2013,** *5* (12), a016949.
3. Guo, W. J.; Giancotti, F. G., Integrin signalling during tumour progression. *Nature Reviews Molecular Cell Biology* **2004,** *5* (10), 816-826.
4. Roberts, M.; Barry, S.; Woods, A.; van der Sluijs, P.; Norman, J., PDGF-regulated rab4-dependent recycling of alpha v beta 3 integrin from early endosomes is necessary for cell adhesion and spreading. *Current Biology* **2001,** *11* (18), 1392-1402.
5. Panetti, T. S.; McKeownlongo, P. J., The Alpha(V)Beta(5) Integrin Receptor Regulates Receptor-Mediated Endocytosis of Vitronectin. *Journal of Biological Chemistry* **1993,** *268* (16), 11492-11495.
6. (a) Webb, D. J.; Parsons, J. T.; Horwitz, A. F., Adhesion assembly, disassembly and turnover in migrating cells - over and over and over again. *Nature Cell Biology* **2002,** *4* (4), E97-E100; (b) Laukaitis, C. M.; Webb, D. J.; Donais, K.; Horwitz, A. F., Differential dynamics of alpha 5 integrin, paxillin, and alpha-actinin during formation and disassembly of adhesions in migrating cells. *Journal of Cell Biology* **2001,** *153* (7), 1427-1440; (c) Pierini, L. M.; Lawson, M. A.; Eddy, R. J.; Hendey, B.; Maxfield, F. R., Oriented endocytic recycling of alpha 5 beta l in motile neutrophils. *Blood* **2000,** *95* (8), 2471-2481.
7. (a) Beningo, K. A.; Dembo, M.; Kaverina, I.; Small, J. V.; Wang, Y. L., Nascent focal adhesions are responsible for the generation of strong propulsive forces in migrating fibroblasts. *Journal of Cell Biology* **2001,** *153* (4), 881-887; (b) Palecek, S. P.; Huttenlocher, A.; Horwitz, A. F.; Lauffenburger, D. A., Physical and biochemical regulation of integrin release during rear detachment of migrating cells. *Journal of Cell Science* **1998,** *111*, 929-940; (c) Huttenlocher, A.; Palecek, S.; Ginsberg, M.; Lauffenburger, D.; Horwitz, R., Regulation of integrin-mediated adhesive release during cell migration. *Molecular Biology of the Cell* **1998,** *9*, 33A-33A; (d) Caswell, P. T.; Norman, J. C., Integrin trafficking and the control of cell migration. *Traffic* **2006,** *7* (1), 14-21; (e) Lee, J.; Leonard, M.; Oliver, T.; Ishihara, A.; Jacobson, K., Traction Forces Generated by Locomoting Keratocytes. *Journal of Cell Biology* **1994,** *127* (6), 1957-1964.
8. (a) Onodera, Y.; Nam, J. M.; Sabe, H., Intracellular trafficking of integrins in cancer cells. *Pharmacology & Therapeutics* **2013,** *140* (1), 1-9; (b) Paul, N. R.; Jacquemet, G.; Caswell, P. T., Endocytic Trafficking of Integrins in Cell Migration. *Current Biology* **2015,** *25* (22), R1092-R1105.
9. Tzeng, H.-T.; Wang, Y.-C., Rab-mediated vesicle trafficking in cancer. *Journal of Biomedical Science* **2016,** *23*.
10. Christoforides, C.; Rainero, E.; Brown, K. K.; Norman, J. C.; Toker, A., PKD Controls alpha v beta 3 Integrin Recycling and Tumor Cell Invasive

Migration through Its Substrate Rabaptin-5. *Developmental Cell* **2012,** *23* (3), 560-572.
11. (a) Wang, T. L.; Ming, Z.; Wu, X. C.; Hong, W. J., Rab7: Role of its protein interaction cascades in endo-lysosomal traffic. *Cellular Signalling* **2011,** *23* (3), 516-521; (b) Rink, J.; Ghigo, E.; Kalaidzidis, Y.; Zerial, M., Rab conversion as a mechanism of progression from early to late endosomes. *Cell* **2005,** *122* (5), 735-749.
12. Ullrich, O.; Reinsch, S.; Urbe, S.; Zerial, M.; Parton, R. G., Rab11 regulates recycling through the pericentriolar recycling endosome. *Journal of Cell Biology* **1996,** *135* (4), 913-924.
13. (a) Smith, M. C.; Gestwicki, J. E., Features of protein-protein interactions that translate into potent inhibitors: topology, surface area and affinity. *Expert reviews in molecular medicine* **2012,** *14*, e16; (b) Cromm, P. M.; Spiegel, J.; Grossmann, T. N.; Waldmann, H., Direct Modulation of Small GTPase Activity and Function. *Angewandte Chemie-International Edition* **2015,** *54* (46), 13516-13537.
14. Macia, E.; Ehrlich, M.; Massol, R.; Boucrot, E.; Brunner, C.; Kirchhausen, T., Dynasore, a cell-permeable inhibitor of dynamin. *Developmental Cell* **2006,** *10* (6), 839-850.
15. Antonny, B.; Burd, C.; De Camilli, P.; Chen, E.; Daumke, O.; Faelber, K.; Ford, M.; Frolov, V. A.; Frost, A.; Hinshaw, J. E.; Kirchhausen, T.; Kozlov, M. M.; Lenz, M.; Low, H. H.; McMahon, H.; Merrifield, C.; Pollard, T. D.; Robinson, P. J.; Roux, A.; Schmid, S., Membrane fission by dynamin: what we know and what we need to know. *Embo Journal* **2016,** *35* (21), 2270-2284.
16. Yamada, H.; Abe, T.; Li, S.-A.; Masuoka, Y.; Isoda, M.; Watanabe, M.; Nasu, Y.; Kumon, H.; Asai, A.; Takei, K., Dynasore, a dynamin inhibitor, suppresses lamellipodia formation and cancer cell invasion by destabilizing actin filaments. *Biochemical and Biophysical Research Communications* **2009,** *390* (4), 1142-1148.
17. (a) Yamauchi, Y.; Miura, Y.; Kanaho, Y., Machineries regulating the activity of the small GTPase Arf6 in cancer cells are potential targets for developing innovative anti-cancer drugs. *Advances in biological regulation* **2017,** *63*, 115-121; (b) Yoo, J. H.; Shi, D. S.; Grossmann, A. H.; Sorensen, L. K.; Tong, Z.; Mleynek, T. M.; Rogers, A.; Zhu, W.; Richards, J. R.; Winter, J. M.; Zhu, J.; Dunn, C.; Bajji, A.; Shenderovich, M.; Mueller, A. L.; Woodman, S. E.; Harbour, J. W.; Thomas, K. R.; Odelberg, S. J.; Ostanin, K.; Li, D. Y., ARF6 Is an Actionable Node that Orchestrates Oncogenic GNAQ Signaling in Uveal Melanoma. *Cancer cell* **2016,** *29* (6), 889-904.
18. (a) Radhakrishna, H.; Donaldson, J. G., ADP-ribosylation factor 6 regulates a novel plasma membrane recycling pathway. *Journal of Cell Biology* **1997,** *139* (1), 49-61; (b) Schweitzer, J. K.; Sedgwick, A. E.; D'Souza-Schorey, C., ARF6-mediated endocytic recycling impacts cell movement, cell division and lipid homeostasis. *Seminars in cell & developmental biology* **2011,** *22* (1), 39-47; (c) Donaldson, J. G., Multiple roles for Arf6: Sorting, structuring, and signaling at the plasma membrane. *Journal of Biological Chemistry* **2003,** *278* (43), 41573-41576; (d) D'Souza-Schorey, C.; Chavrier,

P., ARF proteins: roles in membrane traffic and beyond. *Nature Reviews Molecular Cell Biology* **2006,** *7* (5), 347-358.
19. (a) Schwartz, A. L.; Bolognesi, A.; Fridovich, S. E., Recycling of the Asialoglycoprotein Receptor and hte Effect of Lysosomotropic Amines in Hepatoma-Cells. *Journal of Cell Biology* **1984,** *98* (2), 732-738; (b) Maxfield, F. R., Weak Bases and Ionophores Rapidly and Reversibly Raise the pH of Endocytic Vesicles in Cultured Mouse Fibroblasts. *Journal of Cell Biology* **1982,** *95* (2), 676-681; (c) Drakakaki, G.; Robert, S.; Szatmari, A. M.; Brown, M. Q.; Nagawa, S.; Van Damme, D.; Leonard, M.; Yang, Z. B.; Girke, T.; Schmid, S. L.; Russinova, E.; Friml, J.; Raikhel, N. V.; Hicks, G. R., Clusters of bioactive compounds target dynamic endomembrane networks in vivo. *Proceedings of the National Academy of Sciences of the United States of America* **2011,** *108* (43), 17850-17855.
20. Nieland, T. J. F.; Feng, Y.; Brown, J. X.; Chuang, T. D.; Buckett, P. D.; Wang, J.; Xie, X. S.; McGraw, T. E.; Kirchhausen, T.; Wessling-Resnick, M., Chemical genetic screening identifies sulfonamides that raise organellar pH and interfere with membrane traffic. *Traffic* **2004,** *5* (7), 478-492.
21. Ronan, B.; Flamand, O.; Vescovi, L.; Dureuil, C.; Durand, L.; Fassy, F.; Bachelot, M.-F.; Lamberton, A.; Mathieu, M.; Bertrand, T.; Marquette, J.-P.; El-Ahmad, Y.; Filoche-Romme, B.; Schio, L.; Garcia-Echeverria, C.; Goulaouic, H.; Pasquier, B., A highly potent and selective Vps34 inhibitor alters vesicle trafficking and autophagy. *Nat Chem Biol* **2014,** *10* (12), 1013-1019.
22. (a) Spiegel, J.; Cromm, P. M.; Itzen, A.; Goody, R. S.; Grossmann, T. N.; Waldmann, H., Direct Targeting of Rab-GTPase-Effector Interactions**. *Angewandte Chemie-International Edition* **2014,** *53* (9), 2498-2503; (b) Cromm, P. M.; Spiegel, J.; Kuchler, P.; Dietrich, L.; Kriegesmann, J.; Wendt, M.; Goody, R. S.; Waldmann, H.; Grossmann, T. N., Protease-Resistant and Cell-Permeable Double-Stapled Peptides Targeting the Rab8a GTPase. *Acs Chemical Biology* **2016,** *11* (8), 2375-2382.
23. (a) Wileman, T.; Boshans, R. L.; Schlesinger, P.; Stahl, P., Monensin Inhibits Recycling of Macrophage Mannose-Glycoprotein Receptors and Ligand Delivery to Lysosomes. *Biochemical Journal* **1984,** *220* (3), 665-675; (b) Nuckols, J. T.; McAuley, A. J.; Huang, Y. J. S.; Horne, K. M.; Higgs, S.; Davey, R. A.; Vanlandingham, D. L., pH-Dependent entry of chikungunya virus fusion into mosquito cells. *Virology Journal* **2014,** *11*.
24. (a) Alam, K.; Pahwa, S.; Wang, X. Y.; Zhang, P. Y.; Ding, K.; Abuznait, A. H.; Li, L.; Yue, W., Downregulation of Organic Anion Transporting Polypeptide (OATP) 1B1 Transport Function by Lysosomotropic Drug Chloroquine: Implication in OATP-Mediated Drug-Drug Interactions. *Molecular Pharmaceutics* **2016,** *13* (3), 839-851; (b) Stoorvogel, W.; Geuze, H. J.; Griffith, J. M.; Schwartz, A. L.; Strous, G. J., Relations Between the Intracellular Pathways of the Receptors for Transferrin, Asiaglycoprotein, and Mannose 6-Phosphate in Human Hepatoma-Cells. *Journal of Cell Biology* **1989,** *108* (6), 2137-2148.
25. (a) van Weert, A. W. M.; Geuze, H. J.; Groothuis, B.; Stoorvogel, W., Primaquine interferes with membrane recycling from endosomes to the

plasma membrane through a direct interaction with endosomes which does not involve neutralisation of endosomal pH nor osmotic swelling of endosomes. *European Journal of Cell Biology* **2000,** *79* (6), 394-399; (b) Hiebsch, R. R.; Raub, T. J.; Wattenberg, B. W., Primaquine Blocks Transport by Inhibiting the Formation of Functional Transport Vesicles - Studies in a Cell-Free Assay of Protein-Transport through the Golgi-Apparatus. *Journal of Biological Chemistry* **1991,** *266* (30), 20323-20328; (c) Woods, A. J.; White, D. P.; Caswell, P. T.; Norman, J. C., PKD1/PKC mu promotes alpha v beta 3 integrin recycling and delivery to nascent focal adhesions. *Embo Journal* **2004,** *23* (13), 2531-2543; (d) Manna, P. T.; Smith, A. J.; Taneja, T. K.; Howell, G. J.; Lippiat, J. D.; Sivaprasadarao, A., Constitutive Endocytic Recycling and Protein Kinase C-mediated Lysosomal Degradation Control K-ATP Channel Surface Density. *Journal of Biological Chemistry* **2010,** *285* (8), 5963-5973.

26. (a) Bhuin, T.; Roy, J. K., Rab proteins: The key regulators of intracellular vesicle transport. *Experimental Cell Research* **2014,** *328* (1), 1-19; (b) Khandelwal, P.; Prakasam, H. S.; Clayton, D. R.; Ruiz, W. G.; Gallo, L. I.; van Roekel, D.; Lukianov, S.; Peränen, J.; Goldenring, J. R.; Apodaca, G., A Rab11a-Rab8a-Myo5B network promotes stretch-regulated exocytosis in bladder umbrella cells. *Molecular Biology of the Cell* **2013,** *24* (7), 1007-1019.

27. Verdine, G. L.; Hilinski, G. J., Stapled peptides for intracellular drug targets. *Methods in enzymology* **2012,** *503*, 3-33.

28. (a) Santolini, E.; Salcini, A. E.; Kay, B. K.; Yamabhai, M.; Di Fiore, P. P., The EH network. *Experimental Cell Research* **1999,** *253* (1), 186-209; (b) Miliaras, N. B.; Wendland, B., EH proteins - Multivalent regulators of endocytosis (and other pathways). *Cell Biochemistry and Biophysics* **2004,** *41* (2), 295-318.

29. Fazioli, F.; Minichiello, L.; Matoskova, B.; Wong, W. T.; Difiore, P. P., Eps15, a Novel Tyrosine Kinase Substrate, Exhibits Transforming Activity. *Molecular and Cellular Biology* **1993,** *13* (9), 5814-5828.

30. Carbone, R.; Fre, S.; Iannolo, G.; Belleudi, F.; Mancini, P.; Pelicci, P. G.; Torrisi, M. R.; Di Fiore, P. P., eps15 and eps15R are essential components of the endocytic pathway. *Cancer Research* **1997,** *57* (24), 5498-5504.

31. (a) Benmerah, A.; Poupon, V.; Cerf-Bensussan, N.; Dautry-Varsat, A., Mapping of Eps15 domains involved in its targeting to clathrin-coated pits. *Journal of Biological Chemistry* **2000,** *275* (5), 3288-3295; (b) Hofmann, K.; Falquet, L., A ubiquitin-interacting motif conserved in components of the proteasomal and lysosomal protein degradation systems. *Trends in Biochemical Sciences* **2001,** *26* (6), 347-350.

32. (a) Rumpf, J.; Simon, B.; Jung, N.; Maritzen, T.; Haucke, V.; Sattler, M.; Groemping, Y., Structure of the Eps15-stonin2 complex provides a molecular explanation for EH-domain ligand specificity. *Embo Journal* **2008,** *27* (3), 558-569; (b) Naslavsky, N.; Caplan, S., EHD proteins: key conductors of endocytic transport. *Trends in Cell Biology* **2011,** *21* (2), 122-131.

33. Grant, B. D.; Caplan, S., Mechanisms of EHD/RME-1 Protein Function in Endocytic Transport. *Traffic* **2008,** *9* (12), 2043-2052.

34. van Bergen En Henegouwen, P. M., Eps15: a multifunctional adaptor protein regulating intracellular trafficking. *Cell communication and signaling : CCS* **2009,** *7*, 24.
35. (a) Lin, S. X.; Grant, B.; Hirsh, D.; Maxfield, F. R., Rme-1 regulates the distribution and function of the endocytic recycling compartment in mammalian cells. *Nature Cell Biology* **2001,** *3* (6), 567-572; (b) Caplan, S.; Naslavsky, N.; Hartnell, L. M.; Lodge, R.; Polishchuk, R. S.; Donaldson, J. G.; Bonifacino, J. S., A tubular EHD1-containing compartment involved in the recycling of major histocompatibility complex class I molecules to the plasma membrane. *Embo Journal* **2002,** *21* (11), 2557-2567.
36. (a) Naslavsky, N.; Caplan, S., C-terminal EH-domain-containing proteins: consensus for a role in endocytic trafficking, EH? *J Cell Sci* **2005,** *118* (Pt 18), 4093-101; (b) Simone, L. C.; Naslavsky, N.; Caplan, S., Scratching the surface: Actin' and other roles for the C-terminal Eps15 homology domain protein, EHD2. *Histology and Histopathology* **2014,** *29* (3), 285-292; (c) Simone, L. C.; Caplan, S.; Naslavsky, N., Role of Phosphatidylinositol 4,5-Bisphosphate in Regulating EHD2 Plasma Membrane Localization. *PLOS ONE* **2013,** *8* (9), e74519.
37. (a) Naslavsky, N.; Rahajeng, J.; Sharma, M.; Jovic, M.; Caplan, S., Interactions between EHD proteins and Rab11-FIP2: A role for EHD3 in early endosomal transport. *Molecular Biology of the Cell* **2006,** *17* (1), 163-177; (b) Sharma, M.; Naslavsky, N.; Caplan, S., A role for EHD4 in the regulation of early endosomal transport. *Traffic* **2008,** *9* (6), 995-1018.
38. Jovic, M.; Naslavsky, N.; Rapaport, D.; Horowitz, M.; Caplan, S., EHD1 regulates beta 1 integrin endosomal transport: effects on focal adhesions, cell spreading and migration. *Journal of Cell Science* **2007,** *120* (5), 802-814.
39. (a) Mintz, L.; Galperin, E.; Pasmanik-Chor, M.; Tulzinsky, S.; Bromberg, Y.; Kozak, C. A.; Joyner, A.; Fein, A.; Horowitz, M., EHD1 - An EH-domain-containing protein with a specific expression pattern. *Genomics* **1999,** *59* (1), 66-76; (b) Grant, B.; Zhang, Y. H.; Paupard, M. C.; Lin, S. X.; Hall, D.; Hirsh, D., Evidence that RME-1, a conserved C-elegans EH-domain protein, functions in endocytic recycling. *Nature Cell Biology* **2001,** *3* (6), 573-579.
40. (a) Naslavsky, N.; Boehm, M.; Backlund, P. S.; Caplan, S., Rabenosyn-5 and EHD1 interact and sequentially regulate protein recycling to the plasma membrane. *Molecular Biology of the Cell* **2004,** *15* (5), 2410-2422; (b) Sharma, M.; Panapakkam Giridharan, S. S.; Rahajeng, J.; Naslavsky, N.; Caplan, S., MICAL-L1 Links EHD1 to Tubular Recycling Endosomes and Regulates Receptor Recycling. *Molecular Biology of the Cell* **2009,** *20* (24), 5181-5194.
41. Guilherme, A.; Soriano, N. A.; Furcinitti, P. S.; Czech, M. P., Role of EHD1 and EHBP1 in perinuclear sorting and insulin-regulated GLUT4 recycling in 3T3-L1 adipocytes. *Journal of Biological Chemistry* **2004,** *279* (38), 40062-40075.
42. Rapaport, D.; Auerbach, W.; Naslavsky, N.; Pasmanik-Chor, M.; Galperin, E.; Fein, A.; Caplan, S.; Joyner, A. L.; Horowitz, M., Recycling to the plasma membrane is delayed in EHD1 knockout mice. *Traffic* **2006,** *7* (1), 52-60.

43. Cortez, K. J.; Lyman, C. A.; Kottilil, S.; Kim, H. S.; Roilides, E.; Yang, J.; Fullmer, B.; Lempicki, R.; Walsh, T. J., Functional genomics of innate host defense molecules in normal human monocytes in response to Aspergillus fumigatus. *Infection and Immunity* **2006,** *74* (4), 2353-2365.
44. Jansen, F. H.; Krijgsveld, J.; van Rijswijk, A.; van den Bemd, G. J.; van den Berg, M. S.; van Weerden, W. M.; Willemsen, R.; Dekker, L. J.; Luider, T. M.; Jenster, G., Exosomal Secretion of Cytoplasmic Prostate Cancer Xenograft-derived Proteins. *Molecular & Cellular Proteomics* **2009,** *8* (6), 1192-1205.
45. Shin, Lesional gene expression profiling in cutaneous T-cell lymphoma reveals natural clusters associated with disease outcome (vol 110, pg 3015, 2007). *Blood* **2008,** *111* (1), 49-49.
46. Gao, Y.; Wang, Y.; Sun, L.; Meng, Q.; Cai, L.; Dong, X., Expression of TGF beta-1 and EHD1 correlated with survival of non-small cell Lung cancer. *Tumor Biology* **2014,** *35* (9), 9371-9380.
47. Gao, J.; Meng, Q. W.; Zhao, Y. B.; Chen, X. S.; Cai, L., EHD1 confers resistance to cisplatin in non-small cell lung cancer by regulating intracellular cisplatin concentrations. *Bmc Cancer* **2016,** *16*.
48. Reinecke, J.; Katafiasz, D.; Naslavsky, N.; Caplan, S., Role of MICAL-L1/EHD1 endocytic pathway in regulating the localization and signaling of the non-receptor tyrosine kinase c-Src. *Molecular Biology of the Cell* **2013,** *24*.
49. Rotem-Yehudar, R.; Galperin, E.; Horowitz, M., Association of insulin-like growth factor 1 receptor with EHD1 and SNAP29. *Journal of Biological Chemistry* **2001,** *276* (35), 33054-33060.
50. Braun, A.; Pinyol, R.; Dahlhaus, R.; Koch, D.; Fonarev, P.; Grant, B. D.; Kessels, M. M.; Qualmann, B., EHD proteins associate with syndapin I and II and such interactions play a crucial role in endosomal recycling. *Molecular Biology of the Cell* **2005,** *16* (8), 3642-3658.
51. Sharma, M.; Giridharan, S. S. P.; Rahajeng, J.; Caplan, S.; Naslavsky, N., MICAL-L1: An unusual Rab effector that links EHD1 to tubular recycling endosomes. *Communicative & integrative biology* **2010,** *3* (2), 181-3.
52. Wei, S. H.; Xu, Y.; Shi, H.; Wong, S. H.; Han, W. P.; Talbot, K.; Hong, W. J.; Ong, W. Y., EHD1 is a synaptic protein that modulates exocytosis through binding to snapin. *Molecular and Cellular Neuroscience* **2010,** *45* (4), 418-429.
53. (a) Zhang, J.; Naslavsky, N.; Caplan, S., Rabs and EHDs: alternate modes for traffic control. *Bioscience Reports* **2012,** *32* (1), 17-23; (b) Giridharan, S. S. P.; Cai, B. S.; Vitale, N.; Naslavsky, N.; Caplan, S., Cooperation of MICAL-L1, syndapin2, and phosphatidic acid in tubular recycling endosome biogenesis. *Molecular Biology of the Cell* **2013,** *24* (11), 1776-1790.
54. Cai, B. S.; Giridharan, S. S. P.; Zhang, J.; Saxena, S.; Bahl, K.; Schmidt, J. A.; Sorgen, P. L.; Guo, W.; Naslavsky, N.; Caplan, S., Differential Roles of C-terminal Eps15 Homology Domain Proteins as Vesiculators and Tubulators of Recycling Endosomes. *Journal of Biological Chemistry* **2013,** *288* (42), 30172-30180.

55. Lee, D. W.; Zhao, X. H.; Scarselletta, S.; Schweinsberg, P. J.; Eisenberg, E.; Grant, B. D.; Greene, L. E., ATP binding regulates oligomerization and endosome association of RME-1 family proteins. *Journal of Biological Chemistry* **2005,** *280* (17), 17213-17220.
56. Sharma, M.; Jovic, M.; Kieken, F.; Naslavsky, N.; Sorgen, P.; Caplan, S., A model for the role of EHD1-containing membrane tubules in endocytic recycling. *Commun Integr Biol* **2009,** *2* (5), 431-3.
57. Naslavsky, N.; Rahajeng, J.; Chenavas, S.; Sorgen, P. L.; Caplan, S., EHD1 and Eps15 interact with phosphatidylinositols via their Eps15 homology domains. *Journal of Biological Chemistry* **2007,** *282* (22), 16612-16622.
58. Kieken, F.; Jovic, M.; Naslavsky, N.; Caplan, S.; Sorgen, P. L., EH domain of EHD1. *Journal of Biomolecular Nmr* **2007,** *39* (4), 323-329.
59. Kieken, F.; Jovic, M.; Tonelli, M.; Naslavsky, N.; Caplan, S.; Sorgen, P. L., Structural insight into the interaction of proteins containing NPF, DPF, and GPF motifs with the C-terminal EH-domain of EHD1. *Protein Science* **2009,** *18* (12), 2471-2479.
60. Kieken, F.; Sharma, M.; Jovic, M.; Giridharan, S. S. P.; Naslavsky, N.; Caplan, S.; Sorgen, P. L., Mechanism for the Selective Interaction of C-terminal Eps15 Homology Domain Proteins with Specific Asn-Pro-Phe-containing Partners. *Journal of Biological Chemistry* **2010,** *285* (12), 8687-8694.
61. Jovic, M.; Kieken, F.; Naslavsky, N.; Sorgen, P. L.; Caplan, S., Eps15 Homology Domain 1-associated Tubules Contain Phosphatidylinositol-4-Phosphate and Phosphatidylinositol-(4,5)-Bisphosphate and Are Required for Efficient Recycling. *Molecular Biology of the Cell* **2009,** *20* (11), 2731-2743.
62. (a) Salcini, A. E.; Confalonieri, S.; Doria, M.; Santolini, E.; Tassi, E.; Minenkova, O.; Cesareni, G.; Pelicci, P. G.; DiFiore, P. P., Binding specificity and in vivo targets of the EH domain, a novel protein-protein interaction module. *Genes & Development* **1997,** *11* (17), 2239-2249; (b) Paoluzi, S.; Castagnoli, L.; Lauro, I.; Salcini, A. E.; Coda, L.; Fre, S.; Confalonieri, S.; Pelicci, P. G.; Di Fiore, P. P.; Cesareni, G., Recognition specificity of individual EH domains of mammals and yeast. *Embo Journal* **1998,** *17* (22), 6541-6550.
63. (a) de Beer, T.; Carter, R. E.; Lobel-Rice, K. E.; Sorkin, A.; Overduin, M., Structure and Asn-Pro-Phe binding pocket of the Eps15 homology domain. *Science* **1998,** *281* (5381), 1357-1360; (b) de Beer, T.; Hoofnagle, A. N.; Enmon, J. L.; Bowers, R. C.; Yamabhai, M.; Kay, B. K.; Overduin, M., Molecular mechanism of NPF recognition by EH domains. *Nature Structural Biology* **2000,** *7* (11), 1018-1022.
64. Henry, G. D.; Corrigan, D. J.; Dineen, J. V.; Baleja, J. D., Charge Effects in the Selection of NPF Motifs by the EH Domain of EHD1. *Biochemistry* **2010,** *49* (16), 3381-3392.
65. Nielsen, E.; Christoforidis, S.; Uttenweiler-Joseph, S.; Miaczynska, M.; Dewitte, F.; Wilm, M.; Hoflack, B.; Zerial, M., Rabenosyn-5, a novel Rab5 effector, is complexed with hVPS45 and recruited to endosomes through a FYVE finger domain. *J Cell Biol* **2000,** *151* (3), 601-12.

66. Cullis, D. N.; Philip, B.; Baleja, J. D.; Feig, L. A., Rab11-FIP2, an Adaptor Protein Connecting Cellular Components Involved in Internalization and Recycling of Epidermal Growth Factor Receptors. *Journal of Biological Chemistry* **2002,** *277* (51), 49158-49166.
67. Yamabhai, M.; Hoffman, N. G.; Hardison, N. L.; McPherson, P. S.; Castagnoli, L.; Cesareni, G.; Kay, B. K., Intersectin, a novel adaptor protein with two Eps15 homology and five Src homology 3 domains. *Journal of Biological Chemistry* **1998,** *273* (47), 31401-31407.
68. Kim, S.; Cullis, D. N.; Feig, L. A.; Baleja, J. D., Solution structure of the Reps1 EH domain and characterization of its binding to NPF target sequences. *Biochemistry* **2001,** *40* (23), 6776-6785.
69. Yamabhai, M.; Kay, B. K., Examining the specificity of Src homology 3 domain-ligand interactions with alkaline phosphatase fusion proteins. *Analytical Biochemistry* **1997,** *247* (1), 143-151.
70. Jones, M. C.; Caswell, P. T.; Norman, J. C., Endocytic recycling pathways: emerging regulators of cell migration. *Current Opinion in Cell Biology* **2006,** *18* (5), 549-557.
71. Desgrosellier, J. S.; Cheresh, D. A., Integrins in cancer: biological implications and therapeutic opportunities. *Nature Reviews Cancer* **2010,** *10* (1), 9-22.
72. Hu, C.-T.; Wu, J.-R.; Wu, W.-S., The role of endosomal signaling triggered by metastatic growth factors in tumor progression. *Cellular Signalling* **2013,** *25* (7), 1539-1545.
73. Daumke, O.; Lundmark, R.; Vallis, Y.; Martens, S.; Butler, P. J. G.; McMahon, H. T., Architectural and mechanistic insights into an EHD ATPase involved in membrane remodelling. *Nature* **2007,** *449* (7164), 923-927.
74. Naslavsky, N.; Weigert, R.; Donaldson, J. G., Characterization of a nonclathrin endocytic pathway: Membrane cargo and lipid requirements. *Molecular Biology of the Cell* **2004,** *15* (8), 3542-3552.
75. (a) Hruby, V. J., Designing peptide receptor agonists and antagonists. *Nature Reviews Drug Discovery* **2002,** *1* (11), 847-858; (b) Kessler, H., Peptide Conformations. 19. Conformation and Biological-Activity of Cyclic-Peptides. *Angewandte Chemie-International Edition in English* **1982,** *21* (7), 512-523; (c) Hruby, V. J., Conformational Restrictions of Biologically-Active Peptides via Amino-Acid Side-Chain Groups. *Life Sciences* **1982,** *31* (3), 189-199; (d) Cardote, T. A. F.; Ciulli, A., Cyclic and Macrocyclic Peptides as Chemical Tools To Recognise Protein Surfaces and Probe Protein-Protein Interactions. *Chemmedchem* **2016,** *11* (8), 787-794; (e) Pelay-Gimeno, M.; Glas, A.; Koch, O.; Grossmann, T. N., Structure-Based Design of Inhibitors of Protein-Protein Interactions: Mimicking Peptide Binding Epitopes. *Angewandte Chemie-International Edition* **2015,** *54* (31), 8896-8927.
76. Wang, C. K.; Craik, D. J., Cyclic peptide oral bioavailability: Lessons from the past. *Peptide Science* **2016,** *106* (6), 901-909.
77. (a) Knipp, G. T.; Velde, D. G. V.; Siahaan, T. J.; Borchardt, R. T., The effect of beta-turn structure on the passive diffusion of peptides across Caco-2 cell monolayers. *Pharmaceutical Research* **1997,** *14* (10), 1332-1340; (b)

Sorensen, M.; Steenberg, B.; Knipp, G. T.; Wang, W.; Steffansen, B.; Frokjaer, S.; Borchardt, R. T., The effect of beta-turn structure on the permeation of peptides across monolayers of bovine brain microvessel endothelial cells. *Pharmaceutical Research* **1997,** *14* (10), 1341-1348; (c) Pauletti, G. M.; Okumu, F. W.; Borchardt, R. T., Effect of size and charge on the passive diffusion of peptides across Caco-2 cell monolayers via the paracellular pathway. *Pharmaceutical Research* **1997,** *14* (2), 164-168; (d) Okumu, F. W.; Pauletti, G. M.; VanderVelde, D. G.; Siahaan, T. J.; Borchardt, R. T., Effect of restricted conformational flexibility on the permeation of model hexapeptides across Caco-2 cell monolayers. *Pharmaceutical Research* **1997,** *14* (2), 169-175.

78. (a) Bock, J. E.; Gavenonis, J.; Kritzer, J. A., Getting in Shape: Controlling Peptide Bioactivity and Bioavailability Using Conformational Constraints. *Acs Chemical Biology* **2013,** *8* (3), 488-499; (b) Loosli, H. R.; Kessler, H.; Oschkinat, H.; Weber, H. P.; Petcher, T. J.; Widmer, A., Peptide Conformations .31. The Conformation of Cyclosporin-A in the Crystal and in Solution. *Helvetica Chimica Acta* **1985,** *68* (3), 682-704.

79. Nevola, L.; Giralt, E., Modulating protein-protein interactions: the potential of peptides. *Chemical Communications* **2015,** *51* (16), 3302-3315.

80. (a) Trabi, M.; Craik, D. J., Circular proteins - no end in sight. *Trends in Biochemical Sciences* **2002,** *27* (3), 132-138; (b) Craik, D. J.; Simonsen, S.; Daly, N. L., The cyclotides: Novel macrocyclic peptides as scaffolds in drug design. *Current Opinion in Drug Discovery & Development* **2002,** *5* (2), 251-260.

81. Marsault, E.; Peterson, M. L., Macrocycles Are Great Cycles: Applications, Opportunities, and Challenges of Synthetic Macrocycles in Drug Discovery. *Journal of Medicinal Chemistry* **2011,** *54* (7), 1961-2004.

82. (a) Giordanetto, F.; Kihlberg, J., Macrocyclic Drugs and Clinical Candidates: What Can Medicinal Chemists Learn from Their Properties? *Journal of Medicinal Chemistry* **2014,** *57* (2), 278-295; (b) DeLorbe, J. E.; Clements, J. H.; Teresk, M. G.; Benfield, A. P.; Plake, H. R.; Millspaugh, L. E.; Martin, S. F., Thermodynamic and Structural Effects of Conformational Constraints in Protein-Ligand Interactions. Entropic Paradoxy Associated with Ligand Preorganization. *Journal of the American Chemical Society* **2009,** *131* (46), 16758-16770; (c) DeLorbe, J. E.; Clements, J. H.; Whiddon, B. B.; Martin, S. F., Thermodynamic and Structural Effects of Macrocyclic Constraints in Protein-Ligand Interactions. *ACS Med. Chem. Lett.* **2010,** *1* (8), 448-452.

83. Wahyudi, H.; McAlpine, S. R., Predicting the unpredictable: Recent structure-activity studies on peptide-based macrocycles. *Bioorganic Chemistry* **2015,** *60*, 74-97.

84. Snyder, P. W.; Lockett, M. R.; Moustakas, D. T.; Whitesides, G. M., Is it the shape of the cavity, or the shape of the water in the cavity? *European Physical Journal-Special Topics* **2014,** *223* (5), 853-891.

85. (a) Quartararo, J. S.; Wu, P. P.; Kritzer, J. A., Peptide Bicycles that Inhibit the Grb2 SH2 Domain. *Chembiochem* **2012,** *13* (10), 1490-1496; (b)

Cascales, L.; Henriques, S. T.; Kerr, M. C.; Huang, Y. H.; Sweet, M. J.; Daly, N. L.; Craik, D. J., Identification and Characterization of a New Family of Cell-penetrating Peptides: Cyclic Cell-Penetrating Peptides. *Journal of Biological Chemistry* **2011,** *286* (42), 36932-36943; (c) Navia, M. A.; Chaturvedi, P. R., Design principles for orally bioavailable drugs. *Drug Discov. Today* **1996,** *1* (5), 179-189.
86. Udugamasooriya, D. G.; Spaller, M. R., Conformational constraint in protein ligand design and the inconsistency of binding entropy. *Biopolymers* **2008,** *89* (8), 653-667.
87. Lodish, H.; Berk, A.; Zipursky, S. L., *Molecular Cell Biology (4th Edition)*. W. H. Freeman: New York, 2000.
88. Gao, Y.; Kodadek, T., Direct Comparison of Linear and Macrocyclic Compound Libraries as a Source of Protein Ligands. *Acs Combinatorial Science* **2015,** *17* (3), 190-195.
89. Kamens, A. J.; Eisert, R. J.; Corlin, T.; Baleja, J. D.; Kritzer, J. A., Structured Cyclic Peptides That Bind the EH Domain of EHD1. *Biochemistry* **2014,** *53* (29), 4758-4760.
90. Schrodinger, L., The PyMOL Molecular Graphics System. *Version 1.8*.
91. Kim, S.; Dubelman, A. M.; Goonesekera, S.; Feig, L. A.; Baleja, J. D., Letter to the Editor: H-1, N-15, and C-13 NMR resonance assignments for the Eps15 homology domain of Reps1. *Journal of Biomolecular Nmr* **2000,** *18* (4), 367-368.
92. Timmerman, P.; Beld, J.; Puijk, W. C.; Meloen, R. H., Rapid and quantitative cyclization of multiple peptide loops onto synthetic scaffolds for structural mimicry of protein surfaces. *Chembiochem* **2005,** *6* (5), 821-+.
93. Heinis, C.; Rutherford, T.; Freund, S.; Winter, G., Phage-encoded combinatorial chemical libraries based on bicyclic peptides. *Nature Chemical Biology* **2009,** *5* (7), 502-507.
94. (a) Urech-Varenne, C.; Radtke, F.; Heinis, C., Phage Selection of Bicyclic Peptide Ligands of the Notch1 Receptor. *Chemmedchem* **2015,** *10* (10), 1754-1761; (b) Rebollo, I. R.; McCallin, S.; Bertoldo, D.; Entenza, J. M.; Moreillon, P.; Heinis, C., Development of Potent and Selective S. aureus Sortase A Inhibitors Based on Peptide Macrocycles. *ACS Med. Chem. Lett.* **2016,** *7* (6), 606-611; (c) Diderich, P.; Heinis, C., Phage selection of bicyclic peptides binding Her2. *Tetrahedron* **2014,** *70* (42), 7733-7739; (d) Angelini, A.; Cendron, L.; Chen, S. Y.; Touati, J.; Winter, G.; Zanotti, G.; Heinis, C., Bicyclic Peptide Inhibitor Reveals Large Contact Interface with a Protease Target. *Acs Chemical Biology* **2012,** *7* (5), 817-821; (e) Chen, S. Y.; Rebollo, I. R.; Buth, S. A.; Morales-Sanfrutos, J.; Touati, J.; Leiman, P. G.; Heinis, C., Bicyclic Peptide Ligands Pulled out of Cysteine-Rich Peptide Libraries. *Journal of the American Chemical Society* **2013,** *135* (17), 6562-6569.
95. (a) de Araujo, A. D.; Hoang, H. N.; Kok, W. M.; Diness, F.; Gupta, P.; Hill, T. A.; Driver, R. W.; Price, D. A.; Liras, S.; Fairlie, D. P., Comparative alpha-Helicity of Cyclic Pentapeptides in Water. *Angewandte Chemie-International Edition* **2014,** *53* (27), 6965-6969; (b) Jo, H.; Meinhardt, N.; Wu, Y. B.; Kulkarni, S.; Hu, X. Z.; Low, K. E.; Davies, P. L.; DeGrado, W. F.; Greenbaum, D.

C., Development of alpha-Helical Calpain Probes by Mimicking a Natural Protein-Protein Interaction. *Journal of the American Chemical Society* **2012,** *134* (42), 17704-17713.
96. Diderich, P.; Bertoldo, D.; Dessen, P.; Khan, M. M.; Pizzitola, I.; Held, W.; Huelsken, J.; Heinis, C., Phage Selection of Chemically Stabilized alpha-Helical Peptide Ligands. *Acs Chemical Biology* **2016,** *11* (5), 1422-1427.
97. Inc., C. C. G., Molecular Operating Environment (MOE). **2013,** *08*.
98. Caswell, P. T.; Chan, M.; Lindsay, A. J.; McCaffrey, M. W.; Boettiger, D.; Norman, J. C., Rab-coupling protein coordinates recycling of alpha 5 beta 1 integrin and EGFR1 to promote cell migration in 3D microenvironments. *Journal of Cell Biology* **2008,** *183* (1), 143-155.
99. (a) Dautryvarsat, A.; Ciechanover, A.; Lodish, H. F., pH and the Recycling of Transferrin During Receptor-Mediated Endocytosis. *Proceedings of the National Academy of Sciences of the United States of America-Biological Sciences* **1983,** *80* (8), 2258-2262; (b) Qian, Z. M.; Li, H. Y.; Sun, H. Z.; Ho, K., Targeted drug delivery via the transferrin receptor-mediated endocytosis pathway. *Pharmacological Reviews* **2002,** *54* (4), 561-587.
100. Jović, M.; Naslavsky, N.; Rapaport, D.; Horowitz, M.; Caplan, S., EHD1 regulates β1 integrin endosomal transport: effects on focal adhesions, cell spreading and migration. *Journal of Cell Science* **2007,** *120* (5), 802.
101. (a) Fritzsche, S.; Springer, S., Investigating MHC class I folding and trafficking with pulse-chase experiments. *Molecular Immunology* **2013,** *55* (2), 126-130; (b) Pohl, S.; Hasilik, A., Biosynthesis, targeting, and processing of lysosomal proteins: Pulse-chase labeling and immune precipitation. In *Lysosomes and Lysosomal Diseases*, Platt, F.; Platt, N., Eds. 2015; Vol. 126, pp 63-83.
102. Wileman, T.; Harding, C.; Stahl, P., Receptor-Mediated Endocytosis. *Biochemical Journal* **1985,** *232* (1), 1-14.
103. (a) Lipinski, C. A., Drug-like properties and the causes of poor solubility and poor permeability. *Journal of Pharmacological and Toxicological Methods* **2000,** *44* (1), 235-249; (b) Matsson, P.; Doak, B. C.; Over, B.; Kihlberg, J., Cell permeability beyond the rule of 5. *Advanced Drug Delivery Reviews* **2016,** *101*, 42-61.
104. (a) Gupta, B.; Levchenko, T. S.; Torchilin, V. P., Intracellular delivery of large molecules and small particles by cell-penetrating proteins and peptides. *Advanced Drug Delivery Reviews* **2005,** *57* (4), 637-651; (b) Kristensen, M.; Birch, D.; Nielsen, H. M., Applications and Challenges for Use of Cell-Penetrating Peptides as Delivery Vectors for Peptide and Protein Cargos. *International Journal of Molecular Sciences* **2016,** *17* (2); (c) Skotland, T.; Iversen, T. G.; Torgersen, M. L.; Sandvig, K., Cell-Penetrating Peptides: Possibilities and Challenges for Drug Delivery in Vitro and in Vivo. *Molecules* **2015,** *20* (7), 13313-13323.
105. Rizzuti, M.; Nizzardo, M.; Zanetta, C.; Ramirez, A.; Corti, S., Therapeutic applications of the cell-penetrating HIV-1 Tat peptide. *Drug Discov. Today* **2015,** *20* (1), 76-85.

106. (a) Kahns, A. H.; Buur, A.; Bundgaard, H., Prodrugs of Peptides .18. Synthesis and Evaluation of Various Esters of Desmopressin (DDAVP). *Pharmaceutical Research* **1993,** *10* (1), 68-74; (b) Orioli, M.; Vistoli, G.; Regazzoni, L.; Pedretti, A.; Lapolla, A.; Rossoni, G.; Canevotti, R.; Gamberoni, L.; Previtali, M.; Carini, M.; Aldini, G., Design, Synthesis, ADME Properties, and Pharmacological Activities of beta-Alanyl-D-histidine (D-Carnosine) Prodrugs with Improved Bioavailability. *Chemmedchem* **2011,** *6* (7), 1269-1282.
107. (a) Jensen, L. B.; Riise, E.; Nielsen, L. K.; Dziegiel, M.; Fugger, L.; Engberg, J., Efficient purification of unique antibodies using peptide affinity-matrix columns. *Journal of Immunological Methods* **2004,** *284* (1-2), 45-54; (b) Murray, A.; Sekowski, M.; Spencer, D. I. R.; Denton, G.; Price, M. R., Purification of monoclonal antibodies by epitope and mimotope affinity chromatography. *Journal of Chromatography A* **1997,** *782* (1), 49-54.
108. (a) Powell, M. F.; Stewart, T.; Otvos, L.; Urge, L.; Gaeta, F. C. A.; Sette, A.; Arrhenius, T.; Thomson, D.; Soda, K.; Colon, S. M., Peptide Stability in Drug Development .2. Effect of Single Amino-Acid Substitution and Glycosylation on Peptide Reactivity in Human Serum. *Pharmaceutical Research* **1993,** *10* (9), 1268-1273; (b) Otvos, L.; Bokonyi, K.; Varga, I.; Otvos, B. I.; Hoffmann, R.; Ertl, H. C. J.; Wade, J. D.; McManus, A. M.; Craik, D.; Bulet, P., Insect peptides with improved protease-resistance protect mice against bacterial infection. *Protein Science* **2000,** *9* (4), 742-749.
109. (a) Nguyen, L. T.; Chau, J. K.; Perry, N. A.; de Boer, L.; Zaat, S. A. J.; Vogel, H. J., Serum Stabilities of Short Tryptophan-and Arginine-Rich Antimicrobial Peptide Analogs. *Plos One* **2010,** *5* (9); (b) Pakkala, M.; Hekim, C.; Soininen, P.; Leinonen, J.; Koistinen, H.; Weisell, J.; Stenman, U. H.; Vepsalainen, J.; Narvanen, A., Activity and stability of human kalikrein-2-specific linear and cyclic peptide inhibitors. *Journal of Peptide Science* **2007,** *13* (5), 348-353.
110. White, N. S.; Errington, R. J., Fluorescence techniques for drug delivery research: theory and practice. *Advanced Drug Delivery Reviews* **2005,** *57* (1), 17-42.
111. Zhang, W. T.; Alt-Holland, A.; Margulis, A.; Shamis, Y.; Fusenig, N. E.; Rodeck, U.; Garlick, J. A., E-cadherin loss promotes the initiation of squamous cell carcinoma invasion through modulation of integrin-mediated adhesion. *Journal of Cell Science* **2006,** *119* (2), 283-291.
112. Margulis, A.; Zhang, W. T.; Alt-Holland, A.; Crawford, H. C.; Fusenig, N. E.; Garlick, J. A., E-cadherin suppression accelerates squamous cell carcinoma progression in three-dimensional, human tissue constructs. *Cancer Research* **2005,** *65* (5), 1783-1791.